Chemical Science

ROYAL SOCIETY OF CHEMISTRY

REVIEW

View Article Online
View Journal | View Issue

Cite this: *Chem. Sci.*, 2025, **16**, 12768

Donor–acceptor type covalent organic frameworks: design, optimization strategies and applications

Haiyang Liu,[a] Shanshan Zhu,[a] Yongfeng Zhi, *[b] Huijuan Yue [c] and Xiaoming Liu *[a]

Covalent organic frameworks (COFs) have emerged as one of the hottest research topics in various applications due to their designed structures, adjustable pore sizes, and abundant active sites. However, the high electron–hole recombination rate and short carrier lifetime in non-donor–acceptor type COFs are inevitable issues. The electron donor–acceptor (D–A) type COFs, which are synthesized by introducing donor and acceptor units into the COF skeleton, combined with effective carrier separation, adjustable bandgap, and sensitive photoelectric response, are considered an effective strategy for improving exciton dissociation and optimizing carrier transport. In recent years, D–A type COFs have witnessed exponential expansion in applications spanning photocatalysis, energy storage, and photothermal therapy. Consequently, there exists an imperative necessity to comprehensively summarize and expound upon the challenges and prospects pertaining to the development of D–A type COFs. In this review, we first summarize the common connecting bonds as well as the building blocks for the synthesis of D–A type COFs. Several strategies for optimizing D–A type COFs and their recent progress in photocatalysis, photothermal therapy, and energy storage are then presented. Finally, we delineate the current challenges and impediments of D–A type COFs and offer a forward-looking perspective on the future development of D–A type COFs. This review is poised to encourage researchers with a more profound comprehension of the design strategies and applications of D–A type COFs, thereby inspiring them to conduct more incisive research into the challenges and developmental prospects of D–A type COFs.

Received 18th February 2025
Accepted 23rd June 2025

DOI: 10.1039/d5sc01267h

rsc.li/chemical-science

[a]*College of Chemistry, Jilin University, Changchun, 130012, P.R. China. E-mail: xm_liu@jlu.edu.cn*

[b]*School of Chemistry and Chemical Engineering, Hainan University, Haikou, 570228, China. E-mail: zhiyf@hainanu.edu.cn*

[c]*State Key Laboratory of Inorganic Synthesis and Preparative Chemistry, College of Chemistry, Jilin University, Changchun, 130012, P.R. China*

1. Introduction

The global energy crisis is progressively becoming a pivotal issue constraining sustainable development. With the continuous consumption of fossil fuels and the sharp rise in

Haiyang Liu

Haiyang Liu obtained his B.Sc degree from Inner Mongolia Minzu University in 2020. Now, he is pursuing his PhD degree in Prof. Xiaoming Liu's group at the Jilin University, China. His research topic is the design, synthesis and application of functional covalent organic frameworks in the field of catalysis.

Shanshan Zhu

Shanshan Zhu obtained her B.Sc degree from Xuchang University in 2019 and M.Sc degree from the Zhengzhou University, in 2022. Now, she is pursuing her PhD degree in Prof. Xiaoming Liu's group at the Jilin University, China. Her research focuses on developing novel COFs for catalysis.

global energy demand, the traditional energy system is confronted with formidable challenges.[1,2] Realizing green and low-carbon transformation and developing clean energy technologies have become urgent global needs. Covalent organic framework materials (COFs) are porous materials composed of organic molecules connected by covalent bonds, with high structural tunability and excellent physical chemical properties, which can overcome the limitations of traditional inorganic materials (*e.g.*, smaller specific surface area, insufficiently rich functional and structural diversity, *etc.*).[3–6] Due to their excellent chemical stability, pore structure, adjustable specific surface area, and diverse functionalization possibilities, COFs have been widely used in various fields such as gas storage,[7,8] catalysis,[9–13] separation,[14–17] luminescent materials,[18] wastewater treatment,[19] solvent permeation,[20] and sensors.[21–24] Therefore, COF materials, as a new type of functional material, provide broad application prospects for addressing energy crises and promoting carbon neutrality. Although COFs have shown great potential in materials science, traditional COFs often have certain limitations in electronic and optical properties, especially in optoelectronic device applications, where efficient electronic transmission and light response performance are difficult to achieve. This limitation is mainly due to the insufficient band structure and electronic coupling effect of organic monomers in the intrinsic structure of COFs, which urgently need further optimization.

To address this issue, COFs with donor–acceptor (D–A) structures have emerged. D–A type COFs are materials constructed through carefully designed interactions between donor and acceptor units.[25,26] This design strategy endows D–A type COFs with a unique electronic structure and functional performance, which can significantly improve the performance of materials in applications such as optoelectronics and energy storage. Donor units are usually aromatic amines or thioaromatic compounds with higher electron density, while acceptor units are aromatic carbonyl or nitro compounds with lower electron density. Under the action of these units, D–A type COFs can not only achieve electronic structure control in the microstructure of the material, but also effectively transfer electrons inside the material, as well as enhance its light-absorbing ability, thereby significantly improving its photoelectric performance.[27] Therefore, D–A type COFs have shown wide potential for applications in the field of optoelectronics, especially in photocatalysis, solar cells, and photothermal therapy. For example, under the action of an intramolecular built-in electric field, the photocatalytic hydrogen evolution rate of TeTpb COF with D–A structure composed of truxenone and 1,3,5-tris (*p*-formyl-phenyl) benzene-based materials reached 21.6 mmol g^{-1} h^{-1}.[28] Wang *et al.* incorporated the D–A type BABT-COF (benzotrithiophene as the D unit, tris (4-aminophenyl) amine as the A unit) as an efficient additive into the hole transport layer, and the assembled perovskite solar cell achieved a power conversion efficiency of 18.56%.[29] In addition, the CTCS-COF hydrogel could achieve the rapid separation of electron–hole pairs under the interaction of D–A (curcumin as the D unit, porphyrins as the A unit), resulting in a rapid on-wound photothermal sterilization effect.[30] These studies on D–A type COFs have shown encouraging results, giving us great

Yongfeng Zhi

Yongfeng Zhi is an associate professor at School of Chemistry and Chemical Engineering of Hainan University, China. He obtained his PhD degree in chemistry in Prof. Xiaoming Liu's group at Jilin University in 2019. He then joined Prof Qichun Zhang's Group at the Nanyang Technological University as a research fellow. In October 2020, He worked as a postdoctoral researcher under the guidance of Prof. Qing Wang and Prof. Donglin Jiang at National University of Singapore. His research topics mainly focus on synthesis and exploration of covalent organic frameworks (COFs).

Huijuan Yue

Huijuan Yue is a full professor at State Key Laboratory of Inorganic Synthesis and Preparative Chemistry, College of Chemistry of Jilin University, China. She obtained her PhD degree in Chemistry in 2007 at Jilin University. She worked as a postdoctoral researcher in the lab of Prof. Xiaodong Zou at Stockholm University in 2007–2010. Her current research interests focus on developing dielectric and magnetic nanocomposites for electromagnetic energy absorption.

Xiaoming Liu

Xiaoming Liu is a full professor at College of Chemistry of Jilin University, China. He obtained his PhD degree in Chemistry in 2006 at Jilin University. He worked as a postdoctoral researcher in the lab of Prof. Donglin Jiang at Institute for Molecular Science in 2010–2012. His current research interests focus on functional porous organic polymers (POPs) and covalent organic frameworks (COFs) for energy and catalysis.

expectations for the future development of D–A type COFs. In summary, the design concept and multifunctionality of D–A type COFs have demonstrated excellent performance in optoelectronic and energy storage applications, and with the continuous improvement of synthesis methods and structural design, their future application prospects in multiple technical fields are becoming increasingly broad.

Although there are a handful of reviews on D–A type COFs that cover many important research advances,[31,32] most of them focus on the connection of material bonds, basic characteristics, and some application areas. Summaries on energy storage or how to improve the performance of D–A type COFs by optimizing their electronic structure are not available. In addition, D–A-type COFs are a very hot field, and the number of articles on D–A-type COFs and the speed of their development have exploded in recent years. Therefore, there is an urgent need to summarize the advantages of D–A-type COFs, construction strategies, and recent advances in photocatalysis, photothermal therapy, and energy storage applications. Hence, this review aims to further supplement and improve the construction modules of D–A type COFs and their research in optical and electrical applications, and introduce several strategies for further optimizing the performance of D–A type COFs (Fig. 1). Additionally, the review will highlight the latest research developments, particularly the emergence of novel structures and innovative breakthroughs in enhancing the application performance of D–A type COFs in optoelectronic devices. We believe that in the future, with the continuous development of synthesis technology and in-depth theoretical research, D–A type COFs are expected to play a more important role in fields such as photocatalytic reactions, optoelectronic devices, energy storage and conversion.

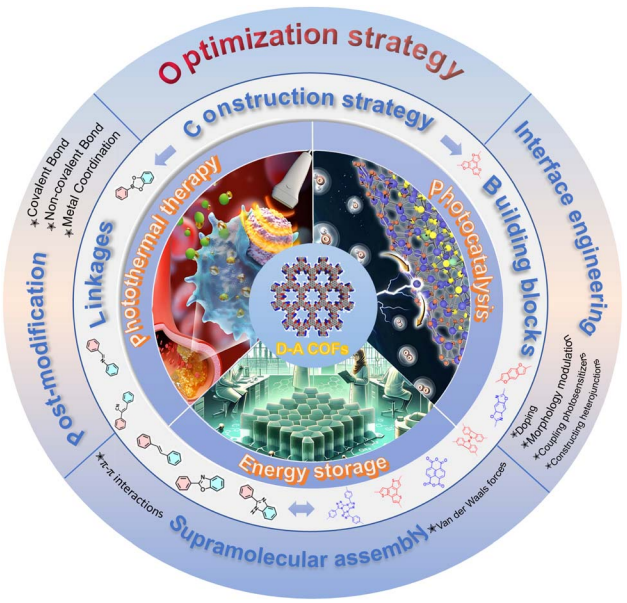

Fig. 1 Schematic diagram of the construction strategy, optimization strategy, and application of D–A type COFs.

2. Definition and advantages of D–A type COFs

D–A type COF is a covalent organic framework material formed by alternating donor and acceptor units. In contrast to conventional COFs, D–A type COFs introduce donor acceptor structures in molecular design, which can endow the material with electronic properties, optical properties, and chemical activity that are different from general COFs. Donor units are typically electron rich aromatic groups, such as nitrogen-containing aromatic hydrocarbons or pyridine groups. These functional groups have strong electron donating ability. The acceptor unit is generally an aromatic group containing electron-withdrawing groups, such as ketone groups, semi carbazide groups, *etc.* These functional groups have strong electron attraction ability. This D–A structure engenders an asymmetric electronic structure of the material, endowing it with special optoelectronic properties such as high light absorption capacity and enhanced electron hole separation efficiency. These characteristics make D–A type COFs exhibit great advantages in photocatalysis, photothermal therapy, and energy storage. Below, we will introduce these advantages in detail:

(1) Advantages of D–A type COFs in photocatalysis.

Efficient electron transport: the donor acceptor structure of D–A type COFs can effectively separate excited electrons and holes, improving the efficiency of photocatalytic reactions. This structural design optimizes the migration path of electrons, allowing electrons and holes to remain separated for a long time and reducing recombination.

Wide spectral absorption: the electronic structure characteristics of D–A type COFs can adjust the band structure of the material, thereby achieving absorption of visible light and even near-infrared light. This gives D–A type COFs significant advantages in photocatalytic water splitting, H_2O_2 generation and organic conversion reactions.[33–35]

Contains built-in electric field: due to the presence of electronic push–pull structures in the molecule, D–A type COFs will form an intrinsic electric field at the microscale. This built-in electric field can promote the migration of electrons from the donor region to the acceptor region in the excited state, while suppressing the recombination of electrons and holes.

(2) Advantages of D–A type COFs in photothermal therapy.

Enhanced light absorption capability: D–A type COF materials can absorb a wide range of light, especially in the near-infrared region, which is crucial for deep tumor treatment. The efficient light absorption ability enables it to generate a large amount of heat during the photothermal conversion process, effectively killing tumor cells.

High photothermal conversion efficiency: the conjugated system and electronic transition behavior of D–A type COFs enable excited state electrons to rapidly convert into thermal energy through non radiative transitions, resulting in high photothermal conversion efficiency.

Good biocompatibility: by designing the surface functional groups of D–A type COFs reasonably, its biocompatibility can be

improved, the toxicity to normal cells can be reduced, and the selectivity of therapeutic effects can be enhanced.

(3) Advantages of D–A type COFs in energy storage.

Enhancement of ion migration ability: in the D–A structure, under external voltage, the electron conduction path and ion diffusion path are often highly coupled, which can achieve synergistic migration of electrons and ions, helping to improve the overall dynamic and rate performance.

Good conductivity: by adjusting the donor and acceptor units, D–A type COFs can optimize the material's conductivity, thereby improving the energy density and power density of batteries or supercapacitors.

Multi-electron redox mechanism: by designing multiple reversible electron donor or acceptor units, D–A type COFs can realize multi-electron transfer reactions and significantly increase the number of electrons that can be stored per unit mass, thus enhancing the specific capacity.

Long cycle life: due to its excellent structural stability and compressive strength, D–A type COFs can maintain high electrochemical performance during long-term charge and discharge processes, exhibiting excellent cycle stability.

As a result, D–A type COFs demonstrate excellent performance in various fields such as photocatalysis, photothermal therapy, and energy storage through their unique donor acceptor structure. Their efficient electronic transmission, wide spectral absorption, adjustable pore structure, and good stability make them a candidate for future high-performance materials. These advantages make D–A type COFs have broad application prospects in fields such as sustainable energy, medical treatment, and intelligent energy storage.

3. Construction strategy of D–A type COFs

D–A type COFs are constructed when donor and acceptor units establish a highly ordered network through covalent bonds. The characteristic of D–A type COFs is that the D and A building units are alternately arranged on the plane to enhance the π–π conjugation effect of the interlayer stacking structure. Owing to the predesign ability of COF structures, the selection of building units and bond connections that make up D–A type COF materials is crucial. The types of D–A units and bonding junctions can affect not only the stability and crystallinity of COFs, but also the in-plane transport mechanisms of carriers. In this section, we provide an overview of the key connections and common donor and acceptor units used for designing D–A type COFs.

3.1 Linkages

The intricacy of synthesis, extent of conjugation, and stability of COFs are mainly influenced by the choice of connection method. Through suitable monomer connections, these monomers undergo reversible condensation reactions to form extended frameworks with specific geometric shapes, which are covalently linked together.[2] At present, various reactive linking groups have been harnessed to construct COFs, and the reactions used to synthesize COFs can be divided into seven categories based on the types of covalent bonds they form. They are: (1) B–O (such as boronic ester,[36] borosilicate,[37] *etc.*); (2) C=N (such as imine,[38] hydrazone,[39] azone);[40] (3) C=C (such as cyanovinylidene,[41] alkene,[42] and benzofuran);[43] (4) $C{=}N_{aromatic}$ (such as triazine,[44] quinoline,[45] phenazine,[46] imidazole,[47] oxazole,[48] *etc.*); (5) C–O (such as dioxane[49] and ester[50]); (6) C–N (such as β-ketoenamine,[51] amide,[52] hydrazine,[53] quinoxaline,[54] *etc.*); and (7) others (such as boron zinc,[55] silicate,[56] and azo[57]). However, not all of the aforementioned connections have been used to form the D–A type COF. Generally speaking, the formation of D–A arrays through condensation between donor and acceptor monomers is crucial for typical D–A type COFs. So far, the connection types of D–A type COFs have been reported as shown in Fig. 2, including but not limited to classic bond linkages such as boronic ester, imine, and ethylene connections.

D–A type COFs linked with boronic esters: Boric acid ester connection represents the initially reported type of connection in COFs and exhibits significant thermal stability. The significant crystallinity observed in COFs connected by boronic acid esters can be attributed to the highly reversible copolymerization reaction between boronic acid and catechol derivatives. However, COFs with boronic ester connections characterized by non-conjugated bonds exhibit limited carrier mobility due to their dependence on the stacking of conjugated units to form channels. To enhance photocatalytic activity, incorporating donor and acceptor units into these COFs can effectively improve carrier mobility. Jiang *et al.* synthesized the first D–A type COF connected by boronic acid ester, which utilized triphenylamine as the electron donor and benzothiazole as the electron acceptor (Fig. 3a).[58] The D–A type COF generates unidirectional columnar arrays and periodicity of D-on-D and A-on-A in an extended and layered crystal framework with AA stacking. This bipolar independent pathway enables the transport of electrons and holes, while the vertically arranged heterojunction with a wide D–A interface significantly improves the photoconductivity. However, their low stability towards hydrolysis and oxidation processes limits their use as heterogeneous catalysts.

D–A type COF linked with imine: The COF connected by imine is synthesized through the Schiff base reaction of aromatic amines and aldehydes. This synthesis method overcomes the problem of easy hydrolysis of boron ester linked COFs, while endowing imine linked COFs with excellent chemical stability (although their formation process is easily reversible).[59] However, the reversibility of imine bonds also makes D–A type COFs connected by imines excellent in crystallinity and specific surface area, making them a widely studied object. The development of imine-based COFs not only significantly improves the chemical stability and applicability of materials, but also greatly expands the research space for new structures, topological structures, synthesis methods, and functions.[60] This is due to the widespread presence and easy availability of amines and aldehydes. Therefore, imine bonds have become the most common connecting bonds in the synthesis of D–A type COFs and other materials. Recently, Li

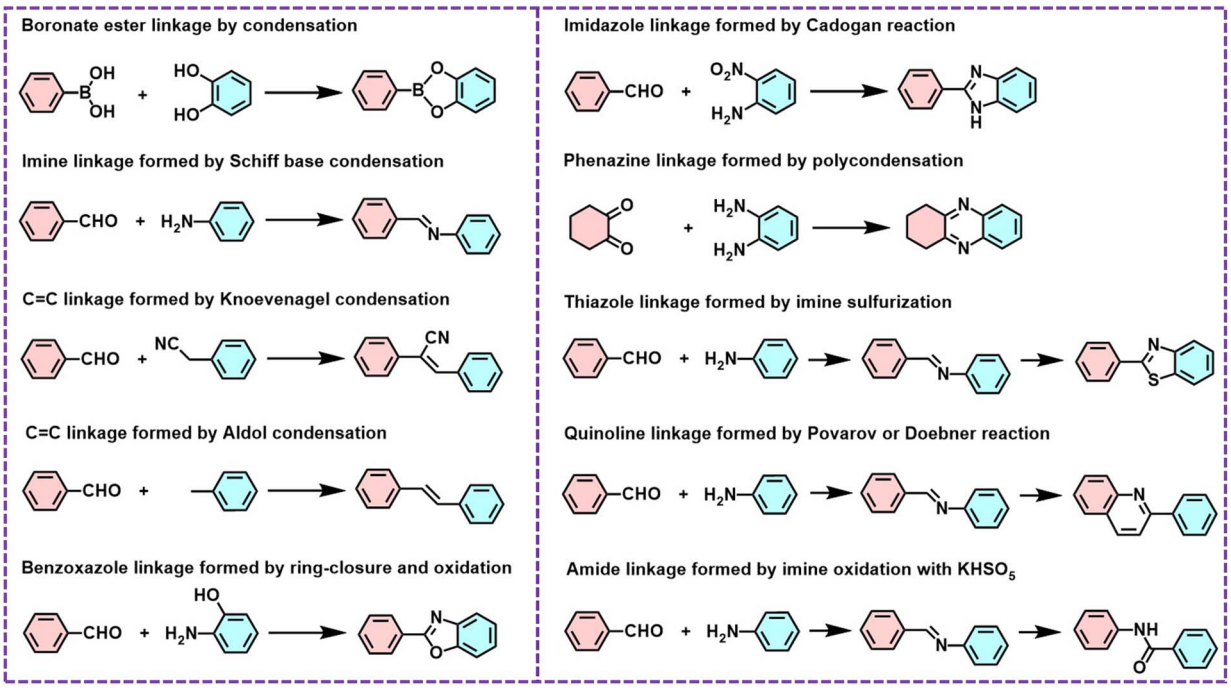

Fig. 2 Formation of linkage bonds for D–A type COFs.

et al. introduced three receptor units containing different heteroatoms (O, S, and Se) and synthesized corresponding photoactive imine linked COFs (Py-BO-COF, Py-BT-COF, and Py-BSE-COF) with different D–A structures.[61] Among them, Py-BT-COF had the best exciton separation ability and interface carrier migration ability, and its hydrogen evolution rate could reach up to 10.0 mmol g^{-1} h^{-1}. In terms of stability, the chemical stability of imine-based COFs in acidic and alkaline media is higher than that of their boron counterparts. However, nucleophilic reagents can affect their integrity and trigger their disassembly, which is not advisable. Therefore, some efforts have been made to increase this stability. For example, an interesting strategy is to convert imines into other more stable functional groups, such as thiazole or quinoline, while maintaining their crystallinity and porosity. For example, Wang and his team utilized an intramolecular Povarov reaction to synthesize imine linked COFs and cyclize them into quinoline linked CQ COFs (Fig. 3b).[62] This CQ COF had excellent chemical stability against strong acids, strong bases, and redox reagents.

D–A type COF linked with ethylene: COFs connected by imines are widely used in the research of D–A type COFs due to their excellent crystallinity and ease of synthesis. However, due to the local conjugation properties of imine bonds, the carrier transport performance of such COFs is somewhat limited. Compared with COFs connected with imines, COFs connected with C=C typically have stronger conjugation and exhibit higher stability to acids or bases.[63] These materials have a complete conjugated system, which enhances their light absorption ability and electron delocalization. In addition, they also retain the inherent characteristics of COFs, such as high specific surface area and excellent crystallinity. The Knoevenagel condensation between aldehydes and benzyl cyanides has been widely used for the preparation of COFs with cyanovinylidene linkages. For example, Zhu and his colleagues successfully prepared fully conjugated Bpy-DAN-COF with the D–A structure using K_2CO_3 as a base catalyst.[64] The bipyridine unit of the acceptor facilitates the formation of a molecular specific electron transport pathway with the donor benzothiophene unit, exhibiting excellent charge separation and transfer efficiency. Specifically, the BTT-BpyDAN-COF exhibited a high hydrogen evolution rate of 10.1 mmol g^{-1} h^{-1} and an excellent apparent quantum efficiency of 4.83% under visible light irradiation. Due to the presence of cyanide substituents on the double bond, the stability of ethylene linked COFs synthesized through Knoevenagel condensation is compromised. To overcome this issue, Aldol condensation can be used to prepare unsubstituted C=C-linked COFs. Guo *et al.* synthesized two types of ethylene linked COFs (TMT-BT-COF and TMT-TT-COF) using benzoic anhydride as a catalyst and aldol condensation reaction (using thienothiophene and benzothiazole groups as the donor and electron-deficient triazine units as the acceptor).[65] Both types of COFs with D–A type vinyl connections exhibited high charge transfer efficiency and significant catalytic activity. As a result, both of them demonstrate remarkably catalytic activity in the oxidation of styrene to benzaldehyde with molecular oxygen, with an exceptionally high conversion rate (≥92%) and selectivity (≥90%).

Therefore, the connecting bonds of D–A type COFs play a crucial role in enhancing material properties, and different types of connecting bonds provide unique performance and advantages for D–A type COFs. In the future, by combining new chemical bonds and self-assembly strategies, D–A type COFs

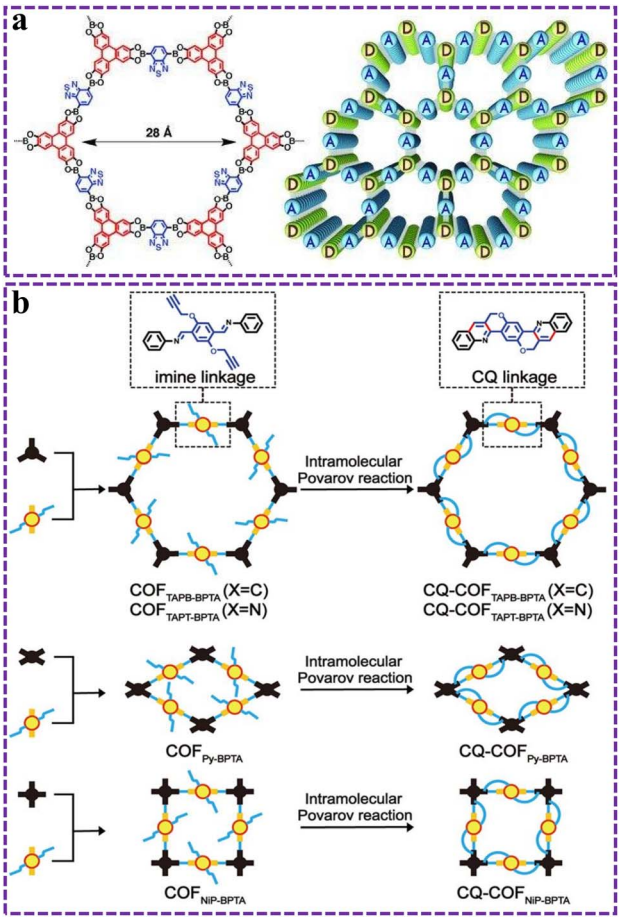

Fig. 3 (a) Schematic representation of 2D D–A COFs with self-sorted and periodic electron donor–accepter ordering and bicontinuous conducting channels. Reproduced from ref. 58 with permission from John Wiley and Sons, copyright 2012. (b) Synthetic Routes to CQ-COFs from imine-linked COFs. Reproduced from ref. 62 with permission from American Chemical Society, copyright 2022.

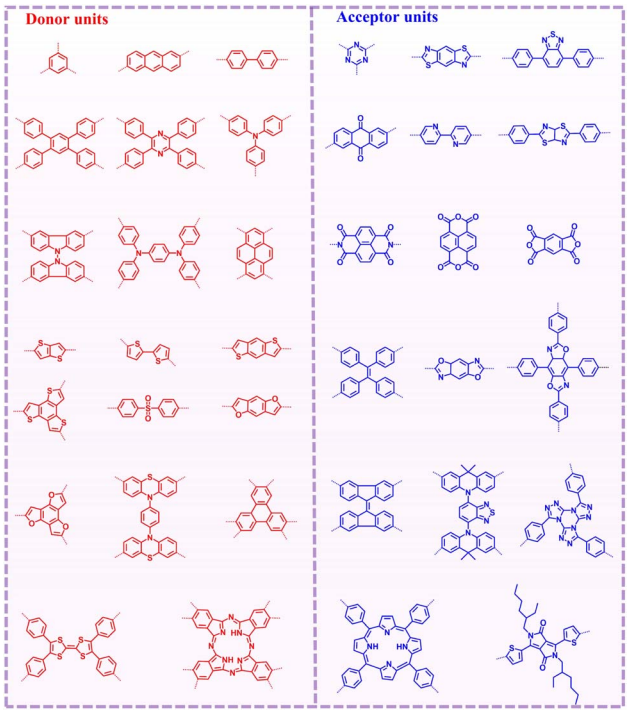

Fig. 4 Partial construction units for D–A type COFs.

featuring higher efficiency, stability, and specific functions can be developed, promoting their applications in energy, catalysis, and drug delivery fields.

3.2 Building blocks

The common donor and acceptor units reported in the literature are shown in Fig. 4. Building blocks play a crucial role in the formation of D–A type COFs. They not only determine the structure and topological characteristics of COFs, but also directly affect their electronic properties, stability, and functionality. In this section, we primarily introduce the common building blocks used to form D–A type COFs, including triazine, thiazolo[5,4-*d*] thiazole, benzothiadiazole, diketopyrrolopyrrole, naphthalene diimides, pyrene, thiophene and benzothiophene unit.

3.2.1 Triazine unit. CTF-1 is the first triazine based COF in two-dimensional (2D) triazine based COFs, which was synthesized by high-temperature ion thermal self-condensation of dicyanobenzene in molten zinc chloride.[44] At present, triazine has become a typical electron acceptor unit, which is combined with donor units to establish an electron transfer platform and generate strong interactions in various fields, greatly improving application performance.[66,67] Lei *et al.* constructed a D–A COF with triazine units and triphenylamine as an efficient electrochemiluminescence (ECL) emitter with adjustable network charge transfer.[68] Research has shown that the ECL strength of triazine based COFs with a strong D–A effect was 123 times stronger than that of phenyl COFs. Density functional theory and proton regulated ECL behavior confirmed that ECL depended on intraparticle charge transfer between donor and acceptor units. Triazine can also serve as a photoactive unit in COFs. The PDI-COF composed of triazine units and donor perylene imide could induce electron-efficient generation of highly oxidative free radicals, which promoted the oxidative coupling reaction of amines and the C-3 thiocyanation reaction of indole.[69] Similarly, triazine-based CzTA-TAPT COF could also serve as an efficient photocatalyst for the aforementioned organic reactions.[70] Matthew V *et al.* prepared a D–A type COF based on triazine-thiophene and demonstrated by transient absorption spectroscopy that it had long-lived excited states (>100 ms).[71] These excited states have lifetimes sufficient for direct photoreduction of uranium at ppm concentration. Triazine-based D–A type COFs with imine linkage could be oxidized to amide-linked COF-TCZ-O, which was used as a photocatalyst for the oxidation reaction of *n*-aryltetrahydroisoquinolines.[72] Similarly, triazine-based TEB-COF containing acetylene groups could photoreduce Cr(VI) due to its superior extended conjugation and planarity.[73] Moreover, triazine units could not only generate stable negative charges under photoexcitation, but also form D–A interactions, improving charge separation efficiency.[74] Recently, Li *et al.*

constructed two types of D–A COFs by combining electron-deficient triazine and electron rich polycyclic aromatic groups.[75] In the absence of an external electron donor, the photocurrent of anthracene-based COFs was enhanced by 5 times compared to naphthyl based COFs. This was mainly due to the enhanced orbital overlap and D–A interaction of anthracene-based COFs, which facilitated effective charge separation. Recently, as shown in Fig. 5, Liu and his group constructed novel D–A type COF materials (COF-JLU42 and COF-JLU32) by introducing electron-deficient triazines and electron-rich benzotrifurans and benzotrithiophenes into the backbone *via* the Schiff base reaction.[76] The photocatalytic hydrogen evolution rate of COF-JLU42 under visible light irradiation was 40 000 μmol g^{-1} h^{-1}.

As is well known, the optical properties and photocatalytic performance of COFs can be adjusted by changing the monomers or making simple modifications.[77,78] However, the key factors affecting the optical, electrical, and photocatalytic performance of COFs still need further exploration. Tang *et al.* synthesized a series of [3 + 3] COFs by the condensation reaction of 1,3,5-tris (4-formylphenyl) benzotriazine units with different substituents (–H, –OH, and $–CF_3$) on the aromatic ring.[79] Research findings have indicated that the existence of –OH substituents could narrow the bandgap and improve conductivity, while COFs with Tz skeletons can improve charge separation efficiency due to the interaction of D–A. Therefore, among these COFs, OH-TFP-TTA with both Tz skeleton and –OH functional group exhibited the highest photocatalytic activity in a visible light induced reduction dehalogenation reaction. Isomers of triazine based COFs with different imine bond directions exhibited significant differences in photocatalytic activity due to differences in imine polarization properties.[80] Among them, the bipyridine unit acted as an electron donor and acceptor in both reverse and forward imine cases, respectively, and these interactions ultimately led to Re-f-COF isomers as effective photocatalysts for CO_2 reduction. Furthermore, density functional theory can be used to predict the optoelectronic properties of the designed COFs. Jiang *et al.* calculated and evaluated the band alignment and charge transfer characteristics of potential D–A COFs.[81] By comparing the charge difference between the ground state and excited state, the effect of D–A action on the charge separation degree and exciton binding energy of different COFs was elucidated. Guided by the above results, corresponding D–A type COFs with different HOMO–LUMO orbitals were synthesized (Fig. 7a), among which TPT-OMe-COF had the best photocatalytic hydrogen production activity, and the activity trends of other COFs were correlated with the activity trends calculated for exciton binding energy. The long reaction time and environmental sensitivity of traditional solvothermal methods limit their practical applications. In view of this, Tz based TzPm-COF with a D–A structure could rapidly generate high crystallinity through the microwave-assisted method.[82] TzPm-COF had a low exciton binding energy and could effectively generate $O_2^{\bullet-}$, ultimately driving the photooxidation amination reaction with high recyclability.

3.2.2 Thiazolo[5,4-*d*] thiazole (Tz) unit. Tz, as an electron-deficient building block with coplanar geometry, a rigid structure, and strong intermolecular p–p stacking properties, has become a commonly used unit for the construction of stable D–A-type COFs.[83,84] Yang *et al.* prepared D–A PETZ-COF with Tz as the acceptor unit and tetraphenylethylene (PE) as the donor unit through a Schiff base reaction.[85] Through photocurrent testing, photoluminescence testing, and DFT calculations, it was shown that PETZ COFs with electronic push–pull properties exhibited stronger photocurrent intensity and fluorescence lifetime compared to PEBP COFs without a D–A structure, thus showing enhanced photocatalytic hydrogen evolution performance. Similarly, the PyTz COF (Fig. 6) constructed by Wen *et al.* also showed similar results to the PETZ-COF mentioned above under the interaction of D–A, making it suitable for the same

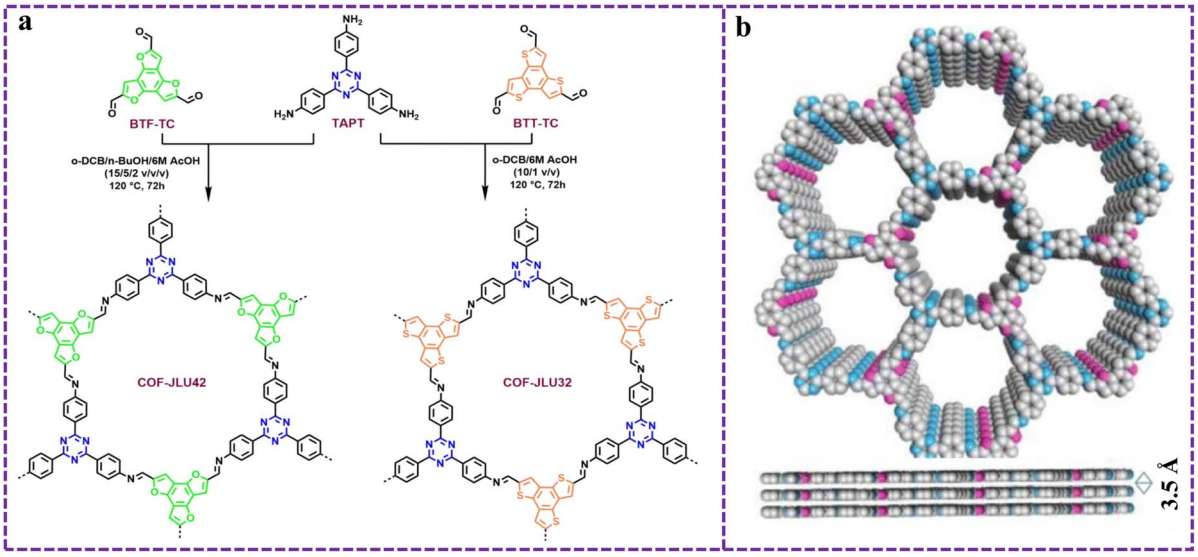

Fig. 5 (a) Synthetic conditions and chemical structures of COF-JLU32 and COF-JLU42, and (b) top and side views of the AA stacking structure of COF-JLU42. Reproduced from ref. 76 with permission from Royal Society of Chemistry, copyright 2024.

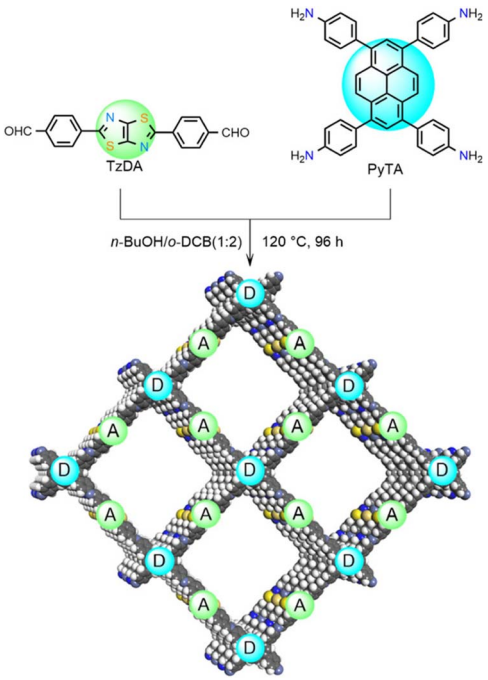

Fig. 6 Synthesis of PyTz-COF under solvothermal conditions. Reproduced from ref. 86 with permission from John Wiley and Sons, copyright 2020.

application.[86] In addition, incorporating TZ units into COFs can effectively improve the light absorption range. Lotsch *et al.* found through solid-state UV-visible absorption spectroscopy that COFs containing Tz units had a broader absorption band edge of approximately 70 nm than COFs without Tz units.[87]

Tz units have abundant heteroatoms with lone pair electrons, which can undergo coordination interactions and improve the crystallinity of COFs, which makes D–A type COFs consisting of the Tz unit have a wide range of applications. Liang and his team designed and prepared a D–A type COF (TPDA-TZDA) based on the Tz unit for enhancing power conversion efficiency in perovskite solar cells.[88] Utilizing the coordination effect generated by the interaction between N atoms on the Tz unit and Pb^{2+}, which effectively increased the grain size and crystallinity, suppressed the defects in the perovskite, and promoted the charge transport within the films. The multi-component COF1-AO based on Tz could also have a certain affinity for uranium in seawater, and the extraction efficiency of uranium could reach a record high of 2.45 mg^{-1} g per day.[89] In addition, Tong and his team prepared two different types of D–A structured COFs containing Tz units (COF-TD1 and COF-TD2), which exhibited excellent degradation activity for various antibiotics.[90] Under the effect of electronic push–pull, COF-TD1 had good degradation performance in complex water environments and real sunlight, which had certain practical application ability.

3.2.3 Benzothiadiazole (BT) unit. Like triazine and Tz units, the BT unit has a coplanar geometry and intermolecular π–π stacking properties, exhibiting strong electron-deficient properties. Combining BT as an acceptor unit with some, *e.g.*, benzene,[91] pyrenyl,[92,93] or other electron-donors to form D–A type COFs can effectively facilitate carrier separation and transport. Lin *et al.* constructed ETTA-Td COF by linking diphenylaldehyde with BT units and electron-rich (4-aminophenyl) ethane (ETTA).[94] This functionalized ETTA-Td COF exhibited excellent oxidase-like activity under light irradiation and could be used as a reliable probe for the detection of sulfide ions in complex biological samples. Highly crystalline COF-C4A-BTD can be synthesized by Schiff base reaction polycondensation using BT as the acceptor unit and cup-shaped aromatic compounds as the donor unit.[95] Due to the length of the linear BT unit and the deformability of the cup-shaped aromatic structure, the lamellar structure of COF-C4A-BTD could show remarkable flexibility. The superior charge transfer behavior within the COF-C4A-BTD molecule resulted in superior visible light driven photocatalytic activity, with removal rates of 99%, 85%, and 66% for organic pollutants such as methylene blue, rhodamine B, and bisphenol A, respectively. Furthermore, OL-COFs containing BT units could accelerate exciton dissociation and prolong charge lifetime under the action of D–A, and could continuously catalyze organic conversion reactions.[96] Inspired by the structural characteristics of natural photosystem I, Chen *et al.* designed and synthesized a series of D–A type COFs (NKCOF–108, −109, −110, −111) containing BT units, which could serve as efficient catalysts for photocatalytic hydrogen evolution reactions.[97] It is well known that the photovoltaic conversion efficiency and carrier mobility in organic photovoltaics could be improved by fine structural modulation (*e.g.*, halogenation) of the building blocks.[92,98,99] As shown in Fig. 7b, Chen and his associates synthesized a series of 2D Py-XTP-BT-COFs (X = H, F, Cl) with strong photoactivity using a solvothermal method.[100] Due to the large electronegativity of the halogen atoms, the electronic structure of the COFs was modulated by halogenation of the BT units, which lowered the energy barrier for H_2 generation as well as increased the charge separation rate, resulting in PyClTP-BT-COFs with ultrahigh photocatalytic H_2 evolution rates.

Among many different bond connections, constructing fully conjugated COFs can achieve ideal light absorption and charge separation.[77,101] Combining the electron-donating pyrene unit with the electron-deficient BT unit enabled the synthesis of a fully conjugated Py-BSZ-COF.[102] The introduction of the BT unit induced a redshift in visible light absorption and a rapid separation of photogenerated charges. The Py-BSZ-COF could mediate the photocatalytic oxidative amine coupling of thioamides and the cyclization to 1,2,4-thiadiazoles with high yields and recoverability. The work demonstrated the great potential of fully conjugated COFs with a D–A structure in light-driven organic synthesis. Wang *et al.* reported two sp^2-c conjugated COFs with BT units (HDU-107 and HDU-108).[103] Among them, the conjugation of the cyano-functional group of HDU-108 provided a concentrated electronegative active center, which made the COF material active site-rich and enhanced the photocatalytic reduction of Cr(VI).

Benzobisthiazole is a derivative of BT, which can serve as a long linker for BT units and has a stronger electron-deficient ability. Zhao and his team fabricated three D–A type COFs (BTH-

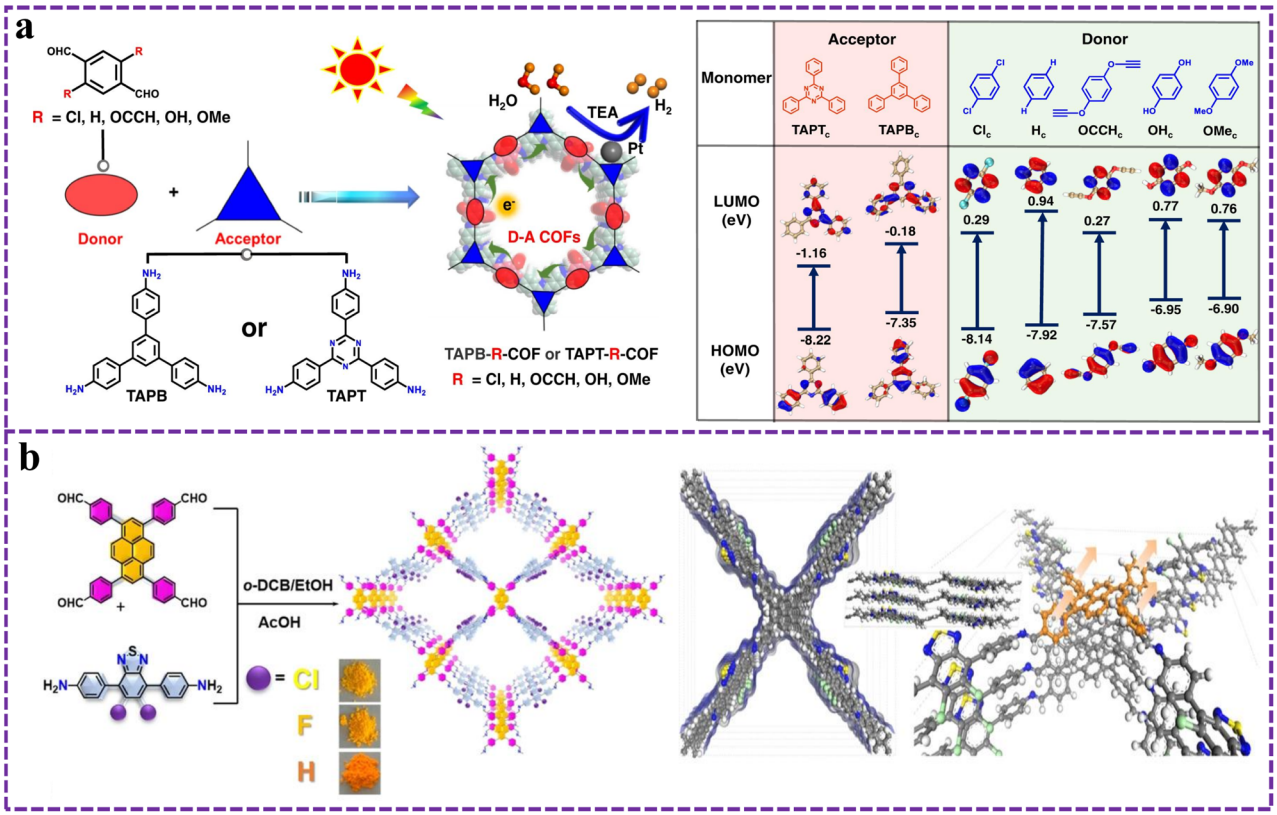

Fig. 7 (a) Construction of D–A COFs composed of amine monomers and functionalized terephthalaldehydes, as well as the corresponding HOMO–LUMO orbitals. Reproduced from ref. 81 with permission from Springer Nature, copyright 2023. (b) Synthetic routes of Py-XTP-BT-COFs under solvothermal conditions, and AA stacking mode of Py-ClTP-BT-COF. Reproduced from ref. 100 with permission from John Wiley and Sons, copyright 2020.

1, 2, 3) with benzobisthiazole as a building unit through Knoevenagel condensation.[104] The integration of the cyanoethylene bond and the BTH unit provided an electron-deficient π-conjugated symmetric structure, and the semiconducting properties of the π-conjugated COFs could be modulated by changing the electronic properties of the other donor units. BTH-3 with benzotrithiophene as the electron-donor unit exhibited the highest photocatalytic hydrogen precipitation ability under visible light irradiation.

Similarly, Chen *et al.* reported a D–A type COF (Tz-COF) linked with benzobisthiazole, which accelerated the exciton dissociation by controlling the D–A interaction and thus prolonged the lifetime of photogenerated carriers.[94] The optimized Tz-COF-3 had an apparent quantum yield of 6.9% at 420 nm.

3.2.4 Diketopyrrolopyrrole (DPP) unit. The dye molecule DPP has excellent coplanarity and strong electron-pulling ability, and it is frequently employed as a photo-functional unit in the formation of D–A type COFs. Moreover, due to the presence of intermolecular hydrogen bonding, DPP possesses excellent solvent resistance and thermal stability properties. Recently, Pachfule and coworkers constructed two D–A-type COFs with DPP as the receptor unit, which have good stability and abundant adsorption sites to efficiently bind iodine in the gas and solution phases.[105] This study demonstrates that the electronic properties of COFs can be tuned to improve charge transport and enhance iodine interactions. This work demonstrates the potential of D–A type COFs with DPP as the receptor unit as efficient and stable iodine adsorbents. The Py-DPP-COF constructed from DPP units could enhance interfacial mass transfer and charge transfer, and a high uranium extraction of 903.6 mg g^{-1} was realized.[106] Moreover, the insertion of DPP units into COFs not only creates a strong electron push–pull effect, but also significantly enhances the light absorption range of COFs. The recently reported TpDPP-Py COFs based on DPP units could cover the UV-visible-near infrared light absorption range and enhanced the two-photon and three-photon effects of the COFs.[107] TpDPP-Py COFs had high photocatalytic conversions and selectivity for both benzylamine and other imine derivatives. Similarly, the DPP-TAPP COF composed of DPP and porphyrin units could reach an absorption atmosphere of about 800 nm and was also capable of spontaneously aggregating into a hollow nanotube structure.[108]

Due to the extended conjugated structure of the DPP units and the ability to contribute to efficient carrier transport, COFs composed of DPP show promising applications in organic optoelectronics. As shown in Fig. 8a, Liu and his partners constructed two 2D COFs (DPP-TBB-COF and DPP-TPP-COF) with high crystallinity and AA stacking structure *via* imine bonding.[109] The ordered intermolecular filling structure and the D–A interaction gave the COFs a wide light absorption range as

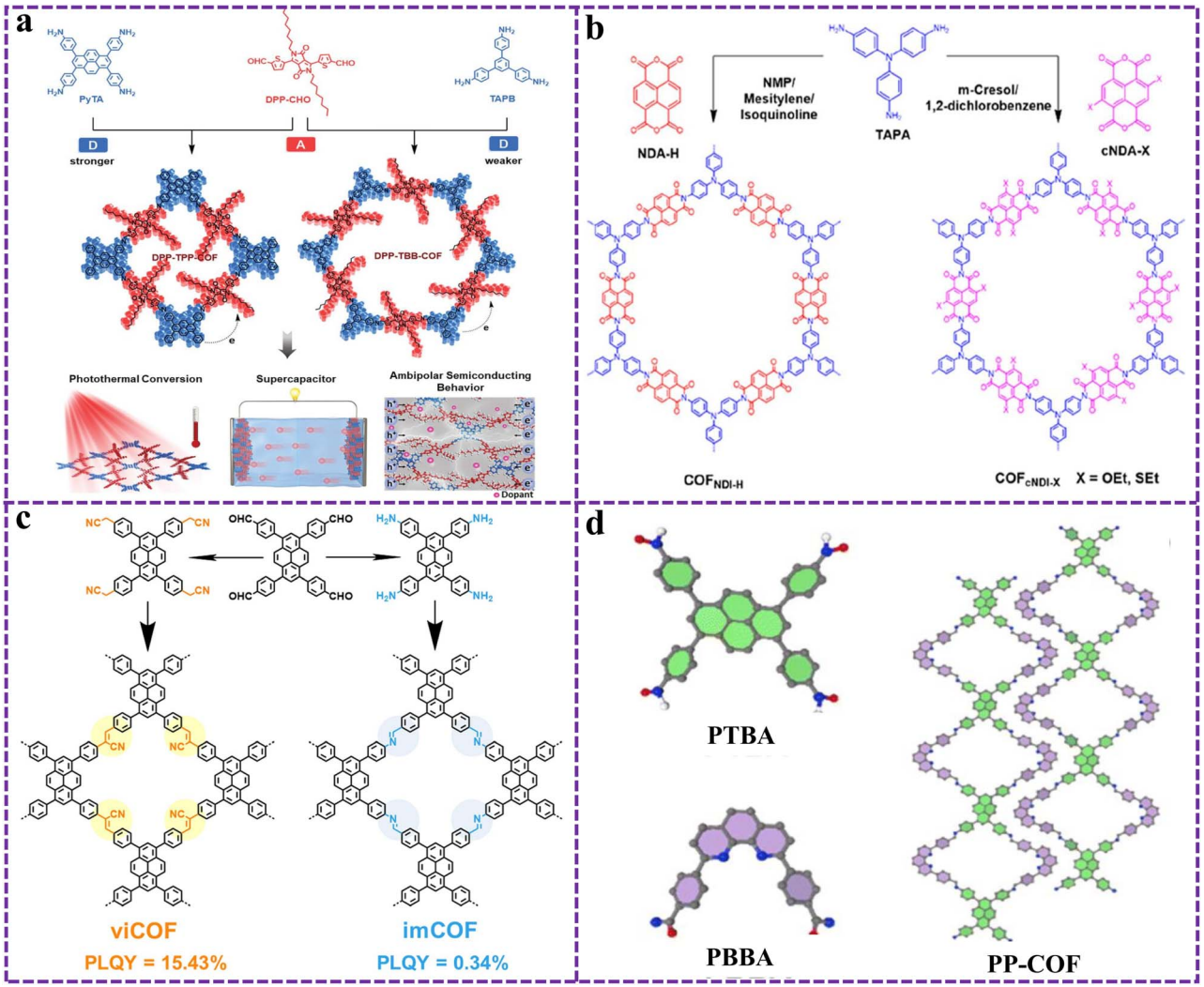

Fig. 8 (a) Schematic diagram of the synthesis of a D–A type COF based on 2D DPP, aiming to achieve multifunctional photoelectric conversion properties. Reproduced from ref. 109 with permission from John Wiley and Sons, copyright 2024. (b) Chemical structures of the COF_{NDI-H}, $COF_{cNDI-OEt}$, and $COF_{cNDI-SEt}$. Reproduced from ref. 117 with permission from American Chemical Society, copyright 2023. (c) Schematic representation of the syntheses of imCOF and viCOF. Reproduced from ref. 127 with permission from John Wiley and Sons, copyright 2023. (d) Construction of PP-COF. Reproduced from ref. 130 with permission from Royal Society of Chemistry, copyright 2024.

well as suitable HOMO/LUMO energy levels, thus the COFs possessed multifunctional photovoltaic properties (photothermal conversion, supercapacitor performance, and bipolar semiconductor behavior). Lee and his team loaded coplanar organic small molecule DPP units into 2D COFs,[110] resulting in stronger conjugation effects within the layered network to enhance light absorption, while a porous polyvinyl alcohol network was used to enhance the hydrophilicity of the overall COFs. Therefore, the prepared layered COFs (COFHS) achieve a high light hot water evaporation rate of 2.5 kg m^{-2} h^{-1} and a good ability to purify polluted water under one solar irradiation. Similarly, the DPP2-HHTP-COF coupled with borate ester had excellent photovoltaic properties with conductivity values up to 10^{-6} S cm^{-1}.[111]

3.2.5 Naphthalene diimide (NDI) unit. NDI is a molecular structure with intramolecular semiconducting properties, and NDI has a direct band gap since its band is mainly contributed by the aromatic C–C π-electron orbitals of the molecule. In addition, NDI is an ideal electron acceptor unit for constructing D–A-type COFs due to its multi-aromatic ring structure with double-electron-withdrawing imine functional groups. The combination of aldehydes or amines with NDI monomers and other donors can be used to construct imine linked NDI D–A COFs. For example, Zhao *et al.* successfully prepared 2D D–A-type COFs with NDI as the A-unit and triphenylamine (PT-N-COF) or triphenylbenzene (PT-B-COF) as the D-unit, which exhibited significant NIR absorption properties.[112] PT-N-COF exhibited a stronger charge transfer effect and D–A interaction, with a photothermal conversion efficiency of 66.4%. Electroactive COFs with similar redox capacities but different porosities and interlayer spacings were obtained by selecting monomers with different planar distortions.[113] NDI-based TAPA-NDI-COF, TAPB-NDI-COF and TAPT-NDI-COF all provided active sites for electrocatalytic reactions under D–A

interactions and had potential as electrocatalysts for oxygen reduction reactions (ORRs). However, due to the effect of interlayer spacing and porosity in the COF, the ORR activity of TAPT-NDI-COF with more pores was higher, which was attributed to the easier access of O_2 to the catalytic center of the electroactive NDI unit. In addition, NT-COF,[114] NDI-COF,[115] and NDTT[116] were COFs synthesized by connecting NDI units through imine bonds.

The bandgap and carrier separation ability are important indicators for evaluating the photoactivity of COFs. Generally, it can be achieved by inserting different substituents on the photoactive unit or changing the interlayer spacing. In view of this, Zhan and his partners obtained NDI COFs ($COF_{cNDI\text{-}OEt}$ and $COF_{cNDI\text{-}SEt}$) with customizable bandgaps by inserting different substituents without changing the global structure, and compared them with $COF_{NDI\text{-}H}$ without substituents (Fig. 8b).[117] The insertion of substituents narrowed the bandgap and interlayer distance of COFs, making it easier for charge delocalization. Moreover, ultrafast spectroscopic data were used to perform kinetic analyses to estimate the lifetime of charge recombination. Overall, current studies remain limited in terms of the correlation between photophysical properties and structural features (*e.g.*, interlayer distances).

3.2.6 Pyrene (Py) unit. Py is a molecule possessing polycyclic aromatic properties and is composed of six carbon atoms and six hydrogen atoms. The π-conjugated structure of Py gives it strong stability and the ability to absorb ultraviolet and visible light. Furthermore, since the Py molecule has many reactive sites, it can be modified by covalent bonding to generate units with strong electron donors. This has led to the Py-based unit being used as the most common donor unit in the formation of D–A type COFs. Yan *et al.* synthesized a novel D–A COF material PyPz COF with an ordered stable π-conjugated structure by combining Py-based units and pyrazine units with aldehyde groups.[118] Since Py acts as a good chromophore group, it can effectively extend the light absorption range. Compared with PyTp-COF without pyrazine, the photocatalytic hydrogen evolution performance of PyPz-COF was improved by about 7 times. When *p*-phenylenediamine was directly polymerized with PDI units, only porous amorphous polymers could be obtained due to insufficient interaction. In contrast, by introducing Py units under the same conditions, the strong D–A interaction between Py and PDI was utilized to promote the formation of ordered structures, and intercalated COFs with good crystallinity were obtained.[119] More specifically, these COFs had a clear and robust heterojunction structure in the vertical direction. In addition, D–A-A type COFs can be constructed by introducing two acceptor units to enhance exciton dissociation and carrier migration. Specifically, TAPPy-DBTDP-COF combines a Py-based donor and two BT acceptors, which allowed efficient transfer of photoexcited electrons to occur in COFs thereby improving photocatalytic performance.[120] Similarly, the performances of DABT-Py-COF,[121] COF-JLU23-25,[122] and TAPFy-PhI[123] were all enhanced by introducing Py units to enhance the light absorption capacity and D–A interactions of the materials.

In addition to the imine linked Py-based COFs generated by the Schiff base reaction mentioned above, the formation of ethylene linked sp^2 conjugated COFs through Knoevenagel condensation is also a common method for generating Py-based D–A COFs. Jiang *et al.* synthesized the first crystalline sp^2 c-COF based on Py groups.[124] The band gap of sp^2 c-COF was 1.9 eV, the aperture was 2 nm, and it had a paramagnetic carbon structure with high spin density. Subsequently, a series of Py-based sp^2 conjugated COFs emerged. Recently, Zhang and his partners prepared two ethylene linked g–COF–DMDP-1 and g–COF–DMDP-2 with a high crystallinity honeycomb structure using 5,10-dimethyl-4,9-diazepene as the key monomer.[125] One of the COFs had a specific surface area of 1238 $m^2\ g^{-1}$. Due to its high hydrophilicity and nitrogen content, g–COF–DMDP-1 produced a high H_2O_2 yield of 3820 $\mu mol\ g^{-1}\ h^{-1}$ in pure water. The 2D D–A type COF with sp^2 carbon connections containing Py and tetra styrene units synthesized by the Knoevenagel condensation method exhibited high thermal stability, with a decomposition temperature of 509 °C.[126] Moreover, the connection of different bonds in COFs can affect the exciton relaxation mode and fluorescence intensity. As shown in Fig. 8c, Han and his collaborators found a significant difference in solid-state photoluminescence quantum yield between vinyl and imino-based Py-COFs, with values of 15.43% and 0.34%, respectively.[127]

Py-based COFs are capable of forming 3D and 1D COFs in addition to the common 2D structures. Initially, Wang *et al.* synthesized 3D COFs (Py-COF) based on a Py-based [4 + 4] imine linkage *via* the solvothermal method.[128] The 3D COF had a dual interpenetrating layer topology and was the first reported fluorescent 3D COF that could be used for explosive detection. Similarly, the two ffc topological structures of D–A type 3D COFs (TFP-Py and TFP-BF) reported by Mahdy exhibit excellent photocatalytic degradation of organic pollutants and hydrogen production performance.[129] In addition to 3D COF, 1D COFs (PP-COF) consisting of pyrene with aniline and phenanthroline with aldehyde groups had been reported recently, and the building units and model diagram of PP-COF are shown in Fig. 8d.[130] Compared with 2D PyTTA-COF, the prepared PP-COF maintains good crystallinity even after 24 h of immersion in different organic solvents as well as strong acids and bases. Moreover, the good photo-responsive properties and excellent light absorption ability of PP-COF could promote the photocatalytic indole functionalization and oxidized thiol coupling reaction.

3.2.7 Carbazole unit. Carbazole is an aromatic amine compound with a tricyclic structure, the basic structure of which is an indole ring conjugated to a benzene ring. The nitrogen atom in carbazole has a lone pair of electrons and the entire structure is highly conjugated, allowing it to efficiently provide electrons to form a strong D–A interaction with the acceptor unit. At first, Kong and his team reported a novel carbazolo-triazine-based D–A type COF (CT-COF).[131] This metal-free CT-COF is capable of efficiently photo-reducing CO_2 to CO. Under the same conditions, the CO release rate (102.7 $mmol\ g^{-1}\ h^{-1}$) was 68.5 times higher than that of g-C_3N_4. The poor chemical and photostability of imine-linked D–A-COFs limits their potential for broader applications. Therefore, Thomas and his collaborators synthesized highly crystalline D–A-type COFs (CzDA-TAPT COFs) by introducing alkyl chains on carbazoles

using molecular engineering.[132] The doping of alkyl-substituted carbazoles not only guided the attachment of continuous layers in different AB stacks, but also provided excellent donor capabilities and significantly improved the photocatalytic efficiency of CzDA-TAPT COFs. Similarly, Su *et al.* oxidized D–A type COFs (COF-TCZ) connected by imine bonds based on carbazole and triazine units to stable amide connected COFs (COF-TCZ-O).[72] COF-TCZ-O has high crystallinity, good thermal and chemical stability, and excellent photoactivity, making it a suitable photocatalyst for the oxidation of *N*-aryltetrahydroisoquinoline. Recent findings suggest that strategically designed D–A-extended structures can significantly improve photocatalytic performance by optimizing electron distribution and charge transfer channels.[133,134] However, most studies on D–A-type COF photocatalysis have focused on 2D conjugated structures, and the counterparts of 3D structures have been less explored. Therefore, Yuan *et al.* synthesized three different D–A-extended COF materials using carbazole based dicyanobenzene derivatives as the intrinsic D–A building block: D–D–A, A–π–D–A, and A–D–A.[135] Among them, 3D-TAPTCOF with the A–D–A structure provides multiple charge transfer pathways, overcoming the inherent electron transport limitations of 2D COFs, thereby exhibiting the highest hydrogen evolution rate of 31.3 mmol g^{-1} h^{-1}.

Bicarbazole is usually composed of two carbazole units connected by covalent bonds. Its structure not only retains the conjugation and electron donating properties of carbazole, but also brings a series of enhancement effects due to molecular extensibility and symmetry. Kaskel and his colleagues reported two novel equi network chemically stable COFs based on carbazole units (COF-DUT-175 and DUT-176).[136] The reversible protonation of imine N in COF can lead to changes in the electronic structure of the conjugated π-system, resulting in characteristic pH responses over a wide pH range without COF decomposition. Both types of COFs are expected to become one of the best materials for indoor humidity control applications. Recently, two D–A type COFs based on carbazole were first used for piezoelectric photocatalytic synthesis of H_2O_2.[137] Vinyl modified Cz-COF achieved record high H_2O_2 production (9212 μmol g^{-1} h^{-1}) from air and pure water through piezoelectric photocatalysis. The efficient production rate of H_2O_2 is due to the synergistic effect between the polarization electric field induced by ultrasound and multiple charge transfer channels separated in space.

3.2.8 Thiophene unit. Thiophene has aromaticity similar to the benzene ring, and its structure contains a sulfur atom and two conjugated double bonds, forming a large conjugated system of six π electrons. Thiophene can be used as a classical donor unit because the d-orbital of the sulfur atom mixes well with the aromatic π-orbitals, thus providing more electrons to the acceptor group. Cao *et al.* constructed a D–A type porphyrin-based COF (TT-Por (Co)-COF) through a Schiff base condensation reaction.[138] The study showed that compared with COF-366-Co without thiophene, the charge transfer ability of TT-por (Co)-COF was enhanced due to the strong D–A interaction of electron rich thiophene, and high current density was generated for the CO_2 electroreduction reaction. Subsequently, the team explored the effect of periodic π-stacking interaction on photocatalysis by preparing a series of D–A-type 2D COFs with thiophene and metalloporphyrin as functional monomers.[139] The yield of photogenerated CO from TT-Por (Co)-COF with tight stacking interaction was 10.05 mmol g^{-1} h^{-1}. This was mainly due to the fact that the periodically ordered structure could efficiently transport the light-irradiated charge to the surface and minimize the charge trapping at the defect site, thus suppressing the recombination of electron–hole pairs.

Thiophene based COF materials are commonly used as photoactive units due to their good dispersibility, developed pore size, and strong light absorption ability. For example, D–A type COF-S materials prepared from thiophene units were used as photo-initiators to synthesize polymethyl methacrylate (PMMA) through free radical polymerization of methyl methacrylate (MMA) under visible light.[140] Similarly, the DTT-ABBO-COF prepared by Chen and his partners had good stability, high activity and recyclability and could be used as an environmentally friendly multiphase catalyst for α-oxidation amination.[141] In addition, TTF-PDI-COF,[142] ThTz COF,[143] TTDA-COF,[144] and JLNU-309 (ref. 145) were all D–A type COFs formed by thiophene as a photoactive unit. However, most COFs are crystalline agglomerated powders, which hinder the exposure of surface catalytic active sites and have poor hydrophilicity. As shown in Fig. 9a, Li *et al.* used a simple electrochemical strategy to exfoliate COFs in water, resulting in exfoliated COFs with more accessible active sites and promoting the dissociation of photoexcited electrons.[146] The specific surface area of Exfo-TTB-PT increased from 762 m^2 g^{-1} to 1056 m^2 g^{-1} after exfoliation, and the hydrogen production also reached a maximum of 27.24 mmol h^{-1} g^{-1}.

Furthermore, the introduction of the thiophene structure can significantly improve the conductivity of COF materials and enhance catalytic activity by optimizing the electronic structure. For example, a thiophene-rich fully conjugated 3D COF (BUCT–COF–11) with excellent metal-free ORR activity and semiconductor properties was reported by Wang *et al.* (Fig. 9b).[147] The introduction of the thiophene ring significantly promoted charge transfer and improved electrocatalytic efficiency. The peak power density of the fuel cell composed of BUCT–COF–11 as the cathode was as high as 493 mW cm^{-2}. This was the first study which reported that the cathode catalyst of fuel cells was an intrinsic COF material, which broadened the application scope of COFs.

As is well known, the catalytic activity of COFs mainly depends on the molecular structure design. Usually, when the building unit is composed of different elements, different bonding directions and angles, it can lead to completely different molecular configurations, stacking methods, and unsaturated states, even for isomers. At present, it is difficult to further explore the relationship between molecular structure and catalytic activity by controlling a single factor. Based on the above problems, as shown in Fig. 9c, Long and his team employed a thiophene positional isomerization strategy to modulate the molecular geometry, and directionally designed and developed 2-thiophene-containing COF-α and 3-thiophene-containing COF-β heterogeneous COF electrocatalysts (COF-α and COF-β).[148] The pentacyclic carbon near the sulfur atom

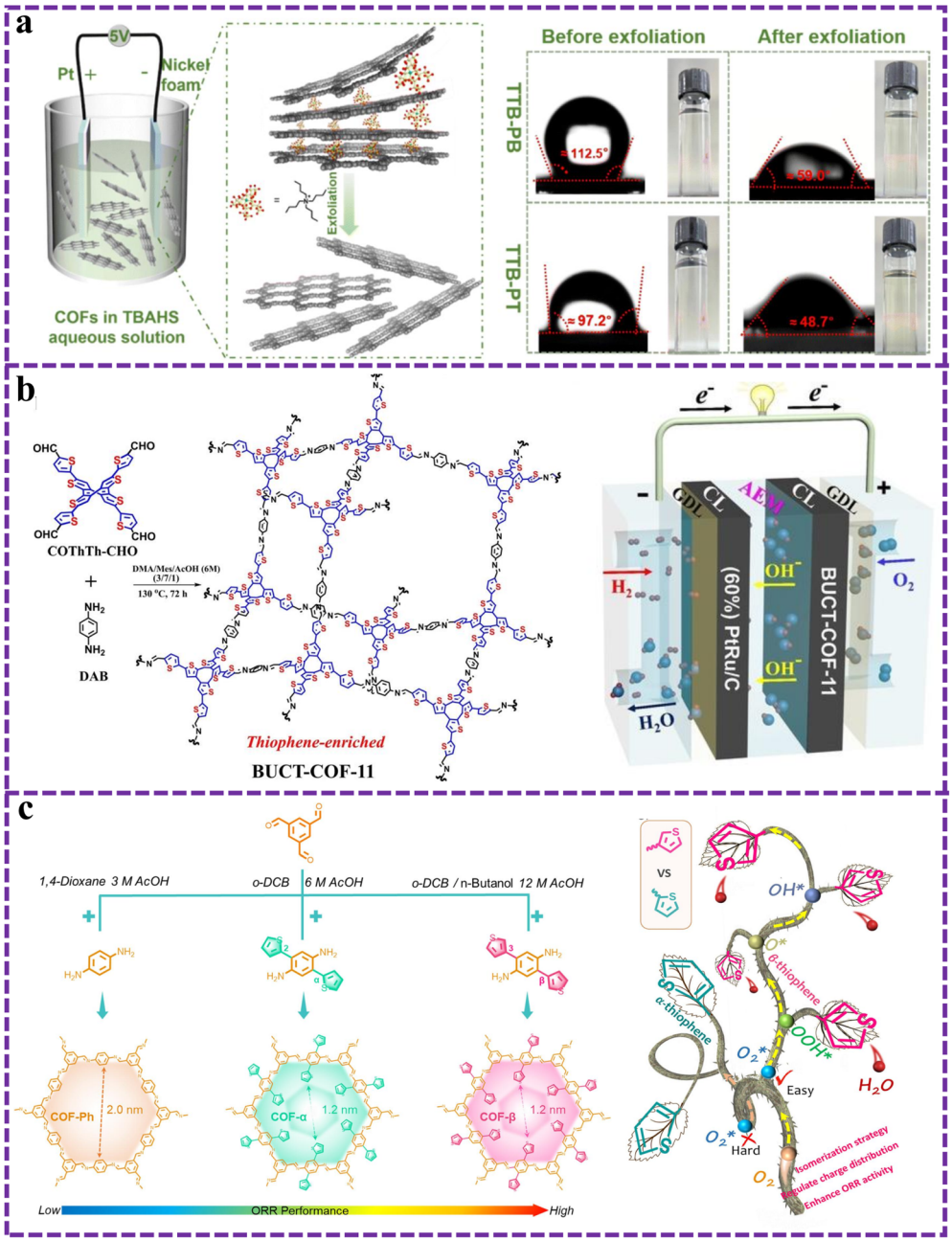

Fig. 9 (a) Schematic diagram of the COF electrochemical stripping device, and water contact angle before and after peeling of two types of COFs. Reproduced from ref. 146 with permission from Royal Society of Chemistry, copyright 2024. (b) The synthetic route of thiophene-enriched BUCT–COF–11, and schematic diagram of devices. Reproduced from ref. 147 with permission from John Wiley and Sons, copyright 2024. (c) The model compound of COF-Ph and the isomeric COFs (COF-α and COF-β) dangling with thiophene units, and schematic illustration of the oxygen reduction process on isomeric COF catalysts. Reproduced from ref. 148 with permission from John Wiley and Sons, copyright 2024.

(thiophene α-position) could be accurately identified as the active site for the catalytic reaction of COFs by a combination of *in situ* Raman spectroscopy and DFT calculations. The ORR reaction mechanism diagram of the COF is shown in Fig. 9c (on the right). Due to the localized charge effect and having more exposed active sites, COF-β exhibited higher ORR performance than COF-α, which had non-localized charge around the dangling thiophene unit.

3.2.9 Benzothiophene unit. Benzothiophene is a derivative of thiophene, which can serve as a long linker for thiophene units and has stronger electron donating ability. Zhao and his colleagues synthesized COFs containing benzothiophene groups (BTTh-Tz COF) and thiophene based TThB-Tz COF.[149] Due to the excellent π-conjugation and flatness of BTTh-Tz COF, its photocatalytic activity was far superior to that of TThB-Tz COF. In addition, the stability of benzothiophene

makes it an interesting candidate for constructing stable D–A-type COFs. Due to the strong interlayer interaction between benzothiophene and Tz units, JUC-607 and JUC-608 COFs had high tolerance to harsh chemical environments.[150] Even when exposed to four acidic or alkaline chemical environments, the original chemical structure can still be maintained after one week.

In general, there exist two methods for the synthesis of D–A type COFs with benzothiophene groups. One is by post-modified bromine functionalization of vinyl-conjugated COFs, followed by further conversion to the thiophene-linked conjugated system 2D COF-S by thiolation cyclization.[151] The high π-conjugation extended the light absorption edge of COF-S from 480 nm to 800 nm, while the intrinsic D–A structure promotes the separation of photogenerated electrons–holes. The second approach is to utilize benzothiophene-containing aldehyde or amine monomers that can synthesize imine-linked benzothiophene-based COFs under mild conditions. For example, Baek and his research group designed and synthesized four benzothiophene-based COFs with aldehyde groups and investigated the effect of conjugation degree on photocatalytic performance.[152] Due to the different degrees of conjugation in the four COFs, the bandgap of their π–π* leaps becomes narrower with the extension of conjugation, and the wavelength of absorption becomes longer. Moreover, the electron affinity increases with the increase of the number of aromatic rings, and the stabilization of the structure increases when the COFs get extra electrons. Similarly, JLNU-310,311,[153] BTT-TAPT-COF,[154] and DADP-COF[155] were all benzothiophene-based COFs synthesized by the Schiff base reaction. Compared to 2D COFs, fully conjugated 3D COFs have abundant open channels and isolated bits, which overcome the interlayer charge transfer bottleneck of 2D COFs and provide more charge transfer pathways. Recently, Wang and his partners synthesized a series of fully conjugated three-dimensional COFs (BUCT–COF–20, 21, 22 and 23) by combining benzothiophene units with saddle shapes and biphenyls with different substituents.[156] The non-conjugated 3D COFs containing sp^3 carbon-based tetrahedral linkages had much lower hydrogen production rates than the four conjugated 3D COF, confirming that the extended π-conjugated structure could provide efficient charge transport channels and enhanced photocatalytic performance. The maximum hydrogen evolution rate of the fully conjugated BUCT–COF–20 was 40.36 mmol g^{-1}. Importantly, this represented the first report of intrinsically metal-free 3D COFs unitized for photocatalytic hydrogen evolution, and the achievement greatly expanded the application scope of 3D COFs.

4. Optimization strategy of D–A type COFs

In D–A type COFs, the different electron affinities between D and A promote charge transfer from D to A in the excited state. Ultimately, the electrons are favorably concentrated on the acceptor unit, which can effectively promote exciton dissociation. However, there are several strategies that can further improve the performance of D–A type COFs, such as post-modification, supramolecular assembly, and interface engineering, which have achieved some remarkable results until now.

4.1 Post-modification

4.1.1 Categorization of post-modification. Post-modification of COF refers to the introduction of additional functional groups or chemical reactions into the COF backbone to change its physical, chemical or electronic properties. Generally speaking, the post-modification strategies of COFs can be divided into the following categories.

4.1.1.1 Covalent bond modification. Nucleophilic substitution reaction: takes advantage of the reactive sites existing in the COF structure, such as aryl halides.[157,158] These sites are capable of reacting with nucleophilic reagents. For example, organic molecules with nucleophilic groups like amino groups and hydroxyl groups can react with the halogenated groups on COFs.[159] Through this nucleophilic substitution reaction, novel functional groups or molecular fragments can be introduced into the COF framework.

Click chemistry: it refers to a class of chemical reactions that are distinguished by high efficiency and high selectivity, which is often employed for the post-modification of COFs.[160] Among them, the copper-catalyzed azide–alkyne cycloaddition reaction stands out as one of the most prevalently used click chemical reactions.[161] By introducing azide groups or alkyne groups onto COFs and then reacting with molecules containing corresponding complementary groups, the functionalization of COFs can be achieved rapidly and efficiently. In this way, a diverse range of functional molecules or groups can be introduced onto the surface or within the framework of COFs.

Condensation reaction: taking advantage of groups such as aldehyde groups and amino groups contained in the COF structure, new functional groups or structural units can be introduced through condensation reactions. For instance, aldehyde groups and amino groups can undergo a Schiff base reaction to form imine bonds.[162,163] Through this approach, functional molecules containing amino groups or aldehyde groups can be linked to COFs, thus achieving the modification of COFs. In addition, common post-modification reactions include the Povarov reaction,[164,165] nitrogen-containing Diels–Alder reaction,[166] and oxidative cyclization reaction.[167]

4.1.1.2 Metal coordination modification. Direct coordination: the solution that contains metal ions is blended with the COF material. Certain coordination sites within the COF structure, such as nitrogen-containing heterocyclic groups including pyridine[168,169] and imidazole,[170] as well as oxygen-containing groups like carboxyl groups and hydroxyl groups, can directly coordinate with metal ions.[171] Consequently, the metal ions are bonded to the COFs, forming metal–COF complexes, which endow COFs with new properties, such as catalytic activity.[172]

Ligand exchange: firstly, COFs are made to coordinate with a ligand to form a stable COF–ligand complex. Subsequently, this complex is immersed in a solution that contains the target metal ions. Through the ligand exchange reaction, the target metal ions substitute the original ligand and coordinate with the COFs, thereby achieving the metal coordination

modification of COFs.[173–175] This method can more precisely control the coordination environment and the loading amount of metal ions.

4.1.2 Examples of post-modification. Generally speaking, introducing π-conjugated aromatic fragments into the periodic lattice of COFs can enhance light collection, but due to the low solubility of highly conjugated linkers, it is difficult to synthesize COFs. Therefore, post modification can be a promising method for synthesizing highly conjugated COFs. Lei and his team successfully prepared two highly conjugated and light-

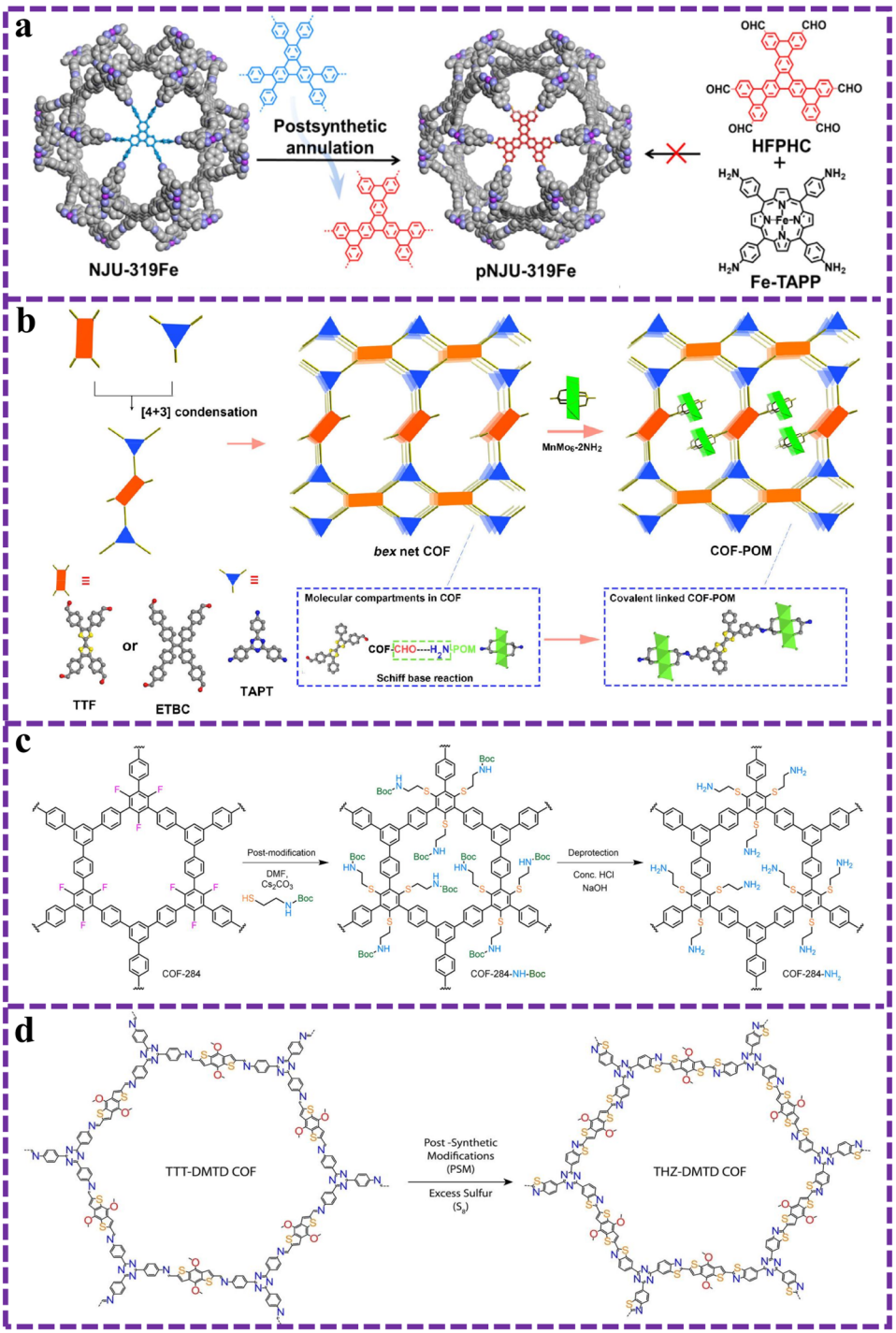

Fig. 10 (a) Post-synthetic annulation of NJU-319Fe. Reproduced from ref. 176 with permission from American Chemical Society, copyright 2023. (b) Schematic diagram of the confinement of uniformly dispersed POM clusters within the pores of COFs through covalent bonds. Reproduced from ref. 183 with permission from American Chemical Society, copyright 2022. (c) Schematics of the synthesis of COF-284-NH_2. Reproduced from ref. 159 with permission from American Chemical Society, copyright 2023. (d) Scheme of the synthesis of the thiazole-linked COF (THZ-DMTD) through post-synthetic modification of TTT-DMTD COF. Reproduced from ref. 185 with permission from John Wiley and Sons, copyright 2023.

absorbing COFs (NJU-318 and NJU-319Fe) through a strategy of synthetic cyclization.[176] The CO yield of pNJU-319Fe after cyclization was 688 μmol g^{-1}, which was 2.5 times higher than that of unmodified NJU-319Fe. It was noteworthy that the direct reaction of cyclized monomers to synthesize highly conjugated COFs was unsuccessful due to the low solubility of the conjugated linker (Fig. 10a). This provides a new idea for the structural design and synthesis of highly conjugated linked COFs.

Some COFs will have poor hydrophilicity and dispersion, which makes it difficult to apply them in liquid-phase reactions. The hydrophilicity of COFs can be well changed by post-modification to solve the above problems. For instance, in order to be able to design a bifunctional material that can fulfill the need of integrating hydrogen supply and proton conduction, Liu *et al.* improved the hydrophilicity and carrier separation of the material itself by converting the cyano-group on the synthesized D–A-type PyBT-COF into a carboxyl group.[177] The water contact angle of PyBT-COF-COOH was much smaller than that of PyBT-COF, which enabled stronger intermolecular interactions with water and easier dispersion in water. As a result, the post-modified PyBT–COF–COOH exhibited a strong photocatalytic hydrogen precipitation rate as well as proton conductivity. Fluorescent COF (TMT-TA) had good crystallinity and stability, but poor dispersibility in water. In view of this, Yan and his team also introduced carboxyl groups into TMT-TA through a post-modification strategy, and the obtained TMT-TA-COOH not only had good dispersibility in water, but also had high sensitivity for the quantitative identification of 5-HIAA.[178] In addition, the application of TMT-TA-COOH in fingerprinting had some potential due to the interaction of residual amino acid bonds and fatty compounds in fingerprints with the carboxyl groups on the surface of TMT-TA-COOH. In the same way, the hydrophilicity of triazinyl COFs could be improved by *in situ* growth of FeOOH clusters on TaTz COFs.[179] The post-modified super-hydrophilic TaTz-FeOOH photocatalysts exhibited effective photo-oxidation of various organic pollutants.

The most common technique for building functional COFs is the post-modification strategy. After modification, some functional groups can be introduced into the COF framework, such as coordinating some metals or connecting organic small molecules with catalytic sites, thereby enhancing the photocatalytic performance of COFs. Initially, Jiang and his partners utilized click reactions to anchor fullerenes covalently in the nanochannels of COFs, transforming them into ordered D–A structured framework materials.[180] Baldwin *et al.* synthesized a series of post-modified COFs by embedding alkyl, alcohol, or aryl groups into the phenol portion of a COF.[181] The grafting of these functional units resulted in COFs that had a good affinity and sensitivity for a number of volatile gases, and also a high selectivity for toluene and isopropanol. Embedding metals atomically into the framework of COFs as catalytic active sites is also a commonly used post-modification strategy. Ye and his team embedded single atom Co into the bipyridine unit of D–A type sp^2 c-COF_{dpy} as a catalytic active site for photocatalytic CO_2 reduction.[182] The structural advantage of this C=C connection allowed carriers to easily reach the Co site through an electronic cascade, resulting in a photocatalytic CO production rate of 17.93 mmol g^{-1} and a selectivity of 81.4% for sp^2 c-COF_{dpy}-Co. Compared with supramolecular interactions such as van der Waals force, hydrogen bonding force, Coulomb force, *etc.*, metal clusters stabilized in pores through covalent bonds are undoubtedly the most stable. TCOF-$MnMo_6$ was a modified COF with a bex topology synthesized by covalently connecting polyoxometalates (POMs) uniformly dispersed in D–A type COFs (Fig. 10b).[183] Specifically, covalent bonds provided efficient electron transfer, and highly dispersed $MnMo_6$ clusters serve as catalytic active sites for CO_2 reduction. The CO yield of TCOF-$MnMo_6$ was 37.25 μmol g^{-1} h^{-1}, which is much higher than that of ECOF-$MnMo_6$. Post-modified functionalized COFs can exhibit better activity in photocatalytic reactions, indicating that the post-modification strategy is an effective and simple functionalization method. Recently, Yaghi *et al.* synthesized two COFs (COF-284 and COF-285) that were stable under extreme conditions through aldehyde alcohol ring trimerization.[159] In Fig. 10c, subsequent post-synthetic modifications of primary amines were carried out to reveal the ability of these two COFs to absorb CO_2 in flue gas and air. Overall, the problem with introducing metal or small molecule strategies is that while they can introduce excellent active sites for COFs, they also reduce their crystallinity, and it is also difficult to ensure that the post-modified groups can be uniformly distributed on the COF backbone.

Converting COFs with poor chemical stability linked to imines into COFs with high chemical stability and conjugation linked to thiazoles is also a common post-modification strategy. At the earliest, Yaghi and his team converted the imine bond into two COFs with thiazole and oxazole bonds by linker substitution and oxidative cyclization, and this derived COF material exhibited higher chemical stability.[184] Byon and his partners compared the stability of COF electrodes in organic lithium batteries with imine connections and those converted to thiazole connections.[167] It was shown that the structural stability of the organic electrodes was enhanced by the π-conjugation and excellent crystallinity of the thiazole moiety, providing extended recyclability and a fast-charging process. The AZO-1 COF electrode connected with thiazole exhibits excellent cycling stability and a power density of approximately 2800 Wk g^{-1}. In contrast, AZO-2 COF connected with imine and AZO-3 COF connected with β-ketoamine were prone to decomposition in azo reactions due to chemical instability and non-coupling, resulting in poor cycling performance. Furthermore, sulfur assisted chemical conversion methods could be used to convert TTT-DMTD COFs containing high-density redox sites into robust thiazole linked D–A type THZ-DMTD COFs (Fig. 10d).[185] Briefly, the reaction of singlet sulfur with the aromatic imine from COF oxidizes the imine to thiamine, followed by further oxidative cyclization of the thiamine to form a thiazole ring. The capacity and stability of Li–S batteries were enhanced while ensuring crystallinity. In addition, this post-sulfurization process can not only maintain crystallinity, but also expand the π-conjugation degree of the COF itself, which is beneficial for light collection. Chen *et al.* similarly utilized singlet sulfur to convert imine-conjugated D–A type 4PE-N COFs

into thiazole-conjugated 4PE-N-S COFs.[186] This strategy extends the conjugated structure of the COFs in both the *x* and *y* directions, which leads to higher electron transport and light absorption. It is worth mentioning that the thiazole-linked 4PE-N-S COFs still have good crystallinity when immersed in common organic solvents or strong acids and bases for 3 days. In contrast, the structures of 4PE-N and 4PE-TT COFs were disrupted when immersed under the same conditions.

4.2 Supramolecular assembly

Supramolecules usually refer to two or more molecules that are bonded together through secondary bonds between molecules to form a multimolecular system at the molecular level. Generally, they are automatically bonded into orderly and organized polymeric systems by non-chemically established weak forces such as hydrogen bonding, coulombic interactions of charges, van der Waals forces, and π–π interactions (formation of stacks of off-domain π-bonds).[187,188] Unlike traditional chemistry which mainly studies covalent bonds, supramolecular chemistry studies weak and reversible non-covalent interactions between molecules, which can be used to significantly accelerate the reaction rate or allow highly selective reactions. As an example, ultra-thin bithiazole-based COF nanosheets (COF-Bta-NSs) with a thickness of about 1.95 nm were prepared in high yield by Zhu *et al.*[189] The COFs were assembled with acetylcholinesterase (AChE) through strong supramolecular interactions, and electrochemical biosensors with excellent performance were constructed, which could be used for the efficient detection of organophosphorus pesticides. The AChE molecules were confirmed to be immobilized on the surface of COF-Bta-NSs through dense hydrogen bonding interactions by various spectroscopic means, which improved the sensitivity and detection durability of the sensor. In addition to this, the heteroatom-hydrogen bonding connection between the COF and the metal coordination played a decisive role in the interfacial transfer in supramolecular systems.[190] Specifically, the photogenerated electrons in the COF were transferred to the metal coordination compounds for CO_2 reduction through the bridge of heteroatoms and hydrogen bonds, and the stronger this hydrogen bonding effect, the higher the photocatalytic CO_2 to CO conversion rate. In supramolecular systems, this heteroatom–hydrogen bond bridging electron transfer pathway confers high photocatalytic performance and provides a way to rationally design efficient supramolecular photosystems.

The π–π supramolecular interactions formed by the stacking of off-domain π-bonds are capable of enhancing the visible light trapping and facilitating charge transfer of D–A type COFs. TT-Por(M)-COFs, for example, had π-stacked column arrays and ordered D–A heterojunction structures that exhibited enhanced intra- and inter-layer charge separation and migration, enabling the efficient photoreduction of CO_2.[139] The vertically oriented D–A separation column of the COF was capable of forming a plate-like interface of periodically ordered heterojunctions, leading to the generation of supramolecular π–π interactions. This will effectively separate the photogenerated carriers and facilitate their migration along the column to the surface, realizing rapid carrier migration and separation. The transient absorption spectra and theoretical computational analyses indicated that the long-term charge retention induced by the intra-layer ordered D–A structure and π-stacked column arrays were the reason for the excellent photoreduction of CO_2.

In general, *z*-direction modulation of 2D COFs relies on spontaneous π–π interactions to form 3D structures, which is difficult to realize. Despite the importance of π–π stacking in the formation, property modulation and stability of COFs, only a few have been proposed to improve the vertical stacking behavior of 2D COF layers. Inspired by the structural modulation mode of graphite intercalation compounds, Lin *et al.* utilized a supramolecular self-assembly system to embed guest molecules between the covalent layers of the COF structure through a bottom-up strategy, thereby generating D–A intercalation COFs capable of modulating the *z*-direction of the lamellar heterostructure (Fig. 11a).[119] Specifically, stabilized intercalated COFs with alternating D–A stacking arrangements were constructed using electron-deficient PDI as the acceptor unit, electron-rich perylene as the donor unit and intercalating agent in the vertical direction, and *p*-phenylenediamine as the polymerizing agent in the lateral direction. This strategy overcame the dispersive interactions between the large π–π surfaces as well as the electrostatic D–A pairs between most of the COFs with insufficient attractive forces. TTF-intercalated COF@C was also an intercalated COF synthesized by supramolecular assembly, which used triazine as the acceptor unit and electron-rich thiofulvalene as the donor unit and intercalating agent. This intercalated COF was able to efficiently convert the light energy into heat energy with a photothermal conversion efficiency of up to 38.1%.[191] Moreover, this intercalated COF could be encapsulated by cancer cell membranes with good biocompatibility and tumor-targeting ability, and can effectively inhibit tumor growth under laser irradiation. Overall, a stable D–A alternate stacking arrangement is a necessary prerequisite for the successful construction of D–A intercalated COFs, and this novel assembly method is expected to be able to provide new nanotechnology applications in the future.

4.3 Interface engineering

The design and construction of interfacial engineering of COF catalysts are the key factors to improve their catalytic performance and stability. Currently, the common optimization of COF interfacial engineering mainly includes doping,[192,193] morphology modulation,[194] coupling photosensitizers[195] and constructing heterojunctions.[196,197] This optimization of interfacial engineering can produce a 1 + 1 > 2 effect with the interaction between D–A type COFs, which can substantially improve the performance and application ability of COFs. Both metal doping and non-metal doping are effective methods to enhance COFs in terms of energy band structure, band gap, properties and other parameters. This facilitates charge carrier separation, optical trapping range expansion, energy band structure optimization and substrate adsorption/desorption. In order to explore new ways with modulating exciton dissociation

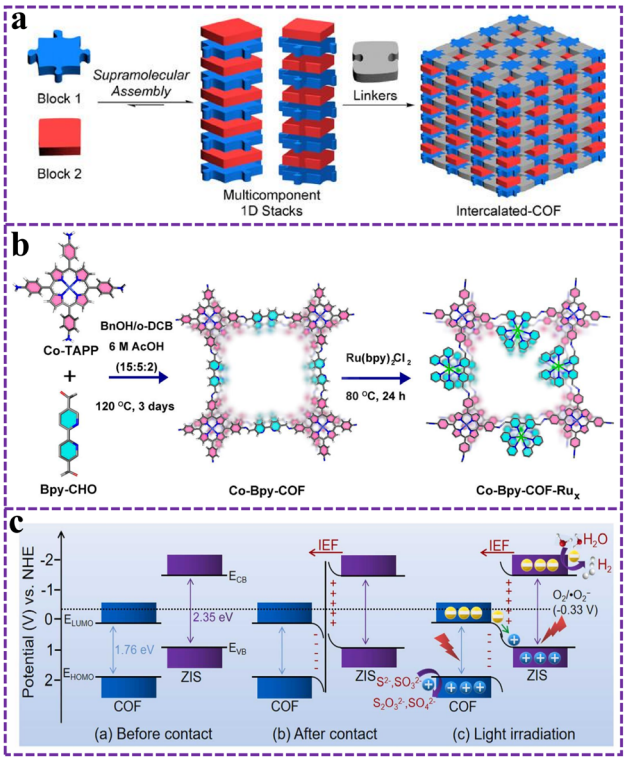

Fig. 11 (a) Schematic illustration of supramolecular multicomponent 1D stacks toward intercalated-COFs. Reproduced from ref. 119 with permission from American Chemical Society, copyright 2020. (b) Schematic illustration of the construction of Co-Bpy-COF and its post-synthetic modification to Co-Bpy–COF–Rux. Reproduced from ref. 201 with permission from American Chemical Society, copyright 2023. (c) Charge-transfer mechanism of the S-scheme COF-ZIS heterostructure before contact, after contact in the dark and light irradiation. Reproduced from ref. 205 with permission from Elsevier, copyright 2024.

in COFs to promote photocatalysis, Li and his team doped the metal Ni into fluorenylketone-based D–A type COFs by doped (Ni–COF-SCAU-1).[198] The addition of Ni significantly modified the exciton effect and promoted the surface hydrogen precipitation reaction under photoexcitation. The results showed that the hydrogen precipitation rate of Ni–COF-SCAU-1 reached 198 mmol g^{-1} h^{-1} at 420 nm under visible light and the AQE was as high as 43.2%, which was much higher than that of COF-SCAU-1. This metal-doping strategy opens up a new pathway for exciton modulation in COFs. Wang and his partners constructed a copper-porphyrin doped D–A type COF (CTF-BTA_{2OH}-Por(Cu)) for multiple efficient sterilization.[199] The Cu-porphyrin doping enhanced the ROS generation and could destroy proteins for sterilization in the absence of light. Non-metallic doping extends the conjugated system, facilitates enhanced light absorption and charge separation and transport rather than recombination. COF-IsoQ-Tp was a controllable N-doped D–A type COF based on bottom-up molecular precursor selection.[200] The N-doped array of ordered photocatalytic sites functioned within the porous β-ketoamine carbon framework in the reticular COF-IsoQ-Tp. Compared with the homostructured COF-Naph-Tp without N doping, COF-IsoQ-Tp provided excellent peak photoelectric activity ($J = -16$ μA cm^{-2}) and its photocatalytic hydrogen evolution rate was also three orders of magnitude higher.

Coupling a photosensitizer on a D–A-type COF enables a long-lived triple excited state photosensitive donor to extend the excited state lifetime of the active site and also generates an internal driving force with a well-defined direction like a built-in electric field to enhance the photovoltaic efficiency. In Fig. 11b, Huang *et al.* used a photosensitizer ($Ru(bpy)_3Cl_2$) with a good excited donor state characterization for photovoltaic CO_2 reduction by integrating it into Co-bpy-COF.[201] The problem that the excited state in the active site is easily dissipated by thermal release, luminescence and electron transfer to nearby substances resulting in short excited state lifetime has been solved. Specifically, the powerful donor photosensitizer $Ru(bpy)_3Cl_2$ with a long-lived triplet excited state could transfer excitation electrons to the Co-bpy-COF, lowering the energy barrier for photo-electrocatalytic CO_2 reduction. Notably, only trace amounts of H_2 and CO production were detected on the Co-bpy-COF in the absence of $Ru(bpy)_3Cl_2$. Strategies for coupling photosensitizers can be constructed not only by coupling to D–A COFs through bonding interactions, but also by loading. Chen and his team constructed magnetic Fe_3O_4@D–A COFs as photoactive materials, which were used as photocurrent–polarity switching factors by loading ZnSe quantum dots onto the COFs.[202] ZnSe quantum dots as photosensitive materials were matched with D–A type COF energy levels to change the polarity of the photocurrent, which were used as mir-138 sensors with high selectivity and sensitivity. However, the system of this strategy is more complicated and it is not possible to determine the real active site or the magnitude of the role played by each player, so in-depth exploratory mechanistic studies are lacking.

It is well known that improving the separation rate of electron holes in D–A type COFs is an important factor to enhance their photocatalytic performance.[203] And the formation of a heterojunction can enable the transfer of photogenerated carriers from the COF to the surface of another semiconductor, thus realizing the effective separation of photogenerated electrons and holes. In addition, heterojunctions may not only inherit the properties of individual components, but may also exhibit new properties, which may synergistically contribute to the enhancement of photoactivity. The more common types of heterojunctions studied are mainly type-II heterojunctions, Z-scheme heterojunctions, and S-scheme heterojunctions. For type-II heterojunction, Ding *et al.* recently obtained heterojunction COF materials with excellent photocatalytic nitrogen fixation performance by compositing a D–A type COF with g-C_3N_4 with N vacancies. The optimized COF composite showed an NH_2 production efficiency of 646 μmol h^{-1} g^{-1} at 420 nm without adding a sacrificial agent.

But the type II heterojunction still has fundamental problems at present, such as the efficiency of the photogenerated electron hole separation is at the cost of reducing the reduction and oxidation ability of the two semiconductor photocatalysts. In addition, the presence of photogenerated electrons and holes in the original photocatalysts inhibits the interfacial transfer of

electron holes in the other catalysts due to electrostatic interactions. Comparatively, the formation of Z-scheme as well as S-scheme heterojunctions can well avoid the above problems. However, due to some defects and irrationality in the mechanism of the Z-scheme heterojunction when it was initially set up, the charge transfer mechanism of the Z-scheme heterojunction has been gradually replaced by that of the S-scheme heterojunction.[204] Wang and his partners formed core–shell structural complexes with S-scheme heterojunctions by growing $ZnIn_2S_4$ nanosheets *in situ* on a porphyrin-based COF with a D–A structure.[205] Specifically, the COF and $ZnIn_2S_4$ form a built-in electric field due to the difference in Fermi energy levels when they are in contact. Under the effect of the built-in electric field and energy band bending, the electrons and holes with strong reducing and oxidizing ability were retained (Fig. 11c). The PHE efficiency of the COF-ZIS composite was 2711 μmol h^{-1} g^{-1} with an AQY of up to 2.45% at 400 nm when Pt was the co-catalyst. However, the biggest disadvantage of heterojunctions is that most of the heterojunctions formed by the compositing of two materials are independent and not in contact with each other, and the number of heterojunctions formed is very small. Therefore, precise control and improvement of the number of heterojunctions formed is the way to greatly improve the photocatalytic efficiency. In addition, lattice mismatches, defects at phase interfaces, and electronic energy band shifts may occur at heterojunctions during long-term cycling tests.

5. Application of D–A type COFs

The previous sections emphasized the advantages of D–A type COFs, including high crystallinity, porosity, and stability. In addition, the selection of D and A molecular units, the choice of connecting bonds, the regulation of crystallinity and conjugation, and the functionalization of active centers give D–A type COFs different properties. This can meet the needs of many applications such as photocatalysis, photothermal therapy and energy storage (Table 1).

5.1 Photocatalysis

5.1.1 Photocatalytic H_2 evolution. As is generally recognized, everything grows due to the light of the sun, and

Table 1 Photocatalytic application of D–A type COFs

Application	Photocatalyst	Linkage	Lightsource	Condition[a]	Performance	Ref.
H_2 evolution	PyPz-COF	Imine	≥420 nm	H_2O/AA	7542 μmol g^{-1} h^{-1}	118
	Py-DNII-COF	Imine	≥420 nm	H_2O/NMP/AA	625 μmol g^{-1} h^{-1}	206
	COF-F	Imine	AM 1.5	H_2O/AA	10 580 μmol g^{-1} h^{-1}	207
	Py-FTP-BT-COF	Imine	>420 nm	H_2O/AA	177.50 μmol h^{-1}	100
	sp^2c-Py-BT COF	Vinylene	>420 nm	H_2O	17.2 μmol g^{-1} h^{-1}	210
	BTT-BpyDAN-COF	Vinylene	>420 nm	H_2O/TEOA	10 100 μmol g^{-1} h^{-1}	64
	COF-JLU45	Vinylene	>420 nm	H_2O/AA	272 500 μmol g^{-1} h^{-1}	209
	COF-alkene	Vinylene	>420 nm	H_2O/TEOA	2330 μmol g^{-1} h^{-1}	211
	DCNA-1	Imine	>420 nm	H_2O/TEOA	27 900 μmol g^{-1} h^{-1}	212
	HIAM-0015	Imine	>420 nm	H_2O/AA	17 990 μmol g^{-1} h^{-1}	213
	COF-JLU35	Vinylene	>420 nm	H_2O/AA	70 800 μmol g^{-1} h^{-1}	214
	HBT-COF	Imine	≥420 nm	H_2O/AA	19.00 μmol h^{-1}	91
	TtaTfa-COF	Imine	>420 nm	H_2O/TEOA	20 700 μmol g^{-1} h^{-1}	215
	BTT-BPy-COF	Vinylene	>420 nm	H_2O/AA	15 800 μmol g^{-1} h^{-1}	216
	MAC-FA1/S-COF	Imine	>420 nm	H_2O/AA	100 000 μmol g^{-1} h^{-1}	218
H_2O_2 production	TAPD-$(Me)_2$ COF	Imine	420–700 nm	H_2O/ethanol/O_2	234.52 μmol g^{-1} h^{-1}	223
	TP-$DPBD_{30}$-COF	Hydrazone	>300 nm	H_2O/air	9200 μmol g^{-1} h^{-1}	224
	TT-DTDA-COF	Imine	>420 nm	H_2O/O_2	1302 μmol g^{-1} h^{-1}	225
	TAPT-TFPA COFs@Pd IC	Imine	AM 1.5	H_2O/ethanol/O_2	2143 μmol g^{-1} h^{-1}	226
	COF-JLU90	Imine	AM 1.5	H_2O/O_2	9800 μmol g^{-1} h^{-1}	221
	COF-N32	Imine	>420 nm	H_2O/O_2	605 μmol g^{-1} h^{-1}	227
	PB-COF	Imide	AM 1.5	H_2O/O_2	2044 μmol g^{-1} h^{-1}	228
	JUC-675	Imine	>420 nm	CH_3CN/benzylamine	22 800 μmol g^{-1} h^{-1}	229
	COF-TPT-Azo	Azobenzene	>420 nm	H_2O/O_2	1498 μmol g^{-1} h^{-1}	230
	COF-1	Imine	>420 nm	Seawater	6930 μmol g^{-1} h^{-1}	231
	EBA-COF	Vinylene	>420 nm	H_2O/ethanol/O_2	1830 μmol g^{-1} h^{-1}	74
	TTF-BT-COF	Imine	AM 1.5	H_2O/O_2	276 000 μmol g^{-1} h^{-1}	232
	TDB-COF	Imine	AM 1.5	H_2O/O_2	723.5 μmol g^{-1} h^{-1}	233
	ECUT-COF-50	Imine	≥400 nm	H_2O/air	4742 μmol g^{-1} h^{-1}	234
Organic conversion	Bpy-sp^2c-BTT-COF	Vinylene	LED	—	Thioether oxidation (93%)	235
	En-COF-P	Ketoenamine	LED	—	Thioether oxidation (99%)	160
	TpAQ-COF	Imine	LED	—	Oxidation of amines (92%)	236
	COF-NUST-36	Imine	LED	—	Oxidation of amines (98%)	237
	TP-PB-COF	Imine	LED	—	Indole derivative C-3 thiocyanation (97%)	238
	COF-JLU24	Imine	LED	—	Indole derivative C-3 thiocyanation (98%)	122

[a] AA: ascorbic acid; TEOA: triethanolamine.

converting sustainable and green solar energy into hydrogen energy is an environmentally friendly solution to environmental problems and energy shortages. Therefore, this photochemical energy conversion process requires photocatalysts with appropriate bond structures and effective charge separation. The D–A type COFs with tunable energy band structure, strong absorption light range, large specific surface area and π-conjugated system can fulfill these requirements. Yan and his partners reported a novel D–A COF (PyPz-COF) with pyrazine as the electron acceptor.[118] The hydrogen production performance of this novel PyPz-COF under Pt as a co-catalyst was up to 7542 μmol g^{-1} h^{-1}, which was much higher than that of PyTp-COF without the pyrazine ring (1714 μmol g^{-1} h^{-1}). The Py-DNII-COF with a dual-receptor structure had an excellent photocatalytic ability under the electron push–pull effect and was able to exhibit a hydrogen precipitation of 625 μmol h^{-1} g^{-1} within 48 hours.[206] The structure of the material affects its performance, and the introduction of electron-withdrawing substituents on the acceptor unit of D–A type COFs can significantly improve photocatalysis. The COF–H, COF–Cl, and COF–F were the COFs with different dihedral angles and photocatalytic activities constructed by introducing chlorine and fluorine atoms on BT.[207] The strong electronegativity of the halogen atoms enhances the π–π interactions as well as charge separation, which prolonged the lifetime of the carriers in the COF interlayer. As a result, COF–F with the strongest electron-withdrawal exhibited the relatively highest photocatalytic hydrogen precipitation rate (10.58 mmol g^{-1} h^{-1}), which was about twice that of COF–H and COF–Cl. Similarly, the chlorinated Py-ClTP-BT-COF and fluorinated Py-FTP-BT-COF prepared by Chen *et al.* reached the same conclusion, both Py-FTP-BT-COF with the introduction of strongly electronegative F atoms in the acceptor unit exhibited the highest HER precipitation rate.[100]

In addition to the effect of substituents, recent studies have shown that covalent bonding between different photoactive units is a key factor in determining the photocatalytic activity of

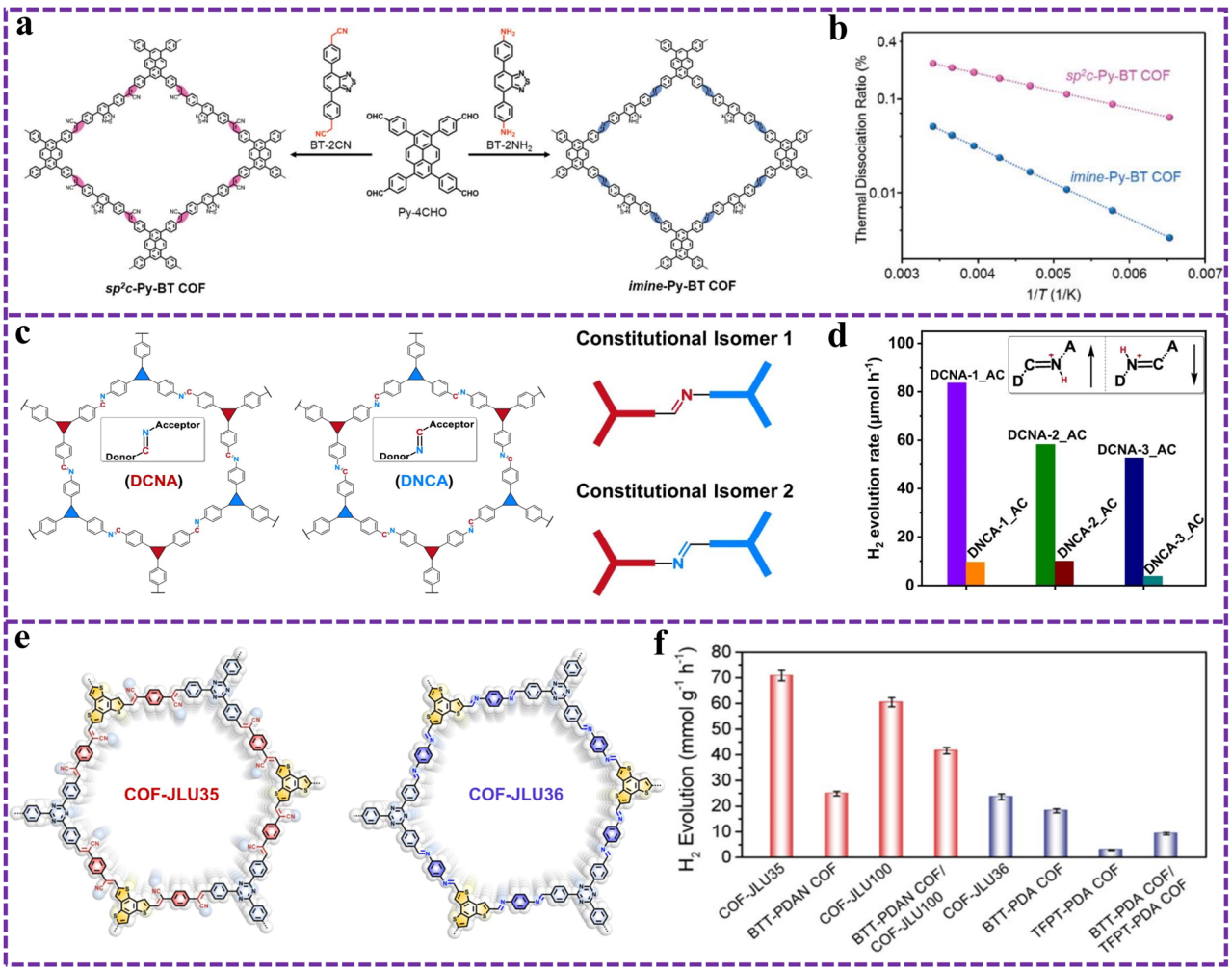

Fig. 12 (a) Synthetic routes and chemical structures and (b) exciton dissociation rates of sp^2c-Py-BT COF and imine-Py-BT COF. Reproduced from ref. 179 with permission from John Wiley and Sons, copyright 2024. (c) The chemical backbones of the isomeric COFs DCNA and DNCA, and (d) comparison of the photocatalytic HER rates of all DCNA_AC and DNCA_AC COFs studied in this project. Reproduced from ref. 212 with permission from Springer Nature, copyright 2022. (e) Syntheses of COF-JLU35 and COF-JLU36 through Knoevenagel and Schiff-base condensation reactions, respectively, and (f) comparison of mass normalized HER performance between COF-JLU35, COF-JLU36 and other COF materials. Reproduced from ref. 214 with permission from American Chemical Society, copyright 2023.

COFs.[208] In contrast, sp^2-linked fully conjugated COFs can enhance charge-carrier mobility and promote charge transfer, which is highly desirable for photocatalytic applications.[209] The imine-Py-BT COFs linked by imine bonds and the cyanoethylene-linked sp^2c-Py-BT COFs then had obvious differences in the photocatalytic activity of water splitting (Fig. 12a).[210] The sp^2c-Py-BT COF with the D–A energy band structure could directly decompose H_2O into H_2 and O_2 under visible light irradiation, whereas the imine-Py-BT COF was not able to catalyze the total water cleavage reaction because of the insufficient OER capacity. Experiments and DFT calculations had showed that cyanoethylene bonding could reduce the exciton binding energy of the COF (Fig. 12b), which was more conducive to promoting charge separation and the dissociation of photo-generated electrons. Similarly, the cyanoethylene-linked COFs constructed from benzotrithiophene as the donor unit exhibited a good photocatalytic hydrogen evolution rate (10.1 mmol g^{-1} h^{-1}) and AQY (4.83%).[64] This was mainly attributed to the fact that the bipyridine unit favored the formation of an intermolecular electron transfer pathway with benzotrithiophene, thus promoting charge separation and transfer efficiency. Yu and his team constructed three COFs with different connecting bonds but the same structure, and similarly found that the photocatalytic hydrogen precipitation performance of the COFs connected by cyanoethylene bonds was much better than that of the imine- and imide-connected COFs, and reached an AQE of 6.7% at 420 nm.[211]

In addition to the aforementioned building block connections and bond types that can influence photophysical properties, the structural isomers of the bonds are equally important for photocatalytic performance studies. Previous work on imine-linked COFs had typically been random in the choice of which was the amino-functionalized monomer as well as whether it was the aldehyde-functionalized monomer, or the monomer that was cheaper or easier to prepare had been chosen. However, this decision may significantly affect the properties of the final material as it predetermines the orientation of the C=N bond to the different linkers. In response to the stoichiometry proposed above, as shown in Fig. 12c, Thomas and his team designed and synthesized imine-bonded D–A-type COFs with differently oriented isomers, (D–C=N–A (DCNA) and D–N=C–A (DNCA)), respectively, in order to study and compare the effects that their structures had on the photovoltaic properties.[212] Although the change in C=N bond orientation did not alter the topology of the COFs, the DCNA-1 COFs were more ordered than DNCA-1, had more than twice the specific surface area of DNCA-1, and had a higher charge transfer efficiency. As a result, all DCNA COFs exhibited stronger photocatalytic hydrogen precipitation performance than the corresponding DNCA COFs (Fig. 12d). Similarly, a series of D–A-type COFs with different imine bond orientations based on BT units also exhibit markedly different photocatalytic hydrogen precipitation abilities.[213] HIAM-0015 with a stronger electron-deficient capacity showed the highest hydrogen precipitation rate, which was about 15 times higher than that of its isomer HIAM-0015v. This strategy provides new ideas for the design and synthesis of COFs, and it is believed that this concept of bond isomerization can be extended to synthesize a wider range of connecting bonds for COFs in addition to imine bonds. Liu and his team constructed two photoactive three component D–π–A materials by introducing electron-deficient triazine and electron-rich benzothiophene groups into the framework (Fig. 12e).[214] This fully π-conjugated bond effectively broadened the visible light capture range of COFs and improved charge transfer and separation efficiency. Among them, COF-JLU35 had a hydrogen evolution rate of 70.8 $\pm$ 1.9 mmol g^{-1} h^{-1} under visible light, which is superior to that of the previously reported COF materials (Fig. 12f).

Subtle structural modifications can significantly modulate the band structure and interfacial properties. For instance, the photocatalytic hydrogen precipitation performance could be improved by changing the hydrophilicity of D–A type COFs. Jiang and his partners reported and compared the photoelectric properties of HBT-COF containing hydroxyl groups and BT-COF without hydroxyl groups.[91] It was found that introducing hydroxyl groups into BT based COFs and polymers improved the hydrophilicity and energy level structure of COF, and enhanced the effective photo-induced charge transfer and segregation. The HER performance of HBT-COF was 5 times higher than that of BT-COF. Furthermore, protonation of the imine bond was also able to improve the hydrophilicity of the D–A-type COF, which enhanced the photocatalytic hydrogen precipitation performance of TtaTfa-COF (20.7 mmol g^{-1} h^{-1}).[215] This post-protonation modification can be applied not only in imine-linked COFs, but also in fully conjugated ethylene-linked COFs. Recently, Wang and his team prepared a protonated sp^2 bonded BTT-BPy-PCOF using bipyridine as a postmodified protonation site.[216] This protonation modification improved the charge separation efficiency and increased the hydrophilicity in the COF pore. The HER rate of the protonated BTT-BPy-PCOF was as high as 15.8 mmol g^{-1} h^{-1}, which was about 6 times higher than that of the unmodified BTT-BPh-COF. Importantly, this post-modified protonation is universal.

In addition to the modulation of D–A COFs described above, compositing with other materials is also an effective way to prepare highly active D–A type COF photocatalysts. Bimetallic Pt-based nanoclusters were loaded onto D–A COFs for photocatalytic hydrogen production.[217] The interaction between COFs and metal nanoclusters promoted the adsorption and activation of H_2O molecules and accelerated the release of hydrogen. Under visible light, $PtCo_2$@COF exhibited the highest photocatalytic activity with a turnover frequency of 486 min^{-1}. Similarly, metal–organic rings with a photosensitizing effect (MAC-FA1) and coral-like S-COF were constructed with direct Z-scheme photocatalysts for the hydrogen evolution reaction through supramolecular interactions.[218] The optimized 4% MAC-FA1/S–COF exhibited a hydrogen evolution rate of 100 mmol g^{-1} h^{-1}, which was much higher than that of S-COF alone, and was one of the best COF-based photocatalytic hydrogen evolution catalysts at that time.

5.1.2 Photocatalytic production of H_2O_2. H_2O_2 is a mild and clean oxidizing agent that also has perfect solubility in water and can be safely transported and stored. In addition, it

has been reported that H_2O_2 can be used as an ideal energy carrier for fuel cells.[219] It is well known that, currently, over 90% of commercial H_2O_2 is produced through a multi-step anthraquinone (AQ) process including the hydrogenation of AQ moiety using expensive palladium (Pd) based catalysts and the subsequent oxidation reaction with O_2, which suffers from intensive energy input and toxic byproduct emission.[220] The green scheme of utilizing clean and renewable solar energy to generate H_2O_2 has a great potential to replace the conventional anthraquinone-based H_2O_2.[221] And the redox centers of D–A-type COFs are spatially separated, which can facilitate the migration and separation of photogenerated carriers for the efficient generation of H_2O_2. The four COFs based on benzotrithiophene were all capable of reducing oxygen in pure water to produce H_2O_2 under visible light due to the carrier generation and transfer facilitated by the D–A interaction.[222] Among them, COF-BTT-TAPT, which used triazine as the A-unit, gave the highest H_2O_2 yield. The 2D COF based on (diarylamino) benzene formed a kgm lattice with high crystallinity and large specific surface area (1165 $m^2\ g^{-1}$) as well as strong visible light absorption, and could serve as an excellent photocatalyst for the production of H_2O_2, as reported by Thoms *et al.*[223] Similarly, Jiang and his partners reported that COFs with dense oxygen reduction and water oxidation catalytic sites only achieved an H_2O_2 yield of 7.2 mmol g^{-1} h^{-1} under light, air, and water conditions, with an optimal apparent quantum yield of 18.0%.[224] As shown in Fig. 13a, this COF could continuously generate over 15 liters of H_2O_2 solution using a flow cell under environmental conditions. Moreover, Dong *et al.* constructed a COF photocatalytic material with asymmetric two-acceptor sites, named TT-DTDA-COF.[225] Two donor units were able to act as multiple efficient adsorption reduction sites for O_2, and the D–A interaction enhanced the separation and migration rate of carriers and thus enhanced the photocatalytic O_2 reduction to H_2O_2 reaction. The H_2O_2 yield can be improved by enhancing the interaction of metal clusters with COF carriers. However, in previously reported photocatalytic systems, the weak binding of metal clusters leads to low catalytic activity and stability. The strongly electronegative fluorine atoms can strongly confine Pd clusters, increase the interaction with the COF, and optimize

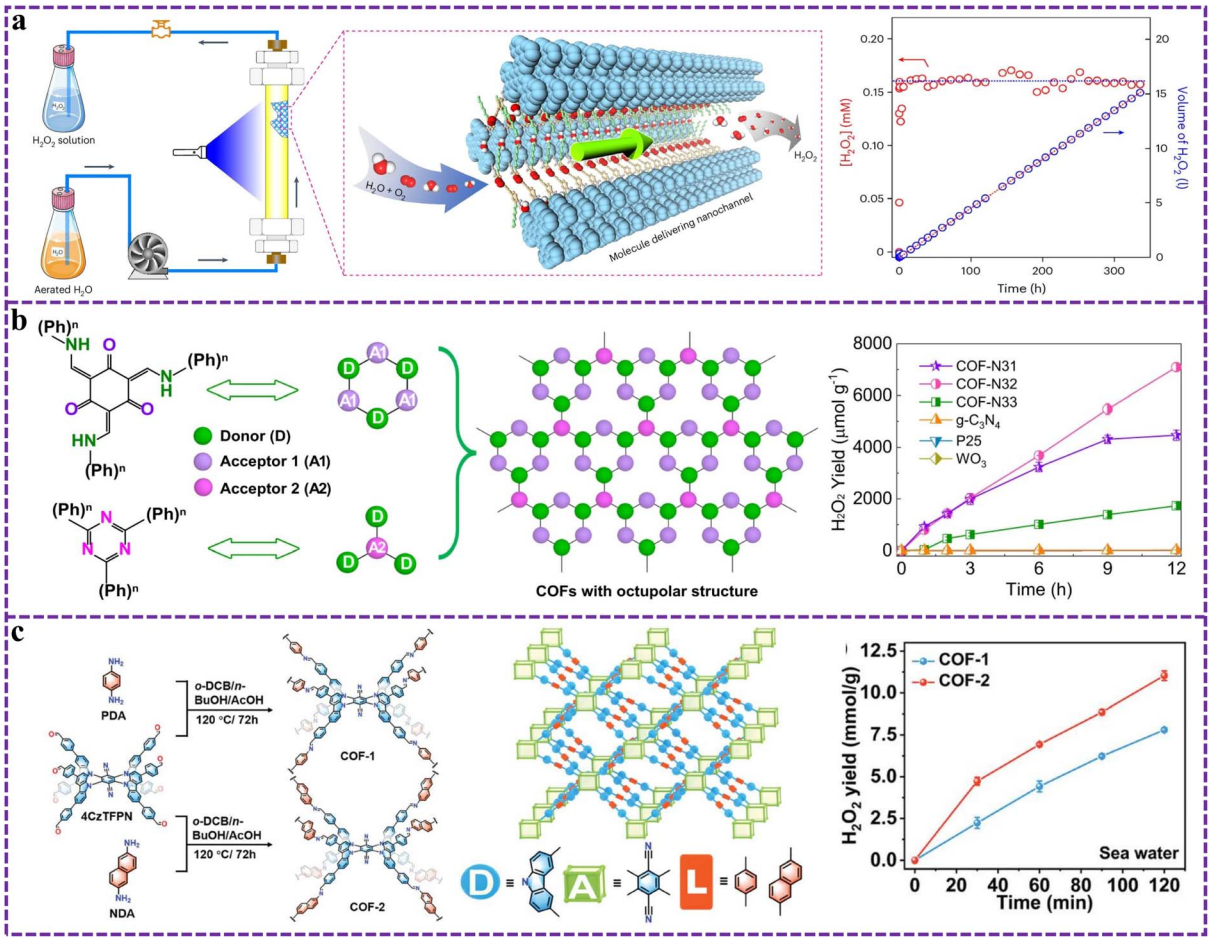

Fig. 13 (a) Schematic of manufacturing H_2O_2 solution *via* continuous photocatalysis in a flow reactor and flow reactor performance for continuous manufacture of pure H_2O_2 solution. Reproduced from ref. 224 with permission from Springer Nature, copyright 2024. (b) Schematic illustration of the octupolar structure and photosynthesis of H_2O_2 using COF-N31, COF-N32 and COF-N33. Reproduced from ref. 227 with permission from Springer Nature, copyright 2023. (c) Illustration of the synthesis and topology representation of 3D COFs, and photocatalytic H_2O_2 production performance of COF-1 and COF-2 in seawater. Reproduced from ref. 231 with permission from John Wiley and Sons, copyright 2024.

the d-band center of Pd clusters. Therefore, TPT-TFPA COFs@Pd exhibited excellent H_2O_2 yield (2143 μmol h^{-1} g^{-1}) and high catalytic stability above 100 hours.[226]

The magnitude of intramolecular polarity in COF has a significant effect on exciton formation and dissociation. Tong and his team found that the effect of the magnitude of intramolecular polarity on the photocatalytic performance also follows the volcano model by varying the number of phenyl groups on the triazine unit.[227] Fig. 13b shows that the polarity of D–A type COFs had a significant impact on the photocatalytic production of H_2O_2. When the polarity is weak, it will limit exciton dissociation, while when the polarity is too strong, it will lead to a weak π-conjugation effect, suppress exciton formation, and thus reduce the photostability of the COF. Therefore, the use of an appropriate amount of phenyl could increase the intramolecular polarity of the COFs themselves and thus regulated the degree of exciton dissociation to efficiently generate H_2O_2. The carbonyl group in polyimide COFs has the property of absorbing and storing electrons, which is an ideal active site for photoreduction of O_2 to H_2O_2.[228] Therefore, the H_2O_2 yield of PB-COF with an electron-rich carbonyl active center was 4.22 times higher than that of PT-COF with a relatively electron-deficient carbonyl active center. The generation of value-added organic chemicals along with the generation of H_2O_2 is an advantage of photocatalysis, and importantly, the substrate of the value-added chemicals also acts as a sacrificial agent to inhibit the electron–hole complexation rate. In view of this, Fang *et al.* synthesized three COFs based on the D–A structure of the BT unit for simultaneous benzylamine oxidation and H_2O_2 generation.[229] As expected, the addition of the sacrificial agent benzylamine allowed the COF to have more e^- to generate $O_2^{\bullet-}$, which captured protons to form $^{\bullet}OOH$ intermediates and subsequently captured protons and electrons for conversion to H_2O_2. In the structure of a COF, even one atom difference can have a great impact on its photoelectric properties as well as the generation of H_2O_2. COF-TPT-Azo was formed through the insertion exchange of COF-TPT-TPA using a linker, and only one N atom was different between the two.[230] The N=N bond in this novel azobenzene-conjugated COF-TPT-Azo was the active site for photocatalysis, exhibiting a narrower band gap and charge transfer ability, and its photocatalytic H_2O_2 yield under alkaline conditions was 7.9 times higher than that of the C=N-conjugated COF-TPT-TPA. Moreover, two 3D COFs (COF-1 and COF-2) reported by Wang *et al.* could reduce the energy loss for filling the triplet excited state and lower the jump energy barrier from the ground state to the singlet excited state, resulting in high selectivity and efficiency of the two COFs in the photocatalytic production of H_2O_2 from natural seawater (Fig. 13c).[231]

As shown in Fig. 14, total H_2O_2 photosynthesis can be achieved by both the oxygen reduction reaction (ORR) and water oxidation reaction (WOR). Mi and his partners reported that the ORR and WOR could occur simultaneously in EBA-COF and BTEA-COF, with H_2O_2 yields up to 1830 μmol g^{-1} h^{-1}.[74] In contrast to the two-electron ORR pathway, the WOR consists of three competing pathways, including a one-electron transfer pathway for $^{\bullet}OH$ generation, a two-electron transfer pathway for H_2O_2 generation, and a four-electron transfer pathway for

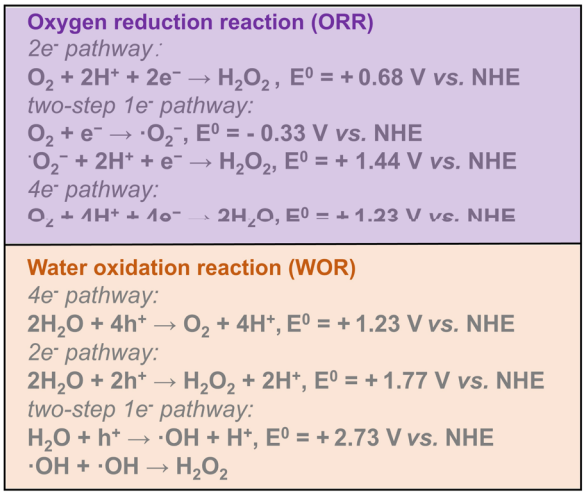

Fig. 14 Mechanism diagram of photocatalytic production of H_2O_2.

photo-induced oxygen precipitation.[239] Therefore, it is crucial to enhance the $2e^-$ WOR pathway rather than the $4e^-$ WOR to achieve simultaneous H_2O_2 production from the WOR/ORR reaction. Lan and his team reported COFs with integrated redox centers, named TTF-BT-COF.[240] Tetrathiafulvalene units were used as oxidation sites for the $2e^-$ WOR and BT units as reduction sites for the ORR, this structure could generate a large amount of H_2O_2 under light irradiation. As a result, TTF-BT-COF could achieve H_2O_2 yields up to 276 000 μmol $h^{-1}g^{-1}$ without sacrificial agents and could produce high concentrations of H_2O_2 (~18.7 wt%) in prolonged batch experiments, which had a great potential for practical applications. The modification of the thioether group can narrow the band gap of TDB-COF and promote the photogenerated mobility.[233] Most importantly, it can effectively modulate the energy band structure for the $2e^-$ WOR and accelerate the $2e^-$ ORR process to generate H_2O_2. Luo and his team synthesized two three-component COFs with D–A–π–D and D–A–π–A structures for the ORR and WOR to efficiently generate H_2O_2 from air and water.[234] It was found that ECUT–COF–50 with the D–A–π–D structure had a higher O_2 adsorption capacity and H_2O_2 generation rate compared to ECUT–COF–51 with the D–A–π–A structure. The C=C in both COFs could serve as the active site for both the ORR and WOR. Currently, significant progress has been made in the study of H_2O_2 production from COF-based photocatalysts.[241] However, this research is still at an early stage with low solar conversion efficiency. Therefore, finding more available monomers to construct COFs with efficient solar energy conversion is an important direction for future development of catalytic generation of H_2O_2.

5.1.3 Photocatalytic organic conversion. Photocatalytic organic conversion is an environmentally friendly and sustainable pathway that utilizes light energy to stimulate chemical reactions, greatly reducing the number of steps involved in traditional synthetic chemistry. Currently, since D–A structured COFs can promote carrier separation and significantly improve catalytic efficiency and selectivity, many D–A

type COF materials have been used as photocatalysts in organic synthesis, such as oxidation, organic coupling and hydrogenation reactions. Thioether oxidation is one of the common photocatalytic organic transformations.[242] Bpy-sp^{2}c-BTT-COF and Bpy-IM-BTT-COF were sp^2 fully conjugated and imine-linked COFs, respectively, both of which had obvious D–A configurations.[235] The sp^2 C=C bond connection had stronger photoreduction and electron transfer abilities than the imine bond connection to COF, and could generate more $O_2^{\bullet-}$ and $^1O_2$ for selective thioether oxidation reaction under green light driving. Lang and his partners designed and synthesized two isomers with different thiazole bond orientations, COFs-Tz-1 and COF-TZ-2.[243] COF-TZ-2 exhibited a higher photocatalytic activity for selective oxidation of sulfides due to its higher dipole moment giving it a better in-plane electron transfer and charge separation ability. En–COF–P was a new type of COFs linked by β-ketoamine, formed by polymerization of amino alkyne clicks, which was a novel approach to synthesize COFs.[160] As shown in Fig. 15a, En–COF–P exhibited a strong visible light absorption range and was able to drive thioether oxidation reactions with up to 99% conversion and 99% selectivity while Im–COF–B polymerized by Schiff base has only a 12% conversion rate. This work expands the types of chemical bonds in COFs.

The formation of benzimidazole derivatives by photosynthetic cyclization is also a common organic transformation reaction. In Fig. 15b, NQ-COFA1 could be formed through a multi-component one pot reaction and two-step post modification, which converts imine bonds in COFs to quinoline linked bonds through cyclization.[244] This one-pot strategy was simpler and had a higher specific surface area as well as crystallinity than the two-step synthetic post-modification approach. NQ-COF$_{A1}$ was an efficient $O_2^{\bullet-}$ mediated photocatalyst for the synthesis reaction of cyclized imidazole derivatives. Subsequently, Xiang *et al.* synthesized ionic NQ-COF$_{D4}$-Me and achieved a yield of 91–98% in photocatalytic benzimidazole synthesis.[245] Similarly, TPT-COF with excellent carrier separation and migration rate exhibited better catalytic performance for the photocatalytic reaction of benzimidazole than TTT-COF, with a yield of 96% and high stability.[246] The next organic conversion reaction is benzylamine coupling reaction. The main reactive oxygen species of the anthraquinone compound TpAQ-COF was $O_2^{\bullet-}$, which could selectively oxidize amines under O_2 and green light, and had good recyclability.[236] Zhang and his partners doped COFs with S and Se atoms and found that doping Se atoms in semimetals could reduce the bandgap and exciton binding energy.[237] Therefore, COF-NUST-36 doped with Se atoms had a high yield of 98% and a selectivity of 97.5% for amine oxidation. Dong and his team designed and synthesized COFs based on the binding energies of COFs with different amine-based monomer linkers by DFT calculations.[247] It was found that the bipyridine-N site of the D–A structured BTT-BPy-COF exhibited enhanced oxygen adsorption and activation, as well as electron transfer ability, which facilitated photocatalytic benzylamine coupling with conversion and selectivity up to 99%.

D–A COFs have been used as photocatalysts for an increasing number of organic small molecule transduction reactions in recent years.[248] By modulating the D–A interactions within the

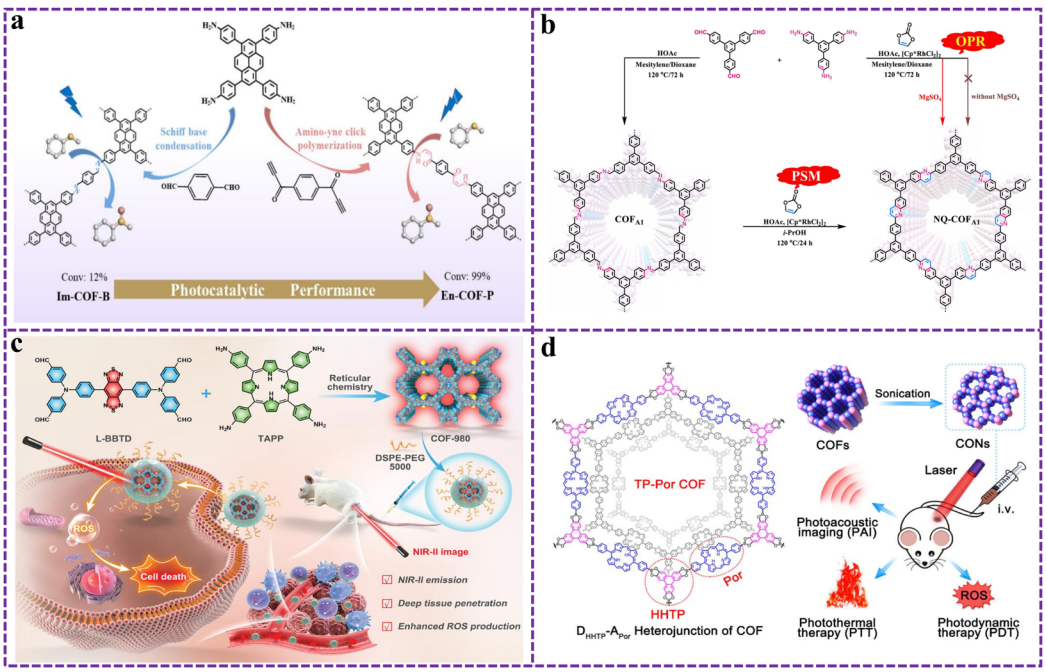

Fig. 15 (a) Schematic diagram of the synthesis and photocatalytic performance of En–COF–P. Reproduced from ref. 160 with permission from American Chemical Society, copyright 2024. (b) Schematic diagram of two methods for constructing NQ-COFA1. Reproduced from ref. 244 with permission from Royal Society of Chemistry, copyright 2023. (c) The design and preparation of COF-980, and its NIR-II fluorescence imaging-guided *in vivo* phototherapy. Reproduced from ref. 256 with permission from John Wiley and Sons, copyright 2024. (d) Schematic illustration of 2D COF fabrication, *in vivo* tumor therapy. Reproduced from ref. 258 with permission from American Chemical Society, copyright 2019.

COFs, the optimized TP-PB COFs had narrower band gaps as well as stronger photocurrent responses, and could be used as highly efficient photocatalysts for indole derivative C-3 thiocyanation.[238] In addition, COF-JLU24 was used for photocatalytic C-3 functionalization of indole, and its catalytic activity was superior to that of the metal free photocatalyst *g*-C_3N_4.[122] The MeO-TBT-COF containing methoxy on the surface showed the highest photocatalytic activity and recoverability in the C-3 thiocyanation reaction conversion of indole derivatives.[249] Moreover, under visible light, BF COFs with the D–A structure could promote the C–S bond formation reaction between β-ketoesters and NH_4SCN, efficiently generating multi-substituted olefins with a yield of up to 98%.[250] The D–A type COF (COF-JLU33) constructed from triazine units and benzothiophene units was used to carry out the photosynthesis of α-trifluoromethyl ketones in heterogeneous photocatalytic systems.[251] Similarly, D–A type PTBC-Por-COF based on porphyrin could effectively generate $O_2^{\cdot-}$ in heterogeneous photocatalytic systems, and served as an efficient photocatalyst for sulfide oxidation and 2-bromoacetophenone reduction dehalogenation.[252] In addition, 3D TAPB-ETTBC COFs with oxidation and reduction active centers could be used as photocatalysts for various organic reactions.[253]

5.2 Photothermal therapy

D–A type COF materials can not only be applied in the fields of photocatalysis and electrocatalysis, but also have important significance in the field of biomedicine. Photothermal therapy (PDT) is a novel non-invasive tumor treatment method that uses photosensitizers to convert light energy into heat energy under light irradiation, killing tumor cells while reducing drug resistance and side effects.[254,255] In addition, the D–A structure can induce photo-generated charge transfer between donor and acceptor units, thereby suppressing fluorescence and enhancing photothermal efficiency. Zhang and his team constructed a D–A type COF (COF-980) capable of second near-infrared (NIR-II) phototherapy and fluorescence bioimaging (Fig. 15c).[256] The COF-980 had good photostability, chemical stability, and excellent reactive oxygen species (ROS) generation efficiency, and was capable of triggering a large amount of intracellular ROS under laser light to kill cancer cells. Furthermore, COF-980 delivers clear *in vivo* images at longer emission wavelengths and could guide efficient photodynamic therapy for 4T1 tumors with minimal side effects. At present, the preparation of monodisperse nanoscale COFs is difficult, and such nanoscale D–A type COFs can facilitate the diffusion of reactive oxygen species. Xie and his team were able to control the size of the COFs (around 400 nm) with uniform spherical morphology and colloidal stability by adjusting the amount of acetic acid catalyst.[257] This nanoscale DPPN COF had the highest photothermal conversion ability under 808 nm laser irradiation, which had significant anti-cancer effects. The synergistic application of photodynamic therapy (PTT) and photothermal therapy (PDT) can achieve better therapeutic results. As shown in Fig. 15d, porphyrin-based COFs (Por-COFs) with a D–A structure could act as photosensitizers enabling the combined action of PTT and PDT to significantly eliminate tumors at 635 nm laser light.[258] Furthermore, another D–A type porphyrin-based HPCOF showed good photo-imaging ability and photothermal conversion efficiency.[259] This HPCOF can be used as both a photothermal agent and a photosensitizer, enabling the combined treatment of tumors with PDT and PTT.

In addition to that, D–A type COFs can be a good carrier for transporting targeted drugs. The D–A structure in COF-PDA-FA can provide multiple channels and pathways for carrier transport, which gives it excellent photothermal properties.[260] And the large specific surface area and porosity in COF-PDA-FA make it a good carrier for targeting and delivering glucose oxidase to tumor cells. Finally, this COF-PDA-FA with high IR absorption could induce endogenous mitochondria and apoptosis in combination with the generated ROS, which ultimately led to the removal of cancer cells with insufficient energy supply. Sun *et al. in situ* loaded heteropolymer blue into a COF by a one-pot method, and the resulting HPB@COF had good pH-responsive release characteristics, biocompatibility, and high tumor inhibition efficiency.[261] Under irradiation with an 808 nm near-infrared laser, HPB@COF could make the tumor temperature rise at high temperature to kill the tumor. In fact, although there are many studies of COFs for photothermal tumor therapy, there is still a long way to go before real clinical cancer treatment. This is because the photothermal conversion efficiency and photodynamic therapy efficiency of COFs have not reached the expected results. In addition, the dispersive stability of COF materials in a short time and at a low concentration in water as well as the lack of selectivity to tumor cells still limits the rapid development of practical applications.

5.3 Energy storage

5.3.1 Supercapacitor. Supercapacitors are a new type of energy storage device that falls between traditional capacitors and batteries. They utilize the double-layer structure formed by charge separation at the electrode–electrolyte interface and reversible redox reactions (pseudo-capacitance) to store energy.[262] Supercapacitors have been widely studied for their advantages such as green environmental protection, high safety, high power density, wide operating temperature range, and long lifespan.[263,264] In the composition of supercapacitors, the properties of electrode materials determine their application performance. D–A type COFs can form highly ordered electronic channels through strong π-conjugation between D–A units, significantly improving the conductivity of the material and promoting rapid charge transfer and storage. In summary, D–A type COF materials have become important candidates for the next generation of high-performance supercapacitor electrode materials due to their excellent electrochemical properties and structural designability. As shown in Fig. 16a, Zhuang and his team synthesized a series of poly (aryl ether)-based COFs with a typical crystal layered structure of the D–A type.[265] Among them, PAE-NiNiPcF$_8$ had ultra-low resistance (1.31×10^{-6} S cm^{-1}), and when assembled into a micro-supercapacitor, it exhibited excellent volumetric capacitance (28.1 F cm^{-3}) and excellent stability after 10 000 charge discharge cycles in acidic

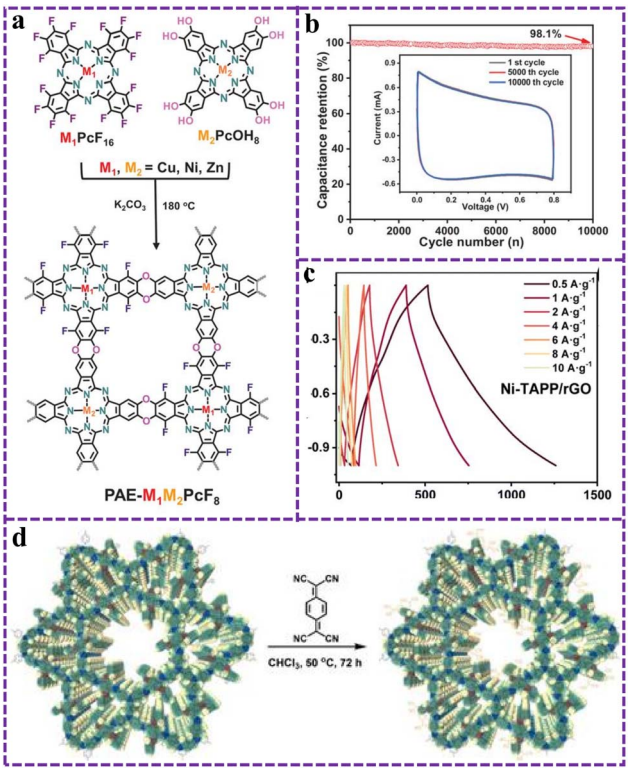

Fig. 16 (a) Synthesis of PAE-$M_1M_2PcF_8$ (M_1, M_2 = Ni, Cu, Zn) with dioxin linkages. Reproduced from ref. 265 with permission from John Wiley and Sons, copyright 2022. (b) The cycling stability of PAE-NiNiPcF_8 for MSC at 50 mV s^{-1} (inset: CV curves at 1st, 5000th, and 10000th cycle). Reproduced from ref. 109 with permission from John Wiley and Sons, copyright 2022. (c) The GCD curves of Ni-TAPP/rGO at different current densities from 0.5 to 10 A g^{-1}. Reproduced from ref. 267 with permission from Royal Society of Chemistry, copyright 2024. (d) Covalent TCNQ immobilization in COF through a [2 + 2] cycloaddition reaction accompanied by a ring opening of the strained intermediate. Reproduced from ref. 269 with permission from American Chemical Society, copyright 2024.

electrolytes (Fig. 16b). Similarly, DPP-TBB-COF composed of DPP and 1,3,5-triphenylbenzene could promote charge transfer under the action of D–A, with a superior specific capacitance of 384 F g^{-1} at a current density of 0.3 A g^{-1} and good durability.[109]

Variations in surface charge density and pore size induced by different electron acceptor units are important for charge storage. Van Der Voort *et al.* investigated the charge storage mechanism of D–A type COFs consisting of TTFs in ionic liquid electrolyte-based supercapacitors.[266] The changes in charge density affect the buildup of ionic liquids in the vicinity of the pores, and the electronic polarity of the pores could influence the confinement process of the ionic liquids in the pores. TTF-Por COF had a wider EDLC window in ionic liquid electrolytes, and the energy density of the EDLC device was 58 Wh kg^{-1}, which was almost 6 times higher than that of organic electrolytes. In addition, TTF–COF–based devices retained about 75–88% capacitance after 100 hours of use in ionic liquid electrolytes. Coupling organic compounds with multiple electron channels and redox reversibility to graphene sheets is expected to overcome the bottleneck of low energy density in organic-based supercapacitors. Ni-TAP/rGO and Ni-TAPP/rGO were D–A type COFs composed of thiofulvalene units and graphene connected by covalent bonding.[267] The formation of a heterojunction at the interface promotes the efficient utilization of COFs and charge transfer, and electrons could be rapidly transferred from the highly conductive graphene oxide to the vertically grown COFs. In Fig. 16c, the capacitance of the Ni-TAPP/rGO electrode at 0.5 A g^{-1} current was 367.5 F g^{-1}. The energy density and power density of the Ni-TAPP/rGO electrode were as high as 51.0 Wh kg^{-1} and 1.78 kW kg^{-1}, respectively. For using D–A type COFs as supercapacitor electrodes, it is important to introduce different donor and acceptor units or further achieve functionalization, for example, enhancing hydrophilicity to improve electrolyte wettability, or introducing active functional groups to enhance pseudocapacitive behavior.

5.3.2 Perovskite solar cells. In addition to the supercapacitors described above, D–A type COFs have also been widely studied in the field of energy storage, including perovskite solar cells (PSCs), lithium-ion batteries, lithium sulfur batteries, and zinc ion batteries (ZIBs). Because the structural effect of D–A can improve charge separation efficiency and transfer, it is beneficial for enhancing battery performance. BPTA-TAPD-COF@TCNQ with a D–A structure synthesized by a post-modification method was used as a multifunctional additive in the cavity transport layer.[268] Thanks to the accelerated carrier extraction and improved conductivity, the addition of BPTA-TAPD-COF@TCNQ (Fig. 16d) in the device achieved a power conversion efficiency (PCE) of up to 24.68%. Similarly, TA-PT COFs with double redox sites and the ability to achieve intramolecular separation provided a reliable 376 mV voltage response in solar responsive cells, with an additional round-trip efficiency of 35%.[269]

Hindering the decomposition of perovskite materials and improving the stability of the materials are of great importance for improving PCE. Doping of $COF_{TPDA\text{-}TZDA}$ in the $FAPbI_3$ layer was able to improve the charge transport within the perovskite membrane and increase the grain size of the perovskite membrane.[88] Importantly, it was able to suppress the perovskite defects through the N-atom coordination effect, thus enhancing the stability of PSCs. After storage for 480 h at approximately 60% relative humidity, the PCE of $COF_{TPDA\text{-}TZDA}$ treated PSCs was as high as 23.51% and had high cycling stability (Fig. 17a). Similarly, doping DA-COFs into the $FAPbI_3$ layer of PSCs could produce the same effect, and the highest power conversion efficiency of the constructed PSCs was 23.19%, with good humidity stability.[270] In addition, this strategy of doping D–A type COFs can also be applied to inverted PSCs. For example, Yu *et al.* used two novel COFTPA and COFICZ to modify inverted PSCs, and this strategy reduced carrier complex losses and improved the stability of the perovskite membrane.[271] The corresponding device structure diagram and PCE performance diagram are shown in Fig. 17b. The energy level matching resulted in a p-type doped interface which effectively enhanced the charge extraction and transport in PSCs, and the maximum PCE of inverted PSCs treated with COFs was 25.68%.

5.3.3 Battery. The D–A effect in COFs can effectively optimize the electronic structure and provide a better platform for

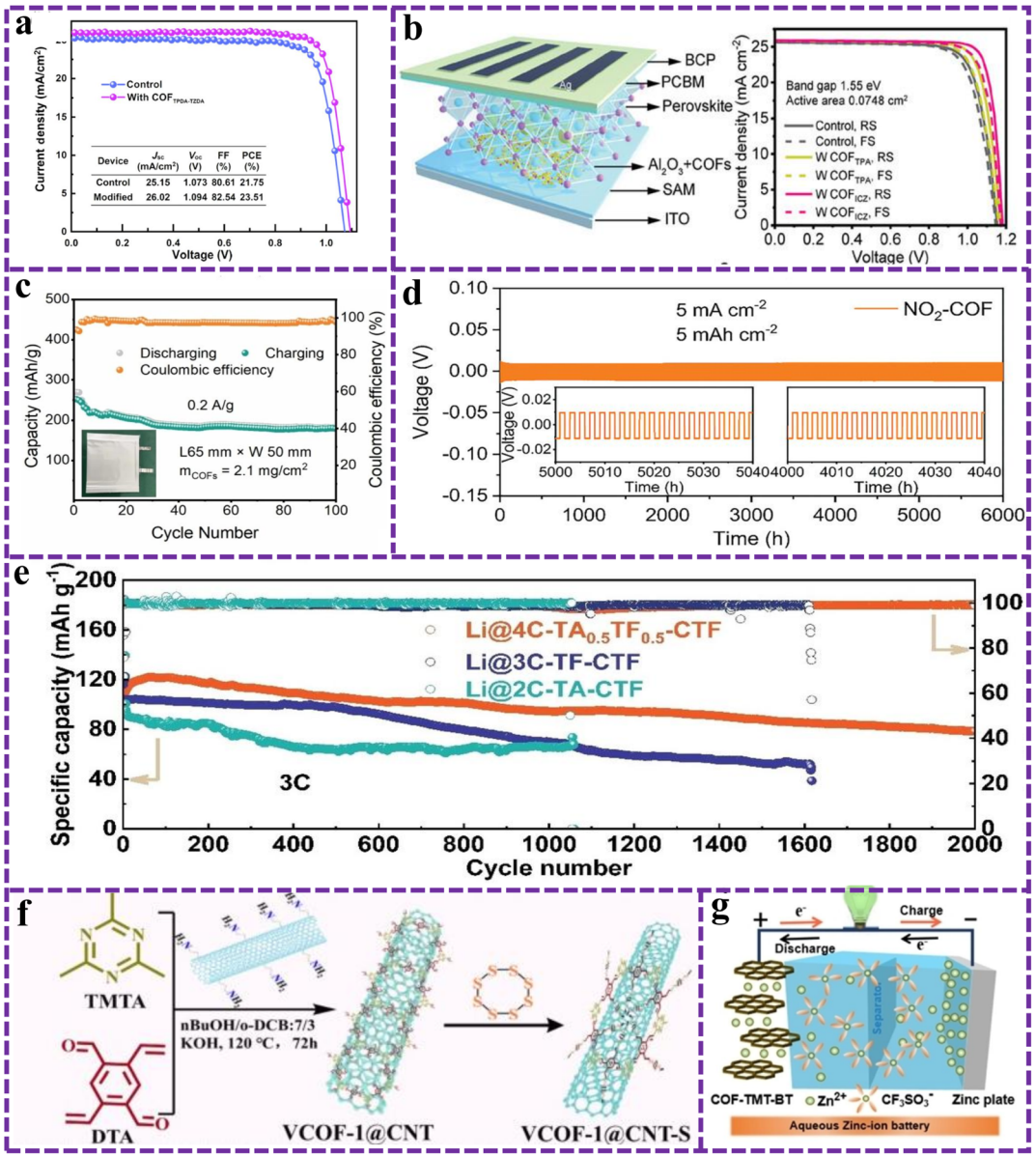

Fig. 17 (a) *J*–*V* characteristics of the PSCs without and with COFTPDA-TZDA under standard illumination conditions. Reproduced from ref. 88 with permission from CCS Chemistry, copyright 2024. (b) Device structure of the inverted PSC and *J*–*V* curves of the COF-modulated inverted PSC devices. Reproduced from ref. 271 with permission from John Wiley and Sons, copyright 2024. (c) Cycling performance of the pouch cell at 0.2 A g^{-1} for 100 cycles. Reproduced from ref. 272 with permission from John Wiley and Sons, copyright 2024. (d) Galvanostatic cycling of Li–Li symmetric cells at a current density of 5 mA cm^{-2}. Reproduced from ref. 274 with permission from John Wiley and Sons, copyright 2023. (e) Long-term cycles of full cells based on Li@2C-TA-CTF, Li@3C-TF-CTF, and Li@4C-$TA_{0.5}TF_{0.5}$-CTF at 3C. Reproduced from ref. 134 with permission from John Wiley and Sons, copyright 2024. (f) Schematic illustration of the synthesis of VCOF-1@CNT and the inverse vulcanization of VCOF-1@CNT with elemental sulfur. Reproduced from ref. 275 with permission from Elsevier, copyright 2024. (g) Schematic of the COF-TMT-BT||$Zn(CF_3SO_3)_2$||Zn energy storage system. Reproduced from ref. 278 with permission from John Wiley and Sons, copyright 2023.

Li^+ migration. For example, D–A COFs with bipolar redox centers (BTT-PTO-COF) had an ideal electron mobility (1.8 cm^2 V^{-1} s^{-1}) for fast ion and electron transport processes.[272] As shown in Fig. 17c, the initial discharge capacity of the pouch battery assembled with BTT-PTO-COF at 0.2 A g^{-1} was 265 mA h g^{-1}, which could exceed 100 cycles. Lithium dendrites can be effectively suppressed by introducing strong electron absorbing units. For example, nitroxide-functionalized NO_2–COF was used as a solid electrolyte interface (SEI) to achieve long-life and dendrite-free Li^+ batteries.[273] The strong electron-absorbing effect of nitroxide gathered the electrons around the material, which enabled Li^+ to be uniformly deposited on the surface of Li with less resistance. The structural effect of D–A facilitates the adjustment of the electronic structure to build a unique Li^+ channel, resulting in an ultra-long cycle life of more than 6000 h for the NO_2–COF/Li modified battery (Fig. 17d). Similarly, introducing strongly electronegative F atoms into COFs can effectively accelerate electron transfer and

enhance Li^+ kinetics. F–COF, as a modified EI, exhibited high ionic conductivity (6.7×10^{-4} S cm^{-1}) and high-capacity retention in Li/$LiFePO_4$ batteries (90.8% after 300 cycles at 5C).[274] The multicomponent 4C-$TA_{0.5}TF_{0.5}$-CTF could also modify the SEI to regulate the interfacial stability of lithium batteries.[134] The dipole moment could be increased by fine-tuning the D–A unit, which promoted the formation of lithophilic sites and achieves uniform lithium deposition behavior. As shown in Fig. 17e, the full battery modified by 4C-$TA_{0.5}TF_{0.5}$-CTF still had a high specific capacity at a current density of 3C for 2000 cycles. In addition, the D–A structured COF can be used as a cathode carrier for Li–S batteries to enhance polysulfide migration and conversion. The homogeneous wrapping of VCOF-1 around carbon nanotubes enhanced the electrical conductivity, while the abundant vinyl content of VCOF-1 promoted the formation of a strong C–S bond with S, which attenuated the shuttling effect and dissolution of polysulfides (Fig. 17f).[275] As a result, the initial discharge specific capacity of VCOF-1@CNT-S reaches 1418 mA h g^{-1}.

The COF materials are renowned for their strong porosity and sustainability, and have enormous potential as cathodes for aqueous ZIBs.[276] Tao and his team designed NT-COF with a D–A structure as a cathode to develop photo-responsive aqueous organozinc batteries.[277] The ordered stacking of D and A fragments establishes a reliable pathway for charge transport and transfer, which results in an effective coupling of intramolecular charge separation and reversible redox chemistry. The NT-COF cathode assembled ZIB battery had a high discharge voltage platform of about 1.4 V, and a discharge capacity of 214 mA h g^{-1}. However, the low stability of COF materials in aqueous solutions limits the long-term cycling of ZIBs. Therefore, COF-TMT-BT formed by aldol condensation had irreversible C=C bonds, making it insoluble in water-based electrolytes and enhancing cycling stability.[278] The BT unit in COF-TMT-BT acted as an electrochemically active group and the assembled ZIBs are shown in Fig. 17g. The specific capacity of the ZIBs was 283.5 mA h g^{-1} with a power density of 23.2 kW kg^{-1} at a current density of 0.1 A g^{-1}, and still had good specific capacity values after 800 cycles.

Overall, in electrochemical energy storage, the precise arrangement of organic units in COF structures can determine their effectiveness, and these structures can be carefully tailored to meet the requirements of specific applications. In addition, structural stability in COFs is important for the long-lasting operation of energy devices. Therefore, it is possible to develop stable structures and suitable charge density distributions by fine-tuning the pore structure and density of D–A type COFs, which will improve ion-selective transport in energy storage and conversion.

6. Conclusion and prospect

This work started with a comprehensive review of the conformational relationships in D–A type (COFs), focusing on those built from common building blocks and bond connections. Understanding these relationships is fundamental as it reveals

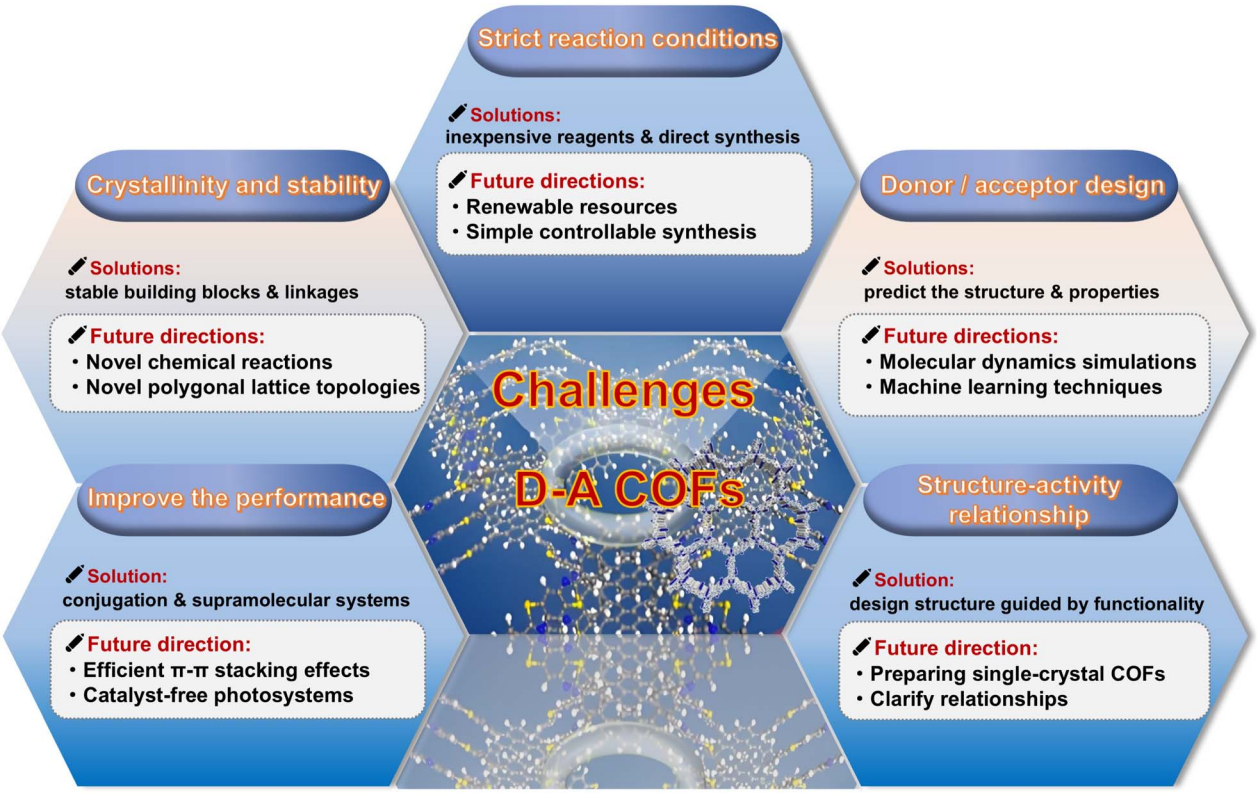

Fig. 18 Current challenges and future prospects of D–A type COFs.

the underlying structural features governing D–A type COFs' properties. Next, it explores strategic approaches for optimizing D–A type COFs. Supramolecular assembly, for instance, arranges molecular components *via* non-covalent interactions to achieve a more favorable structure and enhanced properties. Post-modification synthesis tailors the chemical functionality of pre-synthesized COFs, enabling broader applications. Interfacial engineering, moreover, manipulates COFs' interfaces to enhance their performance. And then this review also summarizes recent progress in photocatalysis, photothermal therapy, and energy storage involving D–A structured COFs. In photocatalysis, they can drive reactions under light due to the favorable charge separation. In photothermal therapy, they convert light to heat for potential cancer treatment, and in energy storage, they may contribute to better devices. In addition, D–A type COFs are a novel material with high research and application value in photovoltaics. Their unique electronic structure allows precise electron control, crucial for charge transfer in photovoltaic devices. Their wide-range light absorption maximizes solar energy use, and high specific surface area offers more reaction sites. Embedding functional groups, choosing bonding modes, and combining donors and acceptors endow them with high structural and optoelectronic tunability. Nevertheless, despite great potential, D–A type COF material research faces challenges like large-scale synthesis, stability under harsh conditions, and performance optimization for specific applications (Fig. 18).

(1) D–A COFs must maintain stability after functionalization in the environment for sustainable and regenerative long-term operation. Therefore, crystallinity and stability of the pore structure must be key to the rational design of D–A COF-based materials for the target application. Employing stable linkers and establishing strong covalent bonds can enhance the durability of COFs, and the environmental conditions (pH, temperature, and presence of solvents) of D–A-type COFs need to be considered and stable building blocks and linkers should be selected accordingly. Furthermore, exploring new irregular polygonal lattice topologies and improving their stability is an important aspect. This is because it enables the growth of the polymer backbone in an anisotropic tiling manner and its structural ordering as compared to the conventional ortho polygonal scheme. In addition, most of the formation of D–A type COFs is specific to the molecular precursor. In other words, only some building blocks with suitable functional groups are able to react with each other to form crystal networks. Therefore, novel chemical reactions involving the use of dynamic covalent bonds should be vigorously explored.

(2) From an economic perspective, the synthesis of D–A COFs generally requires high reaction temperatures, long reaction times, or complex solvent conditions, resulting in poorly controllable synthesis processes as well as high costs. Meanwhile, the use of transition metal catalysts in the cross-coupling reaction introduces trace metals, which affect the objective evaluation of COF catalysts. In addition, some reported D–A-based COFs require high inputs due to multi-step synthesis and harsh reaction conditions. Therefore, the use of inexpensive raw materials and direct synthesis routes can effectively reduce the overall cost of the catalysts. Future research should be devoted to optimizing the synthesis process of D–A type COFs and developing simpler and controllable synthesis methods. For example, the use of microwave radiation and acoustic chemistry can accelerate the reaction rate and improve the yield, but there are fewer related studies. In addition, exploring self-assembly strategies to promote the formation of ordered structures is also an important research direction. In addition, the synthesis of D–A type COFs by utilizing renewable resources (*e.g.*, biomass) or using inexpensive precursors will help to reduce the production cost and promote their realization in large-scale industrial applications.

(3) In D–A type COFs, the selection and arrangement of donor and acceptor units directly affect the electronic structure and their efficiency in photovoltaic and catalytic reactions. However, most of the previous donor and acceptor units are random or empirical and lack a good theoretical basis. In the future, machine learning techniques and molecular dynamics simulations can be used to fine-tune the design of the electronic structure of the D–A interface and predict the electronic structure and physicochemical properties of the material. This will help accelerate the discovery of more exciting and high-performance D–A type COF materials.

(4) The poor electrical conductivity and the lack of active sites for highly selective photocatalytic energy conversion of D–A type COFs have been the limiting factors for the substantial improvement of their performance. Previous researchers have typically used noble metals such as Pt and Pd as co-catalysts to enhance the surface reaction kinetics. However, their limited availability and the heavy metal contamination problem associated with transition metal oxides have hindered their large-scale and widespread application. In the future, efficient π–π stacking effects can be designed, macromolecular conjugation systems can be employed or structures with long-range electron migration can be constructed, which in turn can enhance the electrical conductivity and active sites of D–A type COFs. In addition, it is crucial to vigorously explore low-cost, environmentally friendly, and efficient co-catalysts or develop co-catalyst-free photosystems.

(5) While research in bond chemistry has greatly broadened the structural types of D–A type COFs, a comprehensive understanding of the intrinsic relationship between the selected covalent bonds and the resulting material properties remains a significant challenge. In many cases, covalent bonds act primarily to connect organic units into a well-defined network rather than as a direct source of material functionality. The exact effect of covalent linkages on the overall properties of the resulting materials remains unclear. Due to the complexity of the interactions between organic units as well as between neighboring layers, conducting systematic studies of single-crystal COFs remains a great challenge. Therefore, there is a great need for a generalized method capable of preparing single-crystal COFs to help reveal the mechanism of covalent linkages in these materials.

We are confident that these challenges will be addressed as researchers explore D–A type COFs in depth. In the future, the electronic structure design of D–A type COFs will be optimized

across multiple dimensions, particularly through the precise modulation of donor and acceptor units, fine-tuning the energy band structure, and enhancing electron transfer efficiency. These advancements will significantly enhance their performance in applications such as photovoltaics, catalysis, gas separation, and storage.

Data availability

The type of this manuscript is a review and related data are cited from others. Therefore, there are no raw experimental or computational data associated with this article.

Author contributions

Conceptualization: Haiyang Liu, Yongfeng Zhi, and Xiaoming Liu; writing–original draft: Haiyang Liu, Shanshan Zhu, and Huijuan Yue; writing–review and editing: Yongfeng Zhi and Xiaoming Liu.

Conflicts of interest

There are no conflicts to declare.

Acknowledgements

This work was supported by the project of the National Natural Science Foundation of China (No. 52373210, 52073119), Natural Science Foundation of Jilin Province (No. 20230101029JC), Hainan Provincial Natural Science Foundation of China (224QN181), and State Key Laboratory of Inorganic Synthesis and Preparative Chemistry (No. 2024-7).

Notes and references

1 Z. Zhang, J. Jia, Y. Zhi, S. Ma and X. Liu, *Chem. Soc. Rev.*, 2022, **51**, 2444–2490.
2 S.-Y. Ding and W. Wang, *Chem. Soc. Rev.*, 2013, **42**, 548–568.
3 E. Asayesh-Ardakani, M. Rahmani, A. Hosseinian, S.-B. Ghaffari and M.-H. Sarrafzadeh, *Coord. Chem. Rev.*, 2024, **518**, 216087.
4 X. Kang, E. R. Stephens, B. M. Spector-Watts, Z. Li, Y. Liu, L. Liu and Y. Cui, *Chem. Sci.*, 2022, **13**, 9811–9832.
5 Y. Liu, X. Liu, A. Su, C. Gong, S. Chen, L. Xia, C. Zhang, X. Tao, Y. Li, Y. Li, T. Sun, M. Bu, W. Shao, J. Zhao, X. Li, Y. Peng, P. Guo, Y. Han and Y. Zhu, *Chem. Soc. Rev.*, 2024, **53**, 502–544.
6 Y. Qian and H.-L. Jiang, *Acc. Chem. Res.*, 2024, **57**, 1214–1226.
7 C. Kang, Z. Zhang, A. K. Usadi, D. C. Calabro, L. S. Baugh, K. Chai, Y. Wang and D. Zhao, *J. Am. Chem. Soc.*, 2022, **144**, 20363–20371.
8 Y. Kumar, I. Ahmad, A. Rawat, R. K. Pandey, P. Mohanty and R. Pandey, *ACS Appl. Mater. Interfaces*, 2024, **16**, 11605–11616.
9 Y. Liu, L. Li, Z. Sang, H. Tan, N. Ye, C. Sun, Z. Sun, M. Luo and S. Guo, *Nat. Synth.*, 2024, **4**, 134–141.
10 J. Qiu, K. Meng, Y. Zhang, B. Cheng, J. Zhang, L. Wang and J. Yu, *Adv. Mater.*, 2024, **36**, 2400288.
11 Z. Zhang, Q. Zhang, Y. Hou, J. Li, S. Zhu, H. Xia, H. Yue and X. Liu, *Angew. Chem., Int. Ed.*, 2024, **63**, e202411546.
12 Z. Zhao, W. Chen, G. Zhang and Y. Chen, *J. Mater. Chem. A*, 2023, **11**, 26052–26062.
13 R. Xue, Y.-S. Liu, M.-Y. Wang, H. Guo, W. Yang and G.-Y. Yang, *Mater. Horiz.*, 2023, **10**, 4710–4723.
14 S. Wang, Y. Yang, X. Liang, Y. Ren, H. Ma, Z. Zhu, J. Wang, S. Zeng, S. Song, X. Wang, Y. Han, G. He and Z. Jiang, *Adv. Funct. Mater.*, 2023, **33**, 2300386.
15 K. Xu, Y. Zheng, J. Zhou, Y. Zhao, X. Pang, L. Cheng, H. Wang, X. Zhang, R. Zhang and Z. Jiang, *Adv. Funct. Mater.*, 2024, 2417383.
16 Q. Wang, Y. Guo, Y. Long, Y. Liu, Z. Wang, Y. Liu and X. Zhang, *J. Membr. Sci.*, 2024, **701**, 122766.
17 J. Chang, H. Li, J. Zhao, X. Guan, C. Li, G. Yu, V. Valtchev, Y. Yan, S. Qiu and Q. Fang, *Chem. Sci.*, 2021, **12**, 8452–8457.
18 C. Krishnaraj, A. M. Kaczmarek, H. S. Jena, K. Leus, N. Chaoui, J. Schmidt, R. Van Deun and P. Van Der Voort, *ACS Appl. Mater. Interfaces*, 2019, **11**, 27343–27352.
19 T. Skorjanc, D. Shetty, F. Gándara, L. Ali, J. Raya, G. Das, M. A. Olson and A. Trabolsi, *Chem. Sci.*, 2020, **11**, 845–850.
20 A. Giri, G. Shreeraj, T. K. Dutta and A. Patra, *Angew. Chem., Int. Ed.*, 2023, **62**, e202219083.
21 S. Wang, Y. Fu, F. Wang, X. Wang, Y. Yang, M. Wang, J. Wang, E. Lin, H. Ma, Y. Chen, P. Cheng and Z. Zhang, *J. Am. Chem. Soc.*, 2024, **146**, 33509–33517.
22 S. Wang, Y. Han, V. A. Reddy, M. C.-Y. Ang, G. Sánchez-Velázquez, J. M. Saju, Y. Cao, D. T. Khong, P. K. Jayapal, R. Cheerlavancha, S. I. Loh, G. P. Singh, D. Urano, S. Rajani, B. Marelli and M. S. Strano, *Nat. Commun.*, 2024, **15**, 9300.
23 W. Zhang, Q. Sun, Y. Zhu, J. Sun, Z. Wu and N. Tian, *ACS Sens.*, 2024, **9**, 3262–3271.
24 N. P. Bradshaw, Z. Hirani, L. Kuo, S. Li, N. X. Williams, V. K. Sangwan, L. E. Chaney, A. M. Evans, W. R. Dichtel and M. C. Hersam, *Adv. Mater.*, 2023, **35**, 2303673.
25 G. A. Leith, A. A. Berseneva, A. Mathur, K. C. Park and N. B. Shustova, *Trends. Chem.*, 2020, **2**, 367–382.
26 Y. Liu, X. Jiang, L. Chen, Y. Cui, Q.-Y. Li, X. Zhao, X. Han, Y.-C. Zheng and X.-J. Wang, *J. Mater. Chem. A*, 2023, **11**, 1208–1215.
27 L. Wang and W. Zhu, *Adv. Sci.*, 2023, **11**, 2307227.
28 L. Hao, R. Shen, C. Qin, N. Li, H. Hu, G. Liang and X. Li, *Sci. China Mater.*, 2024, **67**, 504–513.
29 N. Wang, S.-Q. Ye, M. Li, H. Pan and G.-W. Wang, *Sol. RRL*, 2023, **8**, 202300790.
30 P. Li, B. Li, C. Wang, X. Zhao, Y. Zheng, S. Wu, J. Shen, Y. Zhang and X. Liu, *Composites, Part B*, 2023, **252**, 110506.
31 Y. Xia, W. Zhang, S. Yang, L. Wang and G. Yu, *Adv. Mater.*, 2023, **35**, 2301190.
32 J. Zhao, J. Ren, G. Zhang, Z. Zhao, S. Liu, W. Zhang and L. Chen, *Chem. Eur. J.*, 2021, **27**, 10781–10797.
33 M. Lv, X. Ren, R. Cao, Z. Chang, X. Chang, F. Bai and Y. Li, *Polymers*, 2022, **14**, 4893.

34 J. Liu, S. Tang, J. Wang, P. Zhang, Z. Wang, L. Wang, R. Wen and J. Huang, *J. Environ. Chem. Eng.*, 2024, **12**, 114802.
35 X. Wang, H. Li, S. Zhou, J. Ning, H. Wei, X. Li, S. Wang, L. Hao and D. Cao, *Adv. Funct. Mater.*, 2025, 2424035.
36 A. I. B. Adrien, P. Côté, N. W. Ockwig, A. J. M. Michael O'Keeffe and O. M. Yaghi, *Science*, 2005, **310**, 1120411.
37 J. R. Hunt, C. J. Doonan, J. D. LeVangie, A. P. Côté and O. M. Yaghi, *J. Am. Chem. Soc.*, 2008, **130**, 11872–11873.
38 J. R. H. Fernando, J. Uribe-Romo, H. Furukawa, C. Klöck and a. O. M. Y. Michael O'Keeffe, *J. Am. Chem. Soc.*, 2008, **131**, 4570–4571.
39 F. J. Uribe-Romo, C. J. Doonan, H. Furukawa, K. Oisaki and O. M. Yaghi, *J. Am. Chem. Soc.*, 2011, **133**, 11478–11481.
40 S. Dalapati, S. Jin, J. Gao, Y. Xu, A. Nagai and D. Jiang, *J. Am. Chem. Soc.*, 2013, **135**, 17310–17313.
41 X. Zhuang, W. Zhao, F. Zhang, Y. Cao, F. Liu, S. Bi and X. Feng, *Polym. Chem.*, 2016, **7**, 4176–4181.
42 H. Lyu, C. S. Diercks, C. Zhu and O. M. Yaghi, *J. Am. Chem. Soc.*, 2019, **141**, 6848–6852.
43 Y. Su, Y. Wan, H. Xu, K.-i. Otake, X. Tang, L. Huang, S. Kitagawa and C. Gu, *J. Am. Chem. Soc.*, 2020, **142**, 13316–13321.
44 P. Kuhn, M. Antonietti and A. Thomas, *Angew. Chem., Int. Ed.*, 2008, **47**, 3450–3453.
45 X. Li, C. Zhang, S. Cai, X. Lei, V. Altoe, F. Hong, J. J. Urban, J. Ciston, E. M. Chan and Y. Liu, *Nat. Commun.*, 2018, **9**, 2998.
46 J. Guo, Y. Xu, S. Jin, L. Chen, T. Kaji, Y. Honsho, M. A. Addicoat, J. Kim, A. Saeki, H. Ihee, S. Seki, S. Irle, M. Hiramoto, J. Gao and D. Jiang, *Nat. Commun.*, 2013, **4**, 2736.
47 P.-L. Wang, S.-Y. Ding, Z.-C. Zhang, Z.-P. Wang and W. Wang, *J. Am. Chem. Soc.*, 2019, **141**, 18004–18008.
48 D. A. Pyles, J. W. Crowe, L. A. Baldwin and P. L. McGrier, *ACS Macro Lett.*, 2016, **5**, 1055–1058.
49 B. Zhang, M. Wei, H. Mao, X. Pei, S. A. Alshmimri, J. A. Reimer and O. M. Yaghi, *J. Am. Chem. Soc.*, 2018, **140**, 12715–12719.
50 C. Zhao, H. Lyu, Z. Ji, C. Zhu and O. M. Yaghi, *J. Am. Chem. Soc.*, 2020, **142**, 14450–14454.
51 X. Guan, Y. Qian, X. Zhang and H. L. Jiang, *Angew. Chem., Int. Ed.*, 2023, **62**, e202306135.
52 P. J. Waller, S. J. Lyle, T. M. Osborn Popp, C. S. Diercks, J. A. Reimer and O. M. Yaghi, *J. Am. Chem. Soc.*, 2016, **138**, 15519–15522.
53 H. L. Nguyen, C. Gropp, N. Hanikel, A. Möckel, A. Lund and O. M. Yaghi, *ACS Cent. Sci.*, 2022, **8**, 926–932.
54 V. A. Kuehl, P. H. H. Duong, D. Sadrieva, S. A. Amin, Y. She, K. D. Li-Oakey, J. L. Yarger, B. A. Parkinson and J. O. Hoberg, *ACS Appl. Mater. Interfaces*, 2021, **13**, 37494–37499.
55 K. T. Jackson, T. E. Reich and H. M. El-Kaderi, *Chem. Commun.*, 2012, **48**, 8823.
56 O. Yahiaoui, A. N. Fitch, F. Hoffmann, M. Fröba, A. Thomas and J. Roeser, *J. Am. Chem. Soc.*, 2018, **140**, 5330–5333.
57 Z.-B. Zhou, P.-J. Tian, J. Yao, Y. Lu, Q.-Y. Qi and X. Zhao, *Nat. Commun.*, 2022, **13**, 2180.
58 X. Feng, L. Chen, Y. Honsho, O. Saengsawang, L. Liu, L. Wang, A. Saeki, S. Irle, S. Seki, Y. Dong and D. Jiang, *Adv. Mater.*, 2012, **24**, 3026–3031.
59 C. Dai and B. Liu, *Energy Environ. Sci.*, 2020, **13**, 24–52.
60 C. Qian, L. Feng, W. L. Teo, J. Liu, W. Zhou, D. Wang and Y. Zhao, *Nat. Rev. Chem.*, 2022, **6**, 881–898.
61 Z. Song, Y. Xie, X. Song, J. Tang, J. Wang, B. Z. Tang and Z. Li, *J. Mater. Chem. C*, 2024, **12**, 19094–19102.
62 X.-R. Ren, B. Bai, Q. Zhang, Q. Hao, Y. Guo, L.-J. Wan and D. Wang, *J. Am. Chem. Soc.*, 2022, **144**, 2488–2494.
63 A. López-Magano, S. Daliran, A. R. Oveisi, R. Mas-Ballesté, A. Dhakshinamoorthy, J. Alemán, H. Garcia and R. Luque, *Adv. Mater.*, 2023, **35**, 2209475.
64 C.-C. Gu, C.-Q. Ni, R.-J. Wu, L. Deng, J. Zou, H. Li, C.-Y. Tong, F.-H. Xu, B.-C. Weng and R.-L. Zhu, *J. Colloid Interface Sci.*, 2024, **658**, 450–458.
65 J. Wang, S. Qiao, M. Yang and Z. Guo, *Small*, 2024, **21**, 2409292.
66 A. Hayat, H. Ali, Z. Ajmal, A. Alshammari, M. M. Alghamdi, A. A. El-Zahhar, N. Almuqati, M. Sohail, A. M. Abu-Dief, S. Khan, Y. Al-Hadeethi, M. Z. Ansari and Y. Orooji, *Prog. Mater. Sci.*, 2025, **147**, 101352.
67 P. Xiong, S. Zhang, R. Wang, L. Zhang, Q. Ma, X. Ren, Y. Gao, Z. Wang, Z. Guo and C. Zhang, *Energy Environ. Sci.*, 2023, **16**, 3181–3213.
68 R. Luo, H. Lv, Q. Liao, N. Wang, J. Yang, Y. Li, K. Xi, X. Wu, H. Ju and J. Lei, *Nat. Commun.*, 2021, **12**, 6808.
69 X. Li, J. Zhou, W. Yin, B. Xie, Z. Liu and J.-J. Liu, *J. Catal.*, 2024, **437**, 115640.
70 K. Verma, Mohit and K. R. J. Thomas, *Langmuir*, 2024, **40**, 24148–24161.
71 Y. Song, A. Li, P. Li, L. He, D. Xu, F. Wu, F. Zhai, Y. Wu, K. Hu, S. Wang and M. V. Sheridan, *Chem. Mater.*, 2022, **34**, 2771–2778.
72 W. Wang, F. Meng, Y. Bai, Y. Lu, Q. Yang, J. Feng, Q. Su, H. Ren and Q. Wu, *ChemSusChem*, 2024, **17**, e202301916.
73 L. Wang, J. Chakraborty, K. S. Rawat, M. Deng, J. Sun, Y. Wang, V. V. Speybroeck and P. Van Der Voort, *Sep. Purif. Technol.*, 2025, **359**, 130368.
74 L. Zhai, Z. Xie, C.-X. Cui, X. Yang, Q. Xu, X. Ke, M. Liu, L.-B. Qu, X. Chen and L. Mi, *Chem. Mater.*, 2022, **34**, 5232–5240.
75 X. Ma, J. Kang, W. Cao, Y. Wu, C. Pang, S. Li, Z. Yi, Y. Xiong, C. Li, M. Wang, Z. Xu and J. Li, *J. Colloid Interface Sci.*, 2024, **659**, 665–675.
76 C. Yang, Z. Zhang, J. Li, Y. Hou, Q. Zhang, Z. Li, H. Yue and X. Liu, *Green Chem.*, 2024, **26**, 2605–2612.
77 D. N. Ampong, E. Effah, E. A. Tsiwah, A. Kumar, E. Agyekum, E. N. A. Doku, O. Issaka, F. O. Agyemang, K. Mensah-Darkwa and R. K. Gupta, *Coord. Chem. Rev.*, 2024, **519**, 216121.
78 A. Rodríguez-Camargo, K. Endo and B. V. Lotsch, *Angew. Chem., Int. Ed.*, 2024, **63**, e202413096.
79 H. Liu, C. Li, H. Li, Y. Ren, J. Chen, J. Tang and Q. Yang, *ACS Appl. Mater. Interfaces*, 2020, **12**, 20354–20365.
80 D. H. Streater, E. R. Kennehan, D. Wang, C. Fiankor, L. Chen, C. Yang, B. Li, D. Liu, F. Ibrahim, I. Hermans,

K. L. Kohlstedt, L. Luo, J. Zhang and J. Huang, *J. Am. Chem. Soc.*, 2024, **146**, 4489–4499.
81 Y. Qian, Y. Han, X. Zhang, G. Yang, G. Zhang and H.-L. Jiang, *Nat. Commun.*, 2023, **14**, 3083.
82 A. Dey, S. Chakraborty, A. Singh, F. A. Rahimi, S. Biswas, T. Mandal and T. K. Maji, *Angew. Chem., Int. Ed.*, 2024, **63**, e202403093.
83 L. Qin, C. Ma, J. Zhang and T. Zhou, *Adv. Funct. Mater.*, 2024, **34**, 2315157.
84 D.-M. Xue, Y.-J. Zhang, J.-W. Chen, H. Yang, R.-J. Xie, S.-C. Qi, Y.-Q. Bu, F. Liu, H.-H. Zhang and J. Lalevée, *Chem. Eng. J.*, 2024, **502**, 157874.
85 H. Yu, J. Zhang, X. Yan, C. Wu, X. Zhu, B. Li, T. Li, Q. Guo, J. Gao, M. Hu and J. Yang, *J. Mater. Chem. A*, 2022, **10**, 11010–11018.
86 W. Li, X. Huang, T. Zeng, Y. A. Liu, W. Hu, H. Yang, Y. B. Zhang and K. Wen, *Angew. Chem., Int. Ed.*, 2020, **60**, 1869–1874.
87 B. P. Biswal, H. A. Vignolo-González, T. Banerjee, L. Grunenberg, G. Savasci, K. Gottschling, J. Nuss, C. Ochsenfeld and B. V. Lotsch, *J. Am. Chem. Soc.*, 2019, **141**, 11082–11092.
88 L. Yao, S. Liu, L. Li, B. Ge, W. Jiao, S. Zong, X. Song, D. Zhou and Z. Liang, *CCS Chem.*, 2024, **6**, 1721–1730.
89 M. Hao, Y. Xie, X. Liu, Z. Chen, H. Yang, G. I. N. Waterhouse, S. Ma and X. Wang, *JACS Au*, 2023, **3**, 239–251.
90 Y. Hou, F. Liu, B. Zhang and M. Tong, *Environ. Sci. Technol.*, 2022, **56**, 16303–16314.
91 C. Lin, X. Liu, B. Yu, C. Han, L. Gong, C. Wang, Y. Gao, Y. Bian and J. Jiang, *ACS Appl. Mater. Interfaces*, 2021, **13**, 27041–27048.
92 J.-H. Dou, Z.-A. Yu, J. Zhang, Y.-Q. Zheng, Z.-F. Yao, Z. Tu, X. Wang, S. Huang, C. Liu, J. Sun, Y. Yi, X. Cao, Y. Gao, J.-Y. Wang and J. Pei, *J. Am. Chem. Soc.*, 2019, **141**, 6561–6568.
93 M.-Y. Yang, S.-B. Zhang, M. Zhang, Z.-H. Li, Y.-F. Liu, X. Liao, M. Lu, S.-L. Li and Y.-Q. Lan, *J. Am. Chem. Soc.*, 2024, **146**, 3396–3404.
94 F. Liu, Y. He, X. Liu, Z. Wang, H.-L. Liu, X. Zhu, C.-C. Hou, Y. Weng, Q. Zhang and Y. Chen, *ACS Catal.*, 2022, **12**, 9494–9502.
95 J. Xu, W. Liu, L. Jiang, X. Jing, L. L. Liu and Z. Li, *Small*, 2023, **19**, 202304989.
96 J. Zhang, W. Zhou, J. Zhao, L. Xu, X. Jiang, Z. Li, Y. Peng and G. Li, *Small*, 2024, 202408324.
97 Z. Zhao, Y. Zheng, C. Wang, S. Zhang, J. Song, Y. Li, S. Ma, P. Cheng, Z. Zhang and Y. Chen, *ACS Catal.*, 2021, **11**, 2098–2107.
98 X. Zhong, H. Chen, M. Wang, S. Gan, Q. He, W. Chen and F. He, *Macromolecules*, 2019, **52**, 2393–2401.
99 B. McDearmon, Z. A. Page, M. L. Chabinyc and C. J. Hawker, *J. Mater. Chem. C*, 2018, **6**, 3564–3572.
100 W. Chen, L. Wang, D. Mo, F. He, Z. Wen, X. Wu, H. Xu and L. Chen, *Angew. Chem., Int. Ed.*, 2020, **59**, 16902–16909.
101 Z. Wang, P. Yeary, Y. Fan and W. Lin, *Chem. Sci.*, 2024, **15**, 4920–4925.
102 S. Li, L. Li, Y. Li, L. Dai, C. Liu, Y. Liu, J. Li, J. Lv, P. Li and B. Wang, *ACS Catal.*, 2020, **10**, 8717–8726.
103 C. Wang, W. Lu, W. Song, Z. Zhang, C. Xie, Y. Li and J. Wang, *Appl. Catal., B*, 2025, **361**, 124583.
104 Y. Wang, W. Hao, H. Liu, R. Chen, Q. Pan, Z. Li and Y. Zhao, *Nat. Commun.*, 2022, **13**, 100.
105 B. Mishra, S. Dutta, U. Pal, S. Rana, S. K. Mishra, T. Saha-Dasgupta and P. Pachfule, *Small*, 2025, DOI: **10.1002/smll.202411199**.
106 Z. Chen, J. Zhang, F. Yu, Y. He, J. Kang, S. Xiao, F. Song, C. Zhang, R. Liang and J. Qiu, *Sep. Purif. Technol.*, 2025, **359**, 130376.
107 Y. Fang, Y. Liu, H. Huang, J. Sun, J. Hong, F. Zhang, X. Wei, W. Gao, M. Shao, Y. Guo, Q. Tang and Y. Liu, *Nat. Commun.*, 2024, **15**, 4856.
108 B. Gole, V. Stepanenko, S. Rager, M. Grüne, D. D. Medina, T. Bein, F. Würthner and F. Beuerle, *Angew. Chem., Int. Ed.*, 2017, **57**, 846–850.
109 L. Luo, C. Li, Y. Wang, P. Chen, Z. Zhou, T. Chen, K. Wu, S. Y. Ding, L. Tan, J. Wang, X. Shao and Z. Liu, *Small*, 2024, **20**, 202402993.
110 Z. Huang, Y. H. Luo, W. Y. Geng, Y. Wan, S. Li and C. S. Lee, *Small Methods*, 2021, **5**, 2100036.
111 S. Rager, A. C. Jakowetz, B. Gole, F. Beuerle, D. D. Medina and T. Bein, *Chem. Mater.*, 2019, **31**, 2707–2712.
112 Y. Zhang, G. Wu, H. Liu, R. Tian, Y. Li, D. Wang, R. Chen, J. Zhao, S. Liu, Z. Li and Y. Zhao, *Mater. Chem. Front.*, 2021, **5**, 6575–6581.
113 M. Martínez-Fernández, E. Martínez-Periñán, S. Royuela, J. I. Martínez, F. Zamora, E. Lorenzo and J. L. Segura, *Appl. Mater. Today*, 2022, **26**, 101384.
114 J. Lv, Y. X. Tan, J. Xie, R. Yang, M. Yu, S. Sun, M. D. Li, D. Yuan and Y. Wang, *Angew. Chem., Int. Ed.*, 2018, **57**, 12716–12720.
115 S. Royuela, E. Martínez-Periñán, M. P. Arrieta, J. I. Martínez, M. M. Ramos, F. Zamora, E. Lorenzo and J. L. Segura, *Chem. Commun.*, 2020, **56**, 1267–1270.
116 C. Weng, X. Li, Z. Yang, H. Long, C. Lu, L. Dong, S. Zhao and L. Tan, *Chem. Commun.*, 2022, **58**, 6809–6812.
117 Y. Luo, Z. Chang, J. Pei, Z. Guo and H. Zhan, *Nano Lett.*, 2023, **23**, 9266–9271.
118 F. D. Wang, L. J. Yang, X. X. Wang, Y. Rong, L. B. Yang, C. X. Zhang, F. Y. Yan and Q. L. Wang, *Small*, 2023, **19**, 202207421.
119 H. Li, P. Shao, S. Chen, G. Li, X. Feng, X. Chen, H.-J. Zhang, J. Lin and Y.-B. Jiang, *J. Am. Chem. Soc.*, 2020, **142**, 3712–3717.
120 N. Liu, S. Xie, Y. Huang, J. Lu, H. Shi, S. Xu, G. Zhang and X. Chen, *Adv. Energy Mater.*, 2024, **14**, 202402395.
121 G.-B. Wang, H.-P. Xu, K.-H. Xie, J.-L. Kan, J. Fan, Y.-J. Wang, Y. Geng and Y.-B. Dong, *J. Mater. Chem. A*, 2023, **11**, 4007–4012.
122 Z. Li, S. Han, C. Li, P. Shao, H. Xia, H. Li, X. Chen, X. Feng and X. Liu, *J. Mater. Chem. A*, 2020, **8**, 8706–8715.
123 G. Zhang, M. Zhao, L. Su, H. Yu, C. Wang, D. Sun and Y. Ding, *ACS Appl. Mater. Interfaces*, 2023, **15**, 20310–20316.

124 E. Jin, Q. X. Mizue Asada, S. Dalapati, M. A. Addicoat, M. A. Brady, H. Xu, T. Nakamura, T. Heine, Q. Chen and D. Jiang, *Science*, 2017, **357**, 673–676.
125 X. Chi, Z. Zhang, M. Li, Y. Jiao, X. Li, F. Meng, B. Xue, D. Wu and F. Zhang, *Angew. Chem., Int. Ed.*, 2024, 202418895.
126 W. Li, L. Gao, H. Tang, J. Qin, Y. Jiao, L. Wang, S. Xian, Q. Zhou and Z. Wang, *Appl. Mater. Today*, 2024, **37**, 102124.
127 Y. Wang, Y. Z. Cheng, K. M. Wu, D. H. Yang, X. F. Liu, X. Ding and B. H. Han, *Angew. Chem., Int. Ed.*, 2023, **62**, e202310794.
128 G. Lin, H. Ding, D. Yuan, B. Wang and C. Wang, *J. Am. Chem. Soc.*, 2016, **138**, 3302–3305.
129 J. H. Wang, A. E. Hassan, A. M. Elewa and A. F. M. El-Mahdy, *J. Mater. Chem. A*, 2024, **12**, 14005–14021.
130 L. Wang, L. Wang, Q. Zhao, X. Ji, M. Zhao, Y. Zhang and M. Lai, *J. Mater. Chem. A*, 2024, **12**, 28424–28436.
131 K. Lei, D. Wang, L. Ye, M. Kou, Y. Deng, Z. Ma, L. Wang and Y. Kong, *ChemSusChem*, 2020, **13**, 1725–1729.
132 K. Verma, M. A. Addicoat and K. R. Justin Thomas, *ACS Appl. Polym. Mater.*, 2024, **6**, 3909–3917.
133 H. He, R. Shen, Y. Yan, D. Chen, Z. Liu, L. Hao, X. Zhang, P. Zhang and X. Li, *Chem. Sci.*, 2024, **15**, 20002–20012.
134 X. M. Lu, H. Wang, Y. Sun, Y. Xu, W. Sun, Y. Wu, Y. Zhang, C. Yang and Y. Wang, *Angew. Chem., Int. Ed.*, 2024, **63**, e202409436.
135 H. Li, J. Fan, M. Ran, R. A. Borse, S.-X. Lin and D. Yuan, *Angew. Chem., Int. Ed.*, 2025, **64**, e202500937.
136 L. Gilmanova, V. Bon, L. Shupletsov, D. Pohl, M. Rauche, E. Brunner and S. Kaskel, *J. Am. Chem. Soc.*, 2021, **143**, 18368–18373.
137 Z. Li, Z. Dong, Z. Zhang, B. Wei, C. Meng, W. Zhai, Y. Wang, X. Cao, B. Han and Y. Liu, *Angew. Chem., Int. Ed.*, 2025, **64**, e202420218.
138 Q. Wu, M. J. Mao, Q. J. Wu, J. Liang, Y. B. Huang and R. Cao, *Small*, 2020, **17**, 202004933.
139 S. S. Zhao, J. Liang, D.-H. Si, M.-J. Mao, Y. B. Huang and R. Cao, *Appl. Catal., B*, 2023, **333**, 122782.
140 P. Pachfule, A. Acharjya, J. Roeser, R. P. Sivasankaran, M.-Y. Ye, A. Brückner, J. Schmidt and A. Thomas, *Chem. Sci.*, 2019, **10**, 8316–8322.
141 H. Liu, X. Yan, W. Chen, Z. Xie, S. Li, W. Chen, T. Zhang, G. Xing and L. Chen, *Sci. China Chem.*, 2021, **64**, 827–833.
142 H. Xu, S. Xia, C. Li, Y. Li, W. Xing, Y. Jiang and X. Chen, *Angew. Chem., Int. Ed.*, 2024, **63**, e202405476.
143 R.-C. Chen, C.-M. Wu, L.-H. Chung, J. Hu, M.-C. Tang, Z. Lin, X. Yang, Z. Xu and J. He, *Chem. Mater.*, 2024, **36**, 9928–9938.
144 C. Jin, Y. Pang, R. Wang, S. Wu, H. He, L. Gao, J. Liu, L. Chen, Y. Li, X. Yan and B. Wang, *Appl. Catal., A*, 2024, **685**, 119906.
145 Y. Yao, Y. Han, S. Qi, D. Sun, J. Lang, B. Hu, Y. Ma and C. Liu, *Int. J. Hydrogen Energy*, 2024, **63**, 184–192.
146 T. Wang, R. Zhang, P. Zhai, M. Li, X. Liu and C. Li, *J. Mater. Chem. A*, 2024, **12**, 1292–1299.
147 R. Bao, Z. Xiang, Z. Qiao, Y. Yang, Y. Zhang, D. Cao and S. Wang, *Angew. Chem., Int. Ed.*, 2022, **62**, e202216751.
148 Q. Wang, C. Wang, K. Zheng, B. Wang, Z. Wang, C. Zhang and X. Long, *Angew. Chem., Int. Ed.*, 2024, **63**, e202320037.
149 H. Liu, X. Zheng, J. Xu, X. Jia, M. Chao, D. Wang and Y. Zhao, *ACS Appl. Mater. Interfaces*, 2023, **15**, 16794–16800.
150 S. Chang, C. Li, H. Li, L. Zhu and Q. Fang, *Chem. Res. Chin. Univ.*, 2022, **38**, 396–401.
151 Y. Zhao, S. Li, J. Han, G. Fu, L. Liang, M. Chen, X. Wang and T. Zhang, *ACS Mat. Lett.*, 2024, **6**, 3985–3992.
152 J. P. Jeon, Y. J. Kim, S. H. Joo, H. J. Noh, S. K. Kwak and J. B. Baek, *Angew. Chem., Int. Ed.*, 2023, **62**, e202217416.
153 Y. Ma, Y. Yao, S. Qi, C. You, Y. Wu, C. Liu, B. Hu and K. Cui, *Sep. Purif. Technol.*, 2025, **356**, 129972.
154 F. Huang, Y. Wang, X. Dong and X. Lang, *J. Mater. Chem. A*, 2024, **12**, 7036–7046.
155 Y. Ran, M. Yang, J. Li, J. Song, Y. Wang, Z. Li and L. Yuan, *Sep. Purif. Technol.*, 2025, **355**, 129603.
156 Y. Wang, Z. Qiao, H. Li, R. Zhang, Z. Xiang, D. Cao and S. Wang, *Angew. Chem., Int. Ed.*, 2024, **63**, e202404726.
157 Q. Rong, X. Chen, Q. Cheng, Z. Huang and S. He, *ACS Sustainable Chem. Eng.*, 2024, **12**, 13306–13315.
158 H. Ma, B. Liu, B. Li, L. Zhang, Y.-G. Li, H.-Q. Tan, H.-Y. Zang and G. Zhu, *J. Am. Chem. Soc.*, 2016, **138**, 5897–5903.
159 X. Han, Z. Zhou, K. Wang, Z. Zheng, S. E. Neumann, H. Zhang, T. Ma and O. M. Yaghi, *J. Am. Chem. Soc.*, 2023, **146**, 89–94.
160 Z. Gu, J. Tian, Y. Li, H. Li, Y. Chai and X. Chi, *ACS Mat. Lett.*, 2024, **6**, 5292–5299.
161 Z. E. Blastik, S. Voltrová, V. Matoušek, B. Jurásek, D. W. Manley, B. Klepetářová and P. Beier, *Angew. Chem., Int. Ed.*, 2016, **56**, 346–349.
162 H.-Y. Zhang, Y. Yang, C.-C. Li, H.-L. Tang, F.-M. Zhang, G.-L. Zhang and H. Yan, *J. Mater. Chem. A*, 2021, **9**, 16743–16750.
163 M. Kaur, S. Kumar, S. A. Younis, M. Yusuf, J. Lee, S. Weon, K.-H. Kim and A. K. Malik, *Chem. Eng. J.*, 2021, **423**, 130230.
164 B.-J. Yao, W.-X. Wu, L.-G. Ding and Y.-B. Dong, *J. Org. Chem.*, 2021, **86**, 3024–3032.
165 X.-T. Li, J. Zou, T.-H. Wang, H.-C. Ma, G.-J. Chen and Y.-B. Dong, *J. Am. Chem. Soc.*, 2020, **142**, 6521–6526.
166 H. Lyu, H. Li, N. Hanikel, K. Wang and O. M. Yaghi, *J. Am. Chem. Soc.*, 2022, **144**, 12989–12995.
167 V. Singh, J. Kim, B. Kang, J. Moon, S. Kim, W. Y. Kim and H. R. Byon, *Adv. Energy Mater.*, 2021, **11**, 2003735.
168 P. Liu, K. Cai, D.-J. Tao and T. Zhao, *Appl. Catal., B*, 2024, **341**, 123317.
169 Z.-Z. Wu, T. Xia, Y. Liang, Y.-P. Li, Z.-Y. Sui, L.-J. Feng, D.-X. Wu, X.-L. Tian and Q. Chen, *Rare Met.*, 2024, **43**, 3096–3106.
170 G. Matthys, A. Laemont, N. De Geyter, R. Morent, R. Lavendomme and P. Van Der Voort, *Small*, 2024, 20.
171 J. Huang, X. Liu, W. Zhang, Z. Liu, H. Zhong, B. Shao, Q. Liang, Y. Liu, W. Zhang and Q. He, *Chem. Eng. J.*, 2021, **404**, 127136.
172 Y. Hu, G. Liu, T. Song, X. Hu, B. Long and G.-J. Deng, *Appl. Catal., B*, 2025, **361**, 124587.
173 Y. Wang, Y. Zheng, S. han, F. Chen and J. Hu, *Appl. Surf. Sci.*, 2025, **698**, 163089.

174 J. L. Segura, S. Royuela and M. Mar Ramos, *Chem. Soc. Rev.*, 2019, **48**, 3903–3945.
175 Y. Liang, T. Xia, Z. Wu, Y. Yang, Y. Li, Z. Sui, C. Li, R. Fan, X. Tian and Q. Chen, *Mater.Today Chem.*, 2022, **24**, 100777.
176 P. Dong, X. Xu, R. Luo, S. Yuan, J. Zhou and J. Lei, *J. Am. Chem. Soc.*, 2023, **145**, 15473–15481.
177 S. Yang, W. Liu, Y. Zhang, X. Jia, J. Sun, C. Zhang and M. Liu, *J. Mater. Chem. A*, 2024, **12**, 28161–28169.
178 X. Quan and B. Yan, *ACS Sustainable Chem. Eng.*, 2023, **11**, 7466–7474.
179 Y. Wang, Y. Deng, H. Xia, R. Zhang, J. Liu, H. Zhang, Y. Sun, Z. Zhang and X. Lu, *Small Methods*, 2023, **8**, 2300163.
180 L. Chen, K. Furukawa, J. Gao, A. Nagai, T. Nakamura, Y. Dong and D. Jiang, *J. Am. Chem. Soc.*, 2014, **136**, 9806–9809.
181 L. D. Tran, D. C. Moore, B. C. Patra, J. Choi, C. M. Hampton, M. E. Loveday, D. D. Bhagwandin, I. Renggli, C. Muratore, L. F. Drummy, D. Zhao, N. R. Glavin and L. A. Baldwin, *Adv. Funct. Mater.*, 2024, **34**, 202402208.
182 Y. Xiang, W. Dong, P. Wang, S. Wang, X. Ding, F. Ichihara, Z. Wang, Y. Wada, S. Jin, Y. Weng, H. Chen and J. Ye, *Appl. Catal., B*, 2020, **274**, 119096.
183 M. Lu, M. Zhang, J. Liu, T.-Y. Yu, J.-N. Chang, L.-J. Shang, S.-L. Li and Y.-Q. Lan, *J. Am. Chem. Soc.*, 2022, **144**, 1861–1871.
184 P. J. Waller, Y. S. AlFaraj, C. S. Diercks, N. N. Jarenwattananon and O. M. Yaghi, *J. Am. Chem. Soc.*, 2018, **140**, 9099–9103.
185 R. Yan, B. Mishra, M. Traxler, J. Roeser, N. Chaoui, B. Kumbhakar, J. Schmidt, S. Li, A. Thomas and P. Pachfule, *Angew. Chem., Int. Ed.*, 2023, **62**, e202302276.
186 M. Deng, J. Sun, A. Laemont, C. Liu, L. Wang, L. Bourda, J. Chakraborty, K. Van Hecke, R. Morent, N. De Geyter, K. Leus, H. Chen and P. Van Der Voort, *Green Chem.*, 2023, **25**, 3069–3076.
187 K. Dey, S. Mohata and R. Banerjee, *ACS Nano*, 2021, **15**, 12723–12740.
188 Y. Zhang, X. Guan, Z. Meng and H.-L. Jiang, *J. Am. Chem. Soc.*, 2025, **147**, 3776–3785.
189 W. Wei, S. Zhou, D. D. Ma, Q. Li, M. Ran, X. Li, X. T. Wu and Q. L. Zhu, *Adv. Funct. Mater.*, 2023, **33**, 2302917.
190 Y. He, Y. Zhao, X. Wang, Z. Liu, Y. Yu and L. Li, *Angew. Chem., Int. Ed.*, 2023, **62**, e202307160.
191 X. Zhang, Z. Wen, L. Pan, R. Wei, W. Pan, Y. Li, F. Lu, Y. Gao, N. Li and B. Tang, *Mater. Today Nano*, 2023, **24**, 100418.
192 Z. Tang, J. Chen, Y. Xu, Z. Li, L. Sheng, Y. Hu, X. Wang, J. Wang, Y. Tang, X. He and H. Xu, *Chem. Mater.*, 2024, **36**, 4437–4443.
193 Y. Ma, Y. Han, Y. Yao, T. Zhou, D. Sun, C. Liu, G. Che, B. Hu, V. Valtchev and Q. Fang, *Chem. Sci.*, 2024, **15**, 12488–12495.
194 L. Ye, Z. Xia, Q. Xu, Y. Yang, X. Xu, H. Jin and S. Wang, *Chem. Commun.*, 2023, **59**, 9872–9875.
195 Q. An, S. Su, W. Hu, Y. Wang, T. Liang, X. Li and C. Li, *Nanoscale*, 2023, **15**, 19815–19819.
196 Y. Wang, Z. Hu, W. Wang, H. He, L. Deng, Y. Zhang, J. Huang, N. Zhao, G. Yu and Y.-N. Liu, *Chem. Sci.*, 2021, **12**, 16065–16073.
197 M. Zhang, M. Lu, Z. L. Lang, J. Liu, M. Liu, J. N. Chang, L. Y. Li, L. J. Shang, M. Wang, S. L. Li and Y. Q. Lan, *Angew. Chem., Int. Ed.*, 2020, **59**, 6500–6506.
198 R. Shen, X. Li, C. Qin, P. Zhang and X. Li, *Adv. Energy Mater.*, 2023, **13**, 2203695.
199 Z.-W. Zhou, C.-X. Liu, C.-X. Cai, Y.-J. Wei, K. Li, X.-Q. Yu, Y.-H. Liu and N. Wang, *J. Environ. Chem. Eng.*, 2024, **12**, 113533.
200 L. Cognigni, T. Gobbato, E. Benazzi, L. Paoloni, B. D. Vizio, R. Bonetto, F. Rigodanza, A. Bonetto, S. Agnoli, M. Bonchio and P. Costa, *ChemSusChem*, 2024, e202401977.
201 Q.-J. Wu, D.-H. Si, S. Ye, Y.-L. Dong, R. Cao and Y.-B. Huang, *J. Am. Chem. Soc.*, 2023, **145**, 19856–19865.
202 K. Xiao, R. Zhu, C. Du, X. Zhang and J. Chen, *Sens. Actuators, B*, 2023, **380**, 133403.
203 S. Ge, K. Wei, W. Peng, R. Huang, E. Akinlabi, H. Xia, M. W. Shahzad, X. Zhang, B. B. Xu and J. Jiang, *Chem. Soc. Rev.*, 2024, **53**, 11259–11302.
204 Q. Xu, L. Zhang, B. Cheng, J. Fan and J. Yu, *Chem*, 2020, **6**, 1543–1559.
205 C. Cui, X. Xu, X. Zhao, N. Xi, M. Li, X. Wang, Y. Sang, X. Yu, H. Liu and J. Wang, *Nano Energy*, 2024, **126**, 109632.
206 I. M. A. Mekhemer, M. M. Elsenety, A. M. Elewa, K. D. G. Huynh, M. M. Samy, M. G. Mohamed, D. M. Dorrah, D. C. K. Hoang, A. F. Musa, S.-W. Kuo and H.-H. Chou, *J. Mater. Chem. A*, 2024, **12**, 10790–10798.
207 M. Wang, Z. Wang, M. Shan, J. Wang, Z. Qiu, J. Song and Z. Li, *Chem. Mater.*, 2023, **35**, 5368–5377.
208 Y. Yang, N. Luo, S. Lin, H. Yao and Y. Cai, *ACS Catal.*, 2022, **12**, 10718–10726.
209 S. Ma, Z. Li, Y. Hou, J. Li, Z. Zhang, T. Deng, G. Wu, R. Wang, S. w. Yang and X. Liu, *Angew. Chem., Int. Ed.*, 2025, e202501869.
210 J. Cheng, Y. Wu, W. Zhang, J. Zhang, L. Wang, M. Zhou, F. Fan, X. Wu and H. Xu, *Adv. Mater.*, 2023, **36**, 202305313.
211 C. Mo, M. Yang, F. Sun, J. Jian, L. Zhong, Z. Fang, J. Feng and D. Yu, *Adv. Sci.*, 2020, **7**, 1902988.
212 J. Yang, S. Ghosh, J. Roeser, A. Acharjya, C. Penschke, Y. Tsutsui, J. Rabeah, T. Wang, S. Y. Djoko Tameu, M.-Y. Ye, J. Grüneberg, S. Li, C. Li, R. Schomäcker, R. Van De Krol, S. Seki, P. Saalfrank and A. Thomas, *Nat. Commun.*, 2022, **13**, 6317.
213 C. Q. Han, J. X. Guo, S. Sun, Z. Y. Wang, L. Wang and X. Y. Liu, *Small*, 2024, **20**, 202405887.
214 Z. Li, T. Deng, S. Ma, Z. Zhang, G. Wu, J. Wang, Q. Li, H. Xia, S.-W. Yang and X. Liu, *J. Am. Chem. Soc.*, 2023, **145**, 8364–8374.
215 J. Yang, A. Acharjya, M. Y. Ye, J. Rabeah, S. Li, Z. Kochovski, S. Youk, J. Roeser, J. Grüneberg, C. Penschke, M. Schwarze, T. Wang, Y. Lu, R. van de Krol, M. Oschatz, R. Schomäcker, P. Saalfrank and A. Thomas, *Angew. Chem., Int. Ed.*, 2021, **60**, 19797–19803.
216 L. Dai, A. Dong, X. Meng, H. Liu, Y. Li, P. Li and B. Wang, *Angew. Chem., Int. Ed.*, 2023, **62**, e202300224.

217 Y. Liu, Y. Shi, H. Wang and S. Zhang, *Nano Res.*, 2024, **17**, 5835–5844.
218 X. A. Li, Z. Z. Liang, Y. C. Zhou, J. F. Huang, X. L. Wang, L. M. Xiao and J. M. Liu, *Aggregate*, 2023, **5**, e442.
219 K. Mase, M. Yoneda, Y. Yamada and S. Fukuzumi, *Nat. Commun.*, 2016, **7**, 11470.
220 S. Feng, L. Wang, L. Tian, Y. Liu, K. Hu, H. Xu, H. Wang and J. Hua, *Chem. Sci.*, 2024, **15**, 11972–11980.
221 Z. Zhang, Y. Hou, S. Zhu, L. Yang, Y. Wang, H. Yue, H. Xia, G. Wu, S. w. Yang and X. Liu, *Angew. Chem., Int. Ed.*, 2025, e202505286.
222 M. Liu, P. He, H. Gong, Z. Zhao, Y. Li, K. Zhou, Y. Lin, J. Li, Z. Bao, Q. Yang, Y. Yang, Q. Ren and Z. Zhang, *Chem. Eng. J.*, 2024, **482**, 148922.
223 C. Krishnaraj, H. Sekhar Jena, L. Bourda, A. Laemont, P. Pachfule, J. Roeser, C. V. Chandran, S. Borgmans, S. M. J. Rogge, K. Leus, C. V. Stevens, J. A. Martens, V. Van Speybroeck, E. Breynaert, A. Thomas and P. Van Der Voort, *J. Am. Chem. Soc.*, 2020, **142**, 20107–20116.
224 Y. Chen, R. Liu, Y. Guo, G. Wu, T. C. Sum, S. W. Yang and D. Jiang, *Nat. Synth.*, 2024, **3**, 998–1010.
225 Y. Wang, H. Zhao, P. Li, J. Zhang, X. Sun, R. Zhang, Y. Guo, Y. Dong and Y. Zhu, *Chem. Eng. J.*, 2024, **491**, 151825.
226 Y. Liu, L. Li, H. Tan, N. Ye, Y. Gu, S. Zhao, S. Zhang, M. Luo and S. Guo, *J. Am. Chem. Soc.*, 2023, **145**, 19877–19884.
227 F. Liu, P. Zhou, Y. Hou, H. Tan, Y. Liang, J. Liang, Q. Zhang, S. Guo, M. Tong and J. Ni, *Nat. Commun.*, 2023, **14**, 4344.
228 W. Chi, B. Liu, Y. Dong, J. Zhang, X. Sun, C. Pan, H. Zhao, Y. Ling and Y. Zhu, *Appl. Catal., B*, 2024, **355**, 124077.
229 J.-C. Liu, C. Tuo, W.-Y. Xiao, M.-Y. Qi, Y. Yusran, Z.-T. Wang, H. Li, C.-S. Guo, J.-L. Song, S.-L. Qiu, Y.-J. Xu and Q. Fang, *Angew. Chem., Int. Ed.*, 2024, e202416240.
230 H. H. Sun, Z. B. Zhou, Y. Fu, Q. Y. Qi, Z. X. Wang, S. Xu and X. Zhao, *Angew. Chem., Int. Ed.*, 2024, **63**, e202409250.
231 Y. Xie, F. Mao, Q. Rong, X. Liu, M. Hao, Z. Chen, H. Yang, G. I. N. Waterhouse, S. Ma and X. Wang, *Adv. Funct. Mater.*, 2024, 2411077.
232 J. N. Chang, Q. Li, J. W. Shi, M. Zhang, L. Zhang, S. Li, Y. Chen, S. L. Li and Y. Q. Lan, *Angew. Chem., Int. Ed.*, 2023, **62**, e202218868.
233 Z. Zhou, M. Sun, Y. Zhu, P. Li, Y. Zhang, M. Wang and Y. Shen, *Appl. Catal., B*, 2023, **334**, 122862.
234 L. Guo, L. Gong, Y. Yang, Z. Huang, X. Liu and F. Luo, *Angew. Chem., Int. Ed.*, 2024, e202414658.
235 F. Huang, F. Zhang, Y. Wang, K. Zhang and X. Lang, *Appl. Catal., B*, 2025, **361**, 124628.
236 K. Xiong, F. Zhang, Y. Wang, B. Zeng and X. Lang, *J. Colloid Interface Sci.*, 2023, **643**, 340–349.
237 Z. Gu, Z. Shan, Y. Wang, J. Wang, T. Liu, X. Li, Z. Yu, J. Su and G. Zhang, *Chin. Chem. Lett.*, 2024, **35**, 108356.
238 F. Tao, W. Zhou, Z. Li, X. Jiang, L. Wang, Z. Yu, J. Zhang and H. Zhou, *ACS Mat. Lett.*, 2024, **6**, 1120–1129.
239 X. Hu, X. Zeng, Y. Liu, J. Lu and X. Zhang, *Nanoscale*, 2020, **12**, 16008–16027.
240 J. N. Chang, Q. Li, J. W. Shi, M. Zhang, L. Zhang, S. Li, Y. Chen, S. L. Li and Y. Q. Lan, *Angew. Chem., Int. Ed.*, 2023, **62**, e202218868.
241 Z. Yong and T. Ma, *Angew. Chem., Int. Ed.*, 2023, **62**, e202308980.
242 S. Suleman, Y. Zhang, Y. Qian, J. Zhang, Z. Lin, Ö. Metin, Z. Meng and H. L. Jiang, *Angew. Chem., Int. Ed.*, 2023, **63**, e202314988.
243 Y. Wang, F. Zhang, F. Huang, X. Dong, B. Zeng, X.-K. Gu and X. Lang, *Appl. Catal., B*, 2024, **354**, 124103.
244 H. Pang, D. Huang, Y. Zhu, X. Zhao and Y. Xiang, *Chem. Sci.*, 2023, **14**, 1543–1550.
245 D. Huang, Y. Zhang, H. Pang, X. Hu and Y. Xiang, *J. Mater. Chem. A*, 2024, **12**, 18512–18518.
246 Y. Pang, Y. Li, X. Gu, D. Wang, H. He, Y. Gou, B. Yuan, L. Chen and B. Wang, *J. Catal.*, 2024, **433**, 115497.
247 J. Kou, G. Wang, H. Guo, L. Li, J. Fang, J. Ma and Z. Dong, *Appl. Catal., B*, 2024, **352**, 124020.
248 A. Chakraborty, M. Roy, A. Alam, D. Adhikari and P. Pachfule, *Green Chem.*, 2024, **26**, 9619–9651.
249 K. Cai, W. Wang, J. Zhang, L. Chen, L. Wang, X. Zhu, Z. Yu, Z. Wu and H. Zhou, *J. Mater. Chem. A*, 2022, **10**, 7165–7172.
250 W.-K. An, S.-J. Zheng, X. Xu, L.-J. Liu, J.-S. Ren, L. Fan, Z.-K. Yang, Y. Ren and C. Xu, *Appl. Catal., B*, 2022, **316**, 121630.
251 Z. Li, J.-a. Wang, S. Ma, Z. Zhang, Y. Zhi, F. Zhang, H. Xia, G. Henkelman and X. Liu, *Appl. Catal., B*, 2022, **310**, 121335.
252 H. Shan, D. Cai, X. Zhang, Q. Zhu, P. Qin and J. Baeyens, *Chem. Eng. J.*, 2022, **432**, 134288.
253 D. Zhu, Y. Chen, Y. Zhu, C.-Y. Liu, Q. Yan, X. Wu, K. Ling, X. Zhang, P. M. Ajayan, T. P. Senftle and R. Verduzco, *Macromolecules*, 2024, **57**, 1038–1049.
254 Y. Liu, P. Bhattarai, Z. Dai and X. Chen, *Chem. Soc. Rev.*, 2019, **48**, 2053–2108.
255 Q. Zhang, D.-H. Qu, B. L. Feringa and H. Tian, *J. Am. Chem. Soc.*, 2022, **144**, 2022–2033.
256 X. Zhang, Y. Dou, S. Liu, P. Chen, Y. Wen, J. Li, Y. Sun and R. Zhang, *Adv. Healthc. Mater.*, 2024, **13**, 2303842.
257 R. Xia, X. Zheng, C. Li, X. Yuan, J. Wang, Z. Xie and X. Jing, *ACS Nano*, 2021, **15**, 7638–7648.
258 K. Wang, Z. Zhang, L. Lin, J. Chen, K. Hao, H. Tian and X. Chen, *Chem. Mater.*, 2019, **31**, 3313–3323.
259 Y. Liu, K. Yang, J. Wang, Y. Tian, B. Song and R. Zhang, *Mater. Today Bio*, 2024, **25**, 100981.
260 S. Song, D. Wang, K. Zhao, Y. Wu, P. Zhang, J. Liu, G. Yang, P. Gong and Z. Liu, *Chem. Eng. J.*, 2022, **442**, 135963.
261 W. Wang, Y. Song, J. Chen, Y. Yang, J. Wang, Y. Song, J. Ni, M. Tang, J. Zhao, Y. Sun, T. Sun and J. Peng, *J. Mater. Chem. B*, 2022, **10**, 1128–1135.
262 H. Zhang, Y. Geng, J. Huang, Z. Wang, K. Du and H. Li, *Energy Environ. Sci.*, 2023, **16**, 889–951.
263 P. Dubey, V. Shrivastav, T. Boruah, G. Zoppellaro, R. Zbořil, A. Bakandritsos and S. Sundriyal, *Adv. Energy Mater.*, 2024, **14**, 2400521.
264 M. Chafiq, A. Chaouiki and Y. G. Ko, *Energy Storage Mater.*, 2023, **63**, 103014.
265 K. J. Nana Li, F. Rodríguez-Hernández, H. Mao, S. Han, X. Fu, J. Zhang, C. Yang, C. Ke and X. Zhuang, *Adv. Sci.*, 2022, **9**, 2104898.

266 A. Chatterjee, J. Sun, K. S. Rawat, V. Van Speybroeck and P. Van Der Voort, *Small*, 2023, **19**, 202303189.
267 A. Zhang, P. Ran, X. Han, S. Ke, A. Qiu, Z. Zhang, Y. Lv, M. Ding and J.-L. Zuo, *J. Mater. Chem. A*, 2024, **12**, 22037–22044.
268 S. Wang, T. Wu, J. Guo, R. Zhao, Y. Hua and Y. Zhao, *ACS Cent. Sci.*, 2024, **10**, 1383–1395.
269 E. Zhou, X. Zhang, L. Zhu, D. Yuan and Y. Wang, *Adv. Funct. Mater.*, 2023, **33**, 2213667.
270 Z. Li, Z. Zhang, R. Nie, C. Li, Q. Sun, W. Shi, W. Chu, Y. Long, H. Li and X. Liu, *Adv. Funct. Mater.*, 2022, **32**, 2112553.
271 S. Yang, J. He, Z. Chen, H. Luo, J. Wei, X. Wei, H. Li, J. Chen, W. Zhang, J. Wang, S. Wang and G. Yu, *Adv. Mater.*, 2024, **36**, 2408686.
272 C. Li, A. Yu, W. Zhao, G. Long, Q. Zhang, S. Mei and C. J. Yao, *Angew. Chem., Int. Ed.*, 2024, **63**, e202409421.
273 Y. Yang, C. Zhang, G. Zhao, Q. An, Z. y. Mei, Y. Sun, Q. Xu, X. Wang and H. Guo, *Adv. Energy Mater.*, 2023, **13**, 2300725.
274 G. Zhao, H. Ma, C. Zhang, Y. Yang, S. Yu, H. Zhu, Y. Sun and H. Guo, *Nano-Micro Lett.*, 2024, **17**, 21.
275 X. Yu, Y. Zhao, Q. Bao, W. Wang, Y. Li, J. Xiao, Z. Sui, X. Tian and Q. Chen, *J. Colloid Interface Sci.*, 2024, **675**, 970–979.
276 D. Ma, H. Zhao, F. Cao, H. Zhao, J. Li, L. Wang and K. Liu, *Chem. Sci.*, 2022, **13**, 2385–2390.
277 S. Wang, C. Zhu, J. Ji, M. Li, L. Zhao, F. Cai and Z. Tao, *Small Methods*, 2024, 2400557.
278 H. Peng, S. Huang, V. Montes-García, D. Pakulski, H. Guo, F. Richard, X. Zhuang, P. Samorì and A. Ciesielski, *Angew. Chem., Int. Ed.*, 2023, **62**, e202216136.